Strength and Deformation of "Tunable" Clay-Polymer Composites

A Thesis Presented for
the Master of Science
Degree
The University of Tennessee, Knoxville

Matthew David Bishop

August 2013

Copyright © 2013 by Matthew David Bishop
All rights reserved.

DEDICATION

To my fiancée, Anna

ACKNOWLEDGMENTS

First and foremost, I would like to give thanks to God for His many blessings upon my life. During my research I was constantly reminded of Philippians 4:13, "I can do all things through Christ who strengthens me."

I would also like to thank my advisor, Dr. Angel Palomino. Her hard work and support during my research and writing was crucial to my success. She was always available and offering support when I needed it, and I am grateful for the opportunity to work with her over the last year and a half. Also, I could not have done this research without the help of Dr. Palomino's post-doctoral student, Sungho Kim. His great deal of knowledge and willingness to help was incredible. I appreciate the time he dedicated to ensuring my success.

Additionally, I would like to thank the professors that served on my committee: Dr. James Mason and Dr. Khalid Alshibli. They gave me valuable advice and counsel along the way, and helped make my research the best it could be. I greatly appreciate the time they spent working with me during the last year.

I would also like to thank a few of my friends and classmates that gave advice to me along the way, specifically Andrew Druckrey and Mehmet Cil. Their strong work ethic and dedication are traits that I aspire to in my own life.

Finally, I would like to end by thanking my family for their support. This includes my father David, my mother Debbie, my sister Sarah, and my fiancée Anna. They have always encouraged me to be the best I can be, and I am forever grateful.

ABSTRACT

There are many different types of clay that exist throughout the world, and many are characterized by undesirable engineering properties. Soil improvement techniques are often implemented on these soils such as solidification, reinforcement, etc. However, these solutions are a "static" approach, as the soil's properties cannot be modified over time. The development of the specific clay-polymer composites used in this study was motivated by the idea of creating a geomaterial that could be modified over time by adjusting its fabric, namely in the form of controlling interparticle and interlayer spacings. Therefore, the composites that are used in this study are "responsive" to changes in the external environment, which has been proven at the micro-scale in previous studies.

Tests were performed on these clay-polymer composites using two different types of clay, kaolinite and montmorillonite, in order to determine their shear strength and compressibility parameters, as well as their shear wave velocities, and to determine any links between their observed meso-scale behavior and known micro-scale behavior. It was shown that with the addition of polyacrylamide (PAM) polymers, which are sensitive to pH and ionic concentration variations, the normalized shear stress was increased when compared to the control samples under the same conditions. However, no link was found between the known polymer conformation of PAM and the clay-polymer composites' normalized shear stresses.

The compressibility, C_c [compression index], and C_r [recompression index] values of the clay-polymer composites were also shown to be higher than in the control samples. Shear wave velocities, however, were shown to have no significant correlation to the sample type or test conditions, indicating this testing may not be a useful method of distinguishing between the stiffness of control and composite samples. Finally, "tunability" was shown for kaolinite-PAM samples. PAM's extended conformation at high pH and low ionic concentration led to greater increases in compressibility, greater decreases in C_v [coefficient of consolidation], greater increases in C_c, and greater increases in C_r. Thus, an extended polymer conformation was determined to be more compressible and can exhibit greater changes in its behavior than a coiled polymer conformation.

TABLE OF CONTENTS

CHAPTER 1: INTRODUCTION 1

1.1 Motivation 1

1.2 Objectives 2

1.3 Hypotheses 3

1.4 Expected Contributions 4

CHAPTER 2: LITERATURE REVIEW 5

2.1 Montmorillonite 5

2.2 Kaolinite 8

2.3 Clay Surface Properties 10

2.4 Responsive Polymers 13

2.5 “Tunable” Clay-Polymer Composites 17

2.6 Previous Studies 20

2.7 Shear Strength of Clays 23

2.8 Compressibility of Clays 28

CHAPTER 3: SAMPLE PREPARATION 34

3.1 Materials 34

3.1.1 Kaolinite 34

3.1.2 Montmorillonite 35

3.1.3 Polyacrylamide 37

3.2 Na-Kaolinite Process 38

3.3 Solution Intercalation 40

3.4 Pre-Consolidation 44

3.5 Test Matrix 48
CHAPTER 4: SHEAR STRENGTH 50
4.1 Direct Shear Procedure 50
4.1.1 Procedure 50
4.1.2 Test Setup 53
4.1.3 Measurements 56
4.1.3 Undrained Shear Strength 57
4.2 Results 60
4.2.1 Kaolinite (Kt) and Kaolinite Composite (Kt-PAM) 60
4.2.2 Montmorillonite (Mt) and Montmorillonite Composite (Mt-PAM) 66
4.3 Discussion of Results 68
4.4 Conclusions 71
CHAPTER 5: COMPRESSIBILITY AND SHEAR WAVE VELOCITY 73
5.1 1D Consolidation 73
5.1.1 Procedure 73
5.1.2 Test Setup 75
5.1.3 Measurements 79
5.1.4 Void Ratio 79
5.1.5 Coefficient of Consolidation 80
5.1.6 Compression Index and Recompression Index 82
5.2 Shear Wave Velocity Measurement 83
5.2.1 Procedure 83
5.2.2 Test Setup 84
5.2.3 Measurements 88

5.2.4 Shear Wave Velocity 88
5.3 Results 91
5.3.1 Kaolinite (Kt) and Kaolinite Composite (Kt-PAM) 92
5.3.2 Montmorillonite (Mt) and Montmorillonite Composite (Mt-PAM) 105
5.4 Discussion of Results 114
5.5 Conclusions 119
CHAPTER 6: CONCLUSIONS AND FUTURE WORK 121
6.1 Conclusions 121
6.2 Future Work 124
LIST OF REFERENCES 127
APPENDICES 134
Appendix A 135
Appendix B 145
VITA 156

LIST OF TABLES

TABLE 2.1: Typical values of cation exchange capacity (CEC), specific surface (Sa), and surface charge density (σ_0) for clays of interest (Mitchell and Soga 2005; Shang et al. 1994) 13
TABLE 3.1: Elemental Composition of kaolinite (Supplier data) 35
TABLE 3.2: Properties of the kaolinite used in this study (Kim and Palomino 2009) 36
TABLE 3.3: Elemental Composition of montmorillonite (Supplier data) 37
TABLE 3.4: Properties of the montmorillonite used in this study (Kim and Palomino 2011) 37
TABLE 3.5: Mass of each clay and polymer to use for solution intercalation technique based on a batch of 2000 mL or 3500 mL..... 42
TABLE 3.6: Sample calculations showing the resulting water contents for both Kt-PAM and Mt-PAM composites mixed to a total volume of 3500 mL. 44
TABLE 3.7: Test Matrix..... 49
TABLE 5.1: General loading schedule for 1D consolidation testing..... 75
TABLE 5.2: Typical shear wave velocities of different materials (Ashland 2013) .. 85
TABLE 5.3: Void ratio and shear wave velocity results for Kt & Kt-PAM samples under varying pore fluid conditions..... 96
TABLE 5.4: Void ratio and shear wave velocity results for Mt & Mt-PAM samples under varying pore fluid conditions..... 109

LIST OF FIGURES

FIG. 2.1: Mineral composition of dry montmorillonite (Barak and Nater 2003)..... 7
FIG. 2.2: Mineral composition of dry kaolinite (Barak and Nater 2003)..... 9
FIG. 2.3: Representation of a clay particle and the resulting formation of the diffuse double layer (after Mitchell and Soga 2005; Santamarina et al. 2001; Stumm 1992) 11
FIG. 2.4: Schematic of PAM polymer molecule highlighting its amide functional groups (image created using Avogadro Molecule Editor 2012)..... 14
FIG. 2.5: Conformation of polyacrylamide due to pH and ionic concentration (after Kim and Palomino 2011)..... 15
FIG. 2.6: PAM molecules showing highlighted a) undissociated amide groups, and b) dissociated amide groups; red circles highlight the amide functional groups and blue circles highlight the dissociating NH_{2-} and O^{2-} groups (images created using Avogadro Molecule Editor 2012)..... 15
FIG. 2.7: Three formation types of clay-polymer composites (after Kim and Palomino 2011)..... 18
FIG. 2.8: Behavior of clay-polymer composite due to different pH and ionic concentration conditions (after Kim and Palomino 2011)..... 19
FIG. 3.1: Mixer used to prepare the clay-polymer composites 41
FIG. 3.2: Materials used for Kt-PAM composites consist of (a) Kaolinite and (b) PAM..... 43
FIG. 3.3: Pre-consolidation setup showing samples prepared in PVC tubes and consolidated with weights..... 45
FIG. 3.4: Water content and void ratio results for the materials: a) kaolinite; b) kaolinite-PAM composite; c) montmorillonite; and d) montmorillonite-PAM composite..... 47
FIG. 4.1: Procedure showing the steps for extruding each sample from the preconsolidation tube, trimming, and placing into the direct shear box and cell: (a)

extruding, (b) trimming from tube, (c) trimming the diameter, (d) inserting into direct shear box, (e) saturating 54
FIG. 4.2: Direct shear box and cell before the start of a test 55
FIG. 4.3: Direct shear device showing the various components of the test setup 55
FIG. 4.4: Screenshot of the DigiShear program 57
FIG. 4.5: Direct shear tests showing the determination of the undrained shear stresses (S_u, S_{comp}) for: (a) Kt at pH 6 pore fluid and 200 kPa normal stress, and (b) Kt-PAM at pH 6 pore fluid and 200 kPa normal stress 59
FIG. 4.6: Normalized shear stress values (S_u/σ_v or S_{comp}/σ_v) of Kt and Kt-PAM at various pH levels 61
FIG. 4.7: Normalized shear stress values (S_u/σ_v or S_{comp}/σ_v) of Kt and Kt-PAM at various ionic concentrations 62
FIG. 4.8: Test setup for conducting the sedimentation test 63
FIG. 4.9: Sedimentation curves showing inferred fabrics for: (a) Kt at distilled water, (b) Kt at 0.3M NaCl, (c) Kt-PAM at distilled water, and (d) Kt-PAM at 0.3M NaCl 64
FIG. 4.10: Normalized shear stress values (S_u/σ_v or S_{comp}/σ_v) of Mt and Mt-PAM at various pH levels 67
FIG. 4.11: Normalized shear stress values (S_u/σ_v or S_{comp}/σ_v) of Mt and Mt-PAM at various ionic concentrations 68
FIG. 5.1: Procedure showing the steps for extruding each sample from the preconsolidation tube and placing into the consolidation ring: (a) extruding, (b) trimming from tube, (c) inserting into consolidation ring, (d) saturating 76
FIG. 5.2: Modified consolidation cell containing the sample and desired pore fluid condition 77
FIG. 5.3: Soiltest C-220 oedometer used for consolidation testing 78
FIG. 5.4: Example data from a stain vs. log time curve showing the locations of ε_0, ε_{50}, ε_{100}, and t_{50} 81
FIG. 5.5: Sample data from a void ratio vs. effective stress curve showing values for C_c and C_r 83

FIG 5.6: Input and output shear wave signals (Lee 2003) 84
FIG 5.7: Modified consolidation cell, bender element, and modified porous stones 86
FIG 5.8: Shear wave velocity measurement system: waveform generator, consolidation cell, filter/amplifier, oscilloscope, and laptop 87
FIG 5.9: Input sine wave and the resulting output signals for each loading of a consolidation test 89
FIG 5.10: First arrival time calculated using both square and sine waves. The resulting first arrival time is denoted using the blue star (Lee 2003; Lee 2012). 90
FIG 5.11: Void ratio and shear wave velocity curves showing the effects of pH for (a) Kt samples and (b) Kt-PAM samples 93
FIG 5.12: Void ratio and shear wave velocity curves showing the effects of ionic concentration for (a) Kt samples and (b) Kt-PAM samples 94
FIG 5.13: Change in void ratio from start of test to maximum loading of 1643 kPa for Kt and Kt-PAM under varying (a) pH levels and (b) ionic concentrations 97
FIG 5.14: Change in void ratio from maximum loading of 1643 kPa to end of test (after final unloading of 87 kPa) for Kt and Kt-PAM under varying (a) pH levels and (b) ionic concentrations 99
FIG 5.15: Shear wave velocities measured at the initial load of 87 kPa, maximum load of 1643 kPa, and at the end of the test (after final unloading of 87 kPa) for Kt and Kt-PAM under varying (a) pH levels and (b) ionic concentrations 100
FIG 5.16: Coefficient of consolidation results for Kt and Kt-PAM under varying (a) pH levels and (b) ionic concentrations 102
FIG 5.17: Compression index results for Kt and Kt-PAM under varying (a) pH levels and (b) ionic concentrations 103
FIG 5.18: Recompression index results for Kt and Kt-PAM under varying (a) pH levels and (b) ionic concentrations 104
FIG 5.19: Void ratio and shear wave velocity curves showing the effects of pH for (a) Mt samples and (b) Mt-PAM samples 106
FIG 5.20: Void ratio and shear wave velocity curves showing the effects of ionic concentration for (a) Mt samples and (b) Mt-PAM samples 107

FIG 5.21: Change in void ratio from start of test to maximum loading of 87 kPa for Mt and Mt-PAM under varying (a) pH levels and (b) ionic concentrations..... 110
FIG 5.22: Shear wave velocities measured at the initial load of 15 kPa and maximum load of 87 kPa for Mt and Mt-PAM under varying (a) pH levels and (b) ionic concentrations 112
FIG 5.23: Coefficient of consolidation results for Mt and Mt-PAM under varying (a) pH levels and (b) ionic concentrations 113
FIG 5.24: Compression index results for Mt and Mt-PAM under varying (a) pH levels and (b) ionic concentrations 115
FIG 5.25: Recompression index results for Mt and Mt-PAM under varying (a) pH levels and (b) ionic concentrations 116

CHAPTER 1: INTRODUCTION

There are many different types of clay that exist throughout the world, and many are characterized by undesirable engineering properties related to compressibility and shear strength. Many geotechnical projects would benefit from improving the response of these clays. A few examples of clay improvement techniques involve replacement of the clay, solidification, reinforcement of the clay, and others (Rajasekaran and Narasimha Rao 1997). However, these methods are solely focused on a "static" solution, where the modified clay is not "responsive" to changing environments. For example, karst topography gives rise to such a changing environment as the pH of the groundwater changes with the dissolution of limestone.

1.1 Motivation

Creating a "responsive" clay is the next step in the development of clay-polymer composites. At the fundamental level, the fabric of fine-grained soils can have great influence on the macro-scale behavior of the clay, as it can affect the permeability, strength, compressibility, water retention, etc. (Mitchell and Soga 2005; Palomino and Santamarina 2005). For example, soils with flocculated fabric tend to have higher shear strength than those with dispersed fabric (Mitchell and Soga 2005). The development of the specific clay-polymer composites used in this study was motivated by the idea of creating a geomaterial that could be modified over time by adjusting its fabric, namely in the form of controlling interparticle and interlayer

spacings. Therefore, the composites that are used in this study are "responsive" to changes in the external environment, as will be described subsequently.

Prior research into the development of these clay-polymer composites has been conducted, and synthesis techniques have been optimized for creating these materials (Kim and Palomino 2009; Kim and Palomino 2011). Also, the fundamental characterization of the interaction at the polymer-mineral interface has been completed (Kim et al. 2012). Thus, the scope of this project is not to develop methods for creating clay-polymer composites, but to investigate their behaviors at the meso-scale level through laboratory bench-scale testing.

1.2 Objectives

The objectives of this study can be summarized as follows:

(1) Perform testing and analysis on clay-polymer composites to determine the shear strength of these materials

(2) Perform testing and analysis on clay-polymer composites to determine the compressibility of these materials

(3) Use bender elements to characterize the stiffness of these materials throughout a typical 1D consolidation test

(4) Compare composites made of two different clay minerals to determine if the polymers used in this study affect these materials differently

(5) Link known micro-scale particle and particle-polymer response to observations made through bench-scale testing, and determine if the known responses translate into analogous meso-scale behaviors

1.3 Hypotheses

Both the polymer alone and the clay-polymer composite at the micro scale have previously been shown to respond to external stimuli (pore fluid pH and ionic concentration changes). It is hypothesized that the clay-polymer composite at high solids content will respond analogously to different pore fluid conditions. In other words, the composite will maintain its "tunability" at the meso-scale. The purpose of this study is to determine how the shear strength and compressibility parameters are affected when these responsive clay-polymer composites are subjected to differing pore fluid chemistry. Therefore, specific hypotheses are given for these engineering properties:

(1) The behavior of the tunable clay-polymer composites will follow the known micro-scale observations. In other words, these composites will maintain their "tunability" at the meso-scale.

(2) The shear strength of the composites is expected to be higher than that of the clay minerals alone. Polymers are used in many types of engineering applications to increase the strength of a given material, and the same response is expected in this study.

(3) The compressibility of the composites is also expected to be different than that of the clay minerals alone. However, the compressibility of these specific composites is unknown based on current literature. Therefore, it is unclear in which ways the compressibility of the composites will change versus that of the clay minerals alone.

1.4 Expected Contributions

Clay-polymer composites have many practical geotechnical applications such as use in landfill liners, karst mitigation, chemical spill control, etc. (Razakamanantsoa et al. 2012). These materials could be more desirable than traditional clays used in these situations because they are "responsive." While the micro-scale behavior of these materials have been shown through prior research (Kim and Palomino 2009; Kim and Palomino 2011), the meso-scale laboratory testing, such as compressibility and shear strength, has not been performed. Thus, the scope of this project is to investigate some of these engineering properties of these materials, including properties obtained through 1D consolidation testing and direct shear testing.

CHAPTER 2: LITERATURE REVIEW

Much can be learned about the nature of clays, standard methods for which to test these materials, and the nature of polymers and composites. This chapter aims to present an overview of the fundamental concepts addressed in this research. This knowledge will provide the basis of understanding results and observations. Topics discussed in this chapter include an overview of: (1) montmorillonite; (2) kaolinite; (3) clay surface properties; (4) responsive polymers; (5) "tunable" clay-polymer composites; (6) shear strength of clays; and (7) compressibility of clays.

2.1 Montmorillonite

Montmorillonite is a member of the smectite mineral group and has a structure similar to that of the mineral pyrophillite. It consists of one octahedral sheet that is bonded on either side by silica tetrahedral sheets, which is known as a 2:1 layered phyllosilicate crystalline structure (Mitchell and Soga 2005; Newman 1987). This structure is formed by long lines of covalent bonds, where the apical oxygens from the tetrahedral sheets form the vertices of the octahedral sheet (Meunier 2005). In the tetrahedral sheet, trivalent Al can replace a portion of the tetravalent Si. In the octahedral sheet, trivalent Al can also sometimes be replaced by divalent cations such as Mg, but Cr, Fe, Li, and Zn can also serve as replacements (van Olphen 1977). Because of these occurrences, montmorillonitic minerals are quite different from pyrophillite, as there can be a wide range of isomorphous substitution in the

tetrahedral and octahedral sheets. This isomorphous substitution leads to an unbalanced state such that the layers within montmorillonite particles carry a net negative charge (Newman 1987). Depending upon the amount of water that penetrates between the layers, the basal spacing can vary a significant amount: from around 9 Å to complete separation, as shown in Figure 2.1 (Brown and Nadeau 1984; Mitchell and Soga 2005).

The structural formula of a typical montmorillonite with a cation exchange capacity of 70 meq per 100 g can be represented by:

$$\underset{\text{(tetrahedral)}}{[(Si_{3.88}Al_{0.12})^{IV}} \quad \underset{\text{(octahedral)}}{(Al_{1.64}Fe^{3}_{0.05}\,Mg_{0.36})^{VI}}\; O_{10}(OH)_2]_2 \; M_{0.67}$$

where M represents a monovalent exchangeable cation. The superscripts IV and VI refer to tetrahedral and octahedral coordination, respectively (Brown and Nadeau 1984; van Olphen 1977). The layers of montmorillonite particles are bonded together by relatively weak van der Waals forces and cations that balance the net negative charges of the structure. Because these bonds are weak, they can be separated easily through water adsorption or cleavage, thus leading montmorillonite to exhibit swelling behavior (Mitchell and Soga 2005; Newman 1987).

Montmorillonite's swelling behavior is influenced by its relatively large surface area compared to other clays (700 – 800 m^2/g) and the fact that most of the charge balancing cations are found within the crystal structure (Giannelis et al. 1999; Theng 1979). Within the interlayer space, the swelling behavior can be attributed to the ability of the counterions to keep their polar molecule shell behavior; however,

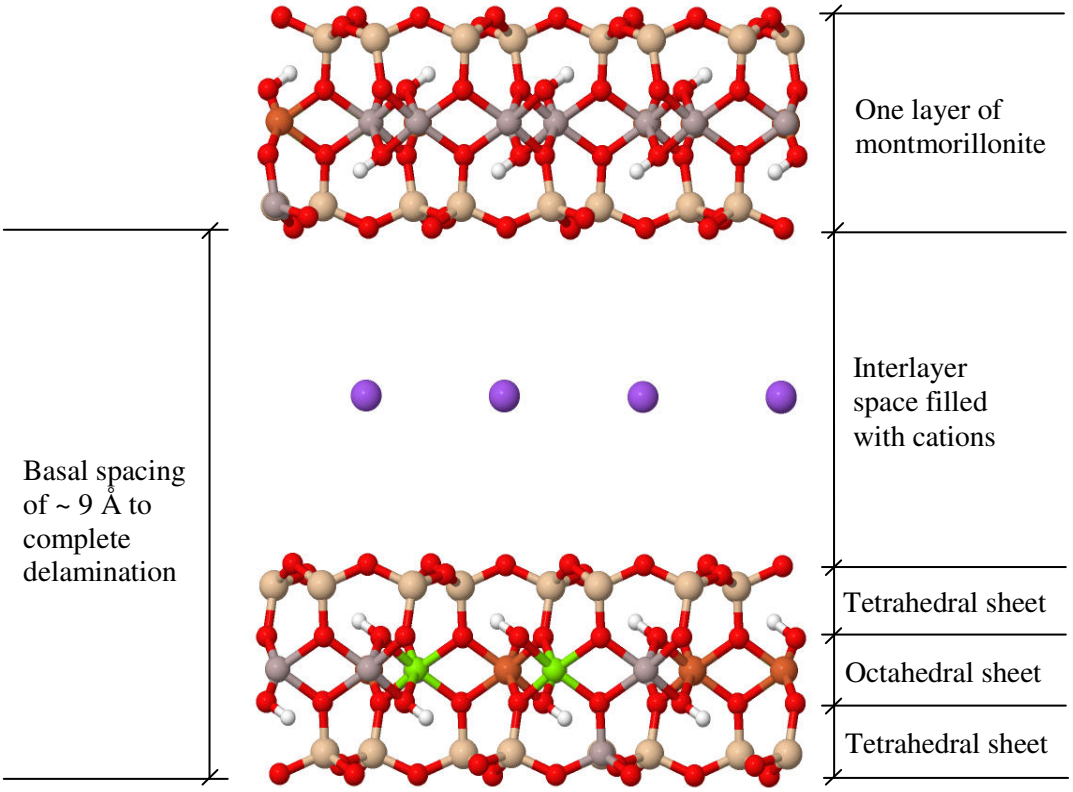


FIG. 2.1: Mineral composition of dry montmorillonite (Barak and Nater 2003)

swelling will not occur under the conditions of a high or zero layer charge (Meunier 2005). This swelling behavior of montmorillonite can be explained by different viewpoints. In one viewpoint, the interlayer cations become hydrated, which leads to a higher hydration energy than the weaker van der Waals forces exhibited between the layers of the particles. With this higher hydration energy, the hydration of the interlayer cations is preferred, and the layer attraction is overcome. In another viewpoint, the water that penetrates the layers does not hydrate the counterions but instead absorbs onto the oxygen termination sites by establishing strong hydrogen bonds (van Olphen 1977).

The amount of swelling between the layers can also vary based upon which cations occupy the interlayer spaces. Montmorillonite that is saturated with monovalent cations such as Li^+ and Na^+ may intercalate as much as four sheets of water molecules, which can lead to basal spacings from about 9.5 Å to 22.5 Å, or further, a complete delamination of the particle into individual layers. However, montmorillonite that is saturated with divalent cations such as Ca^{2+} or Mg^{2+} does not swell to a basal spacing larger than 19 Å (Berend et al. 1995; Chang et al. 1995; Douillard et al. 2007; Theng 1979; Whitley and Smith 2004). Montmorillonite that is saturated with monovalent cations will swell to higher levels versus a montmorillonite saturated with polyvalent cations because the electrostatic attraction that exists between the silicate layers and the cation will be offset by the ion hydration's repulsive effect (Luckham and Rossi 1999).

2.2 Kaolinite

Kaolinite is a member of the kaolinite-serpentine mineral group and has a much different layer structure than that of montmorillonite. Kaolinite consists of one silica tetrahedral sheet that is bonded with one aluminum octahedral sheet, resulting in a 1:1 crystalline structure, shown in Figure 2.2 (Meunier 2005; Mitchell and Soga 2005; Rao et al. 2011; van Olphen 1977). Like montmorillonite, it is a plate-like mineral and has basal planes made up of Al-OH sites contained on the octahedral sheet and of Si-O sites contained on the tetrahedral sheet. In the mineral structure,

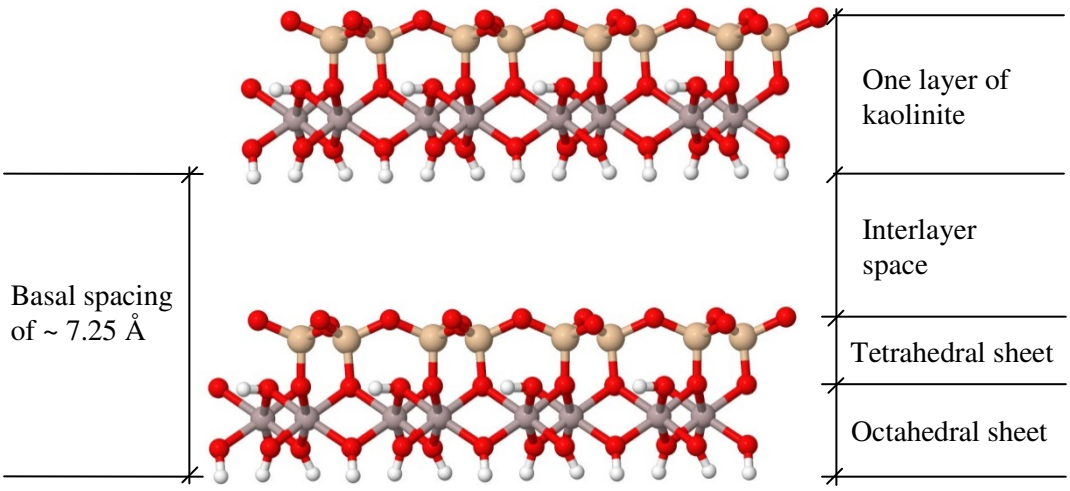


FIG. 2.2: Mineral composition of dry kaolinite (Barak and Nater 2003)

the adjacent layer positions are determined by the required pairing of the oxygens from the basal tetrahedral sheet with the hydroxyls from the next layer's octahedral sheet. This forms a long row of hydrogen bonds, with approximately 3 Å separating the anion centers, which bond the layers together. The basal spacing of kaolinite is composed of the combined thicknesses of the tetrahedral and octahedral sheets and the aforementioned 3 Å interlayer spacing. The theoretical thickness of the combined sheets is 4.26 Å, making the basal spacing around 7.25 Å (Bailey 1993; Brindley and Brown 1980; Meunier 2005; Rao et al. 2011).

The structural formula of an ideal kaolinite can be represented by:

$$Al_4Si_4O_{10}(OH)_8$$

which represents a well-packed mineral structure (Brindley and Brown 1980; Mitchell and Soga 2005). Because of this well-packed structure and the hydrogen bonding between the layers, kaolinite particles do not break down easily, and the

layers are hard to separate. Because of these occurrences, only a very small amount of sorption activity can take place within the internal structure of the particles (Miranda-Trevino and Coles 2003).

Kaolinite particles possess a net negative charge that could be attributed to 3 possible explanations: 1) substitution for Si^{4+} by Al^{3+} in the tetrahedral sheet or for Al^{3+} by a divalent cation in the octahedral sheet, 2) kaolinite particles are only finite in length; therefore, exchangeable cations are attracted to these broken edges, and 3) the hydrogen of these exposed hydroxyls on broken particles may be exchanged by other cations. The cation exchange capacity of the kaolinite minerals is also quite low and usually measures to around 1-15 meq per 100 g. Kaolinite particles experience this quite low cation exchange capacity because of their extremely small degree of isomorphous substitution. Furthermore, kaolinite particles do not allow water molecules to penetrate between the layers because of the strong hydrogen bonding between the layers, meaning that kaolinite does not exhibit swelling behavior (Grim 1968; Miranda-Trevino and Coles 2003; Mitchell and Soga 2005; van Olphen 1977).

2.3 Clay Surface Properties

It is also necessary to discuss general clay mineral surface properties, in order to properly understand the fundamentals of the material behavior. To begin, clay mineral particles tend to interact with one another due to their diffuse double layer. Clay particles contain a surface charge, and nature favors equilibrium and neutrality.

Therefore, this surface charge must be compensated with absorbed counterions in order for the sum of the charges in the system to be equal to zero (Sposito 1989). This double layer consists of the negative surface charge of the clay particle and the area around the particle that contains balancing cations, which help to neutralize the surface charge (Mitchell and Soga 2005; Theng 1979; van Olphen 1977). The basis of this idea was developed as the Gouy-Chapman and Stern model and is shown visually in Figure 2.3. As shown, cations are attracted to the surface of the negatively charged clay particle, but at the same time tend to diffuse away from the surface into the bulk electrolyte of the solution (van Olphen 1977). The Stern layer consists of cations that are attracted to the surface of the particle. These cations form inner

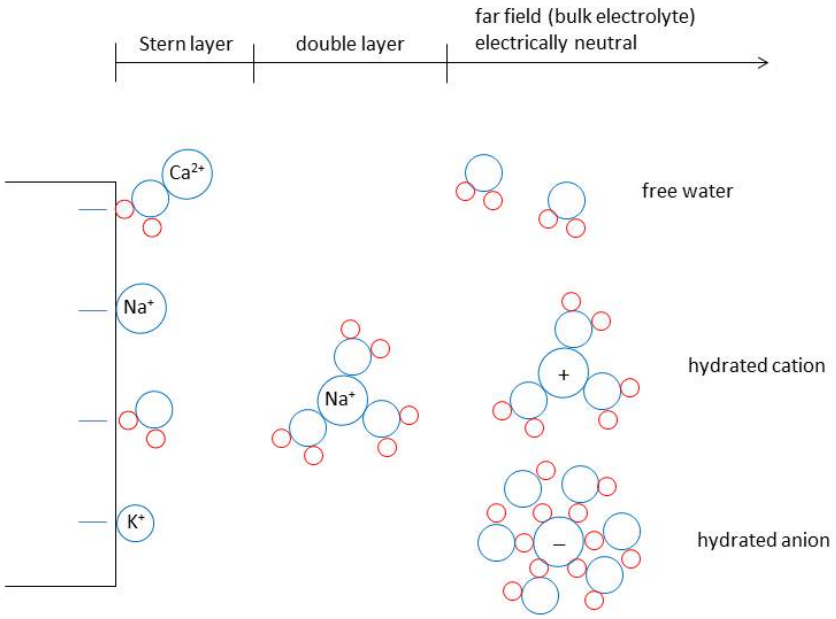


FIG. 2.3: Representation of a clay particle and the resulting formation of the diffuse double layer (after Mitchell and Soga 2005; Santamarina et al. 2001; Stumm 1992)

sphere complexes, where there are no water molecules that separate the cation from the clay particle. Further away from the clay particle in the double layer, cations form outer sphere complexes as shown, where the ion is completely surrounded by water molecules (Santamarina et al. 2001).

When two clay particles' double layers approach each other, there is interference between the two. This leads to a redistribution of the counterions in each of these layers, which requires energy. This energy required to move these cations around is represented as a repulsion force between the two double layers (van Olphen 1977).

As shown in the stern layer from Figure 2.3, counterions are attracted to the negatively charged surface of clay particles. Many of these cations are exchangeable and are easily replaced by other cations in the double layer. The number of these exchangeable charges is known as the cation exchange capacity (CEC) and is denoted in milliequivalents/100g (Mitchell and Soga 2005; van Olphen 1977). Another electrical property that builds upon this concept is called the surface charge density and is defined as the cation exchange capacity per specific surface area, or CEC/Sa (Shang et al. 1994). The specific surface area (Sa) is represented by the surface area of a clay particle per its mass. Typical values for these properties are shown in Table 2.1.

TABLE 2.1: Typical values of cation exchange capacity (CEC), specific surface (Sa), and surface charge density (σ_0) for clays of interest (Mitchell and Soga 2005; Shang et al. 1994)

Clay Mineral	CEC (meq/100g)	Sa (m^2/g)	σ_0 (C/m^2)
Kaolinite	5	15	0.32
Na-montmorillonite	100	800	0.12

2.4 Responsive Polymers

Polymers are made up of chains of monomers, which combine to form large molecules called macromolecules (Painter and Coleman 1997). The use of responsive polymers in clay systems is a unique and developing solution for soil improvement techniques. A polymer is deemed "responsive" when its conformation changes based on environmental triggers. These triggers can consist of many different factors, including but not limited to: temperature, pH level, ionic concentration, and electrical potential (Gudeman and Peppas 1995; Kim et al. 2006; Park and Hoffman 1992). "Conformation" is defined as the polymer molecule orientation, as in a coiled or extended orientation.

The polymer used in this study is called polyacrylamide (PAM), which is a responsive polymer due to the interactions between its amide functional groups and the environment. This is shown schematically in Figure 2.4, with its amide functional groups highlighted. It is a widely used, water-soluble polymer that has current applications in areas such as agriculture, water treatment, oil wells, erosion control, and others (Kulicke et al. 1982; Kurenkov 1997; Ranjbar and Schaffie 2000). It is a

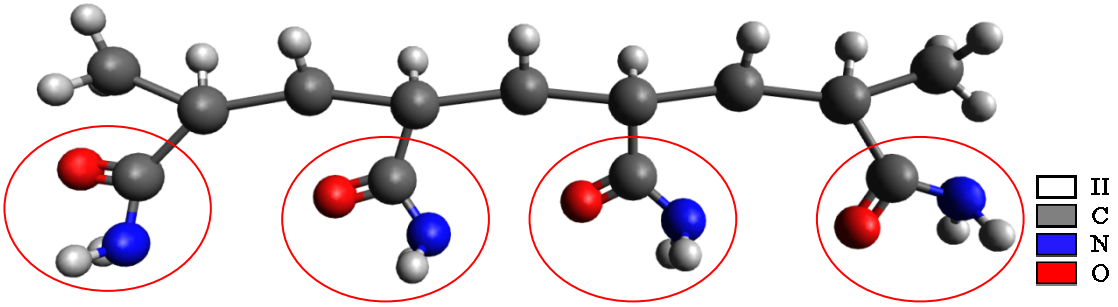


FIG. 2.4: Schematic of PAM polymer molecule highlighting its amide functional groups (image created using Avogadro Molecule Editor 2012)

white, odorless polymer that is also non-toxic (Brandrup and Immergut 1989). The chemical formula of polyacrylamide is denoted as $(C_3H_5NO)_n$ (Maltesh et al. 1991).

The conformation of PAM in the bulk solution is affected by two environmental triggers: pH level and ionic concentration. The polymer conformation simply refers to its physical behavior in its environment. For example, at low pH and/or high ionic concentration, PAM exhibits a "coiled" conformation. At high pH and/or low ionic concentration, PAM exhibits an "extended" conformation. These concepts are shown in Figure 2.5.

pH will first be considered to highlight the changes in the conformation of the polymer. In a low pH condition, there is a high concentration of H^+ ions in the bulk solution. As these ions surround the polymer molecule, the amide groups tend to remain undissociated as shown in Figure 2.6a. Because the excess H^+ ions in the solution do not initiate any chemical changes to the molecule, a low pH condition results in a neutrality or slight attraction within the polymer chain as the amide groups are not negatively charged and, thus, do not repulse each other. Due to the

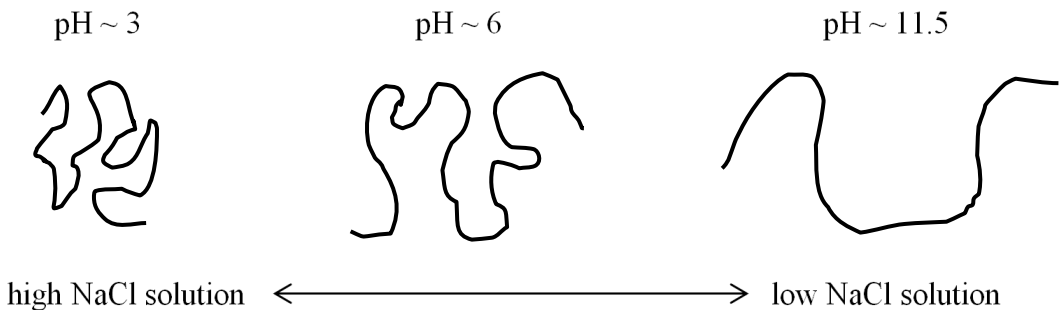


FIG. 2.5: Conformation of polyacrylamide due to pH and ionic concentration (after Kim and Palomino 2011)

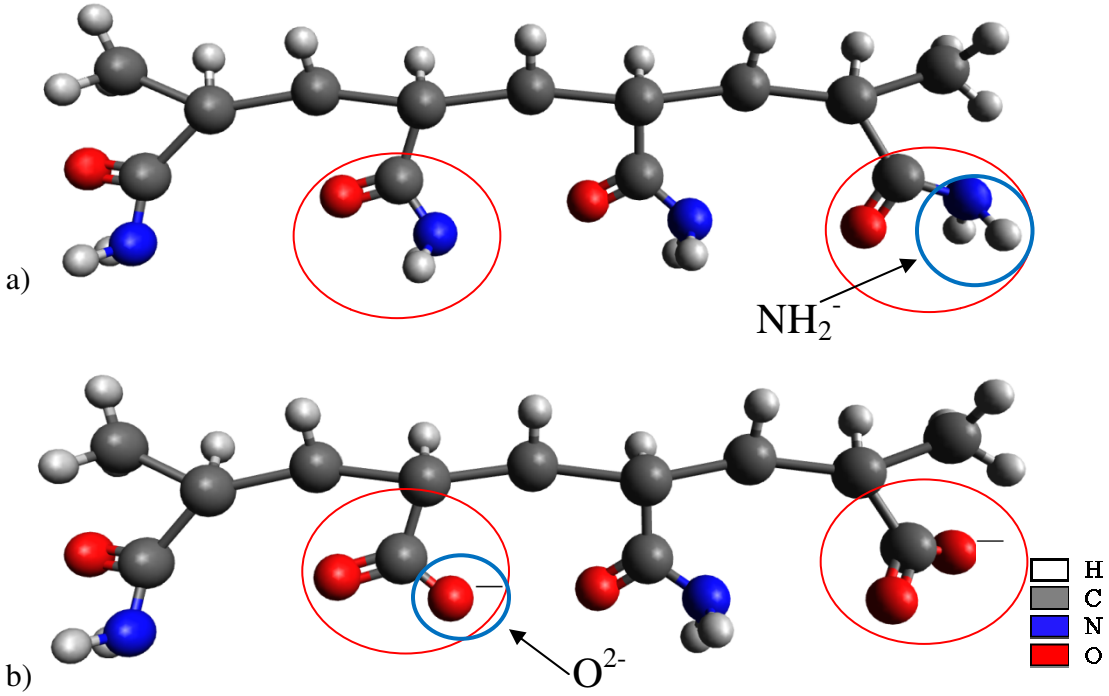


FIG. 2.6: PAM molecules showing highlighted a) undissociated amide groups, and b) dissociated amide groups; red circles highlight the amide functional groups and blue circles highlight the dissociating NH_2- and O^{2-} groups (images created using Avogadro Molecule Editor 2012)

lack of repulsion/slight attraction along the molecule, the molecule adopts a more compact and coiled structure. However, a high pH condition results in a high concentration of OH^- ions in the bulk solution. In this environment, the hydroxyls react with the NH_2^- groups from the amide groups of the polymer according to the following reaction:

$$OH^- + NH_2^- \rightarrow NH_3 + O^{2-} \quad (2.1)$$

The H^+ ions from the hydroxyls bind with the NH_{2-} groups to form the neutral NH_3 in the bulk solution. This reaction leaves the remaining O^{2-} ions to bind to the available site on the polymer chain. Therefore, the polymer's amide groups are then left with a net negative charge at the amide group locations ($O^{2-} > NH_2^-$). This process leaves the PAM molecule with an excess of electrically negative amide groups that will repulse each other, thus forcing an extended conformation along the molecule (Besra et al. 2002; Maltesh et al. 1991).

Figure 2.5 also highlights the changes that ionic concentration can have on the conformation of PAM. This polymer adopts an extended conformation at low ionic concentrations (< 0.005 mol/L NaCl) and a coiled conformation at higher ionic concentrations (> 0.05 mol/L NaCl). This is due to the amount of salt ions in the solution, as salt ions tend to neutralize negatively charged amide groups on the polymer chain. When the negative charges on the amide groups are neutralized by salt ions at higher ionic concentrations, the polymer does not repulse itself and tends to take on a coiled conformation. The opposite is true at low ionic concentrations, as the negative charges on the amide group are not neutralized. Thus, PAM exhibits an

extended conformation under low ionic concentration conditions (Klenina and Lebedeva 1983; Kurenkov 1997).

2.5 "Tunable" Clay-Polymer Composites

Since many in-situ clays, as well as samples prepared in this study, will contain fluid in the pore spaces of the soil, this discussion will focus on the adsorption of polymers onto clay surfaces in aqueous solutions.

Polymers can adsorb onto the surface of a clay mineral through different mechanisms including electrostatic attraction, van der Waals forces, and hydrogen bonding. Such factors that can influence polymer adsorption include the type of polymer, temperature, molecular weight of polymer, and the overall nature of the solvent. Because the adsorption of a polymer can also affect the surface properties of the clay, the surface charge and interparticle forces will be affected as well (Theng 1979; van Olphen 1977). The specific type of polymer can have great influence on this absorption, based on whether the polymer has a nonionic, anionic, or cationic charge in its natural state (Deng et al. 2006; Laird 1997; Theng 1982).

A polymer molecule may have a random orientation in an aqueous solution. However, the adsorption of that molecule onto a clay surface leads to conformational changes. As the polymer is adsorbed, it will adopt a more extended conformation at the surface of the mineral, with tails and loops extending out from the particle (Theng 1982). Studies on the polymer of interest, PAM, have shown that this absorption is also irreversible (Gao and Heimann 1993; Stutzmann and Siffert 1977). Flocculation

of clay particles due to this adsorption can occur through different mechanisms including polymer bridging, the formation and depletion flocculation of the polymer-particle surface complex, charge compensation (neutralization), or any combination of these mechanisms. For a polymer with a nonionic charge, polymer bridging and charge compensation are the primary mechanisms found to occur (Gregory 1988; Mpofu et al. 2003). For a polymer with a cationic charge, electrostatic interactions (specifically Coulombic attraction) are the cause of the charge compensation mechanism between the negatively charged clay mineral surface, and the positively charged polymer (Theng 1982; van Olphen 1977).

When a clay is subjected to an aqueous polymer solution, there are three main types of clay-polymer composites that can be formed: phase-separated, intercalated, and exfoliated structures (Alexandre and Dubois 2000; Giannelis et al. 1999). Shown in Figure 2.7, the phase-separated structure consists of clay particles (shown by blue lines) with resulting polymer (shown by irregular lines) adsorption surrounding the

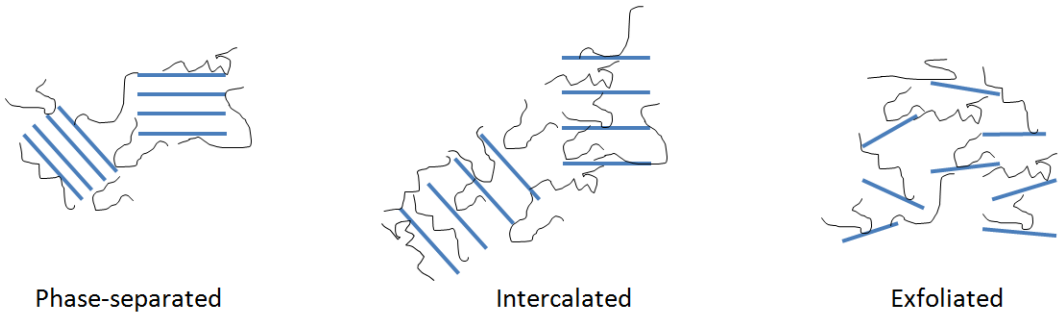


FIG. 2.7: Three formation types of clay-polymer composites (after Kim and Palomino 2011)

particles. These structures are referred to as "microcomposites," and there is no penetration of polymer into the interlayer spaces. In this study, microcomposites are formed with the clay mineral kaolinite, as the strong hydrogen bonds between the layers do not allow for this polymer adsorption within the particles (Kim and Palomino 2009). In the intercalated structure, however, the polymers can also absorb in the interlayer spacings as well as surrounding the clay particle. These composites are referred to as "nanocomposites," and are formed when montmorillonite is used. Because montmorillonite has weakly bonded layers, the counterions in the interlayer spaces are exchanged for polymer adsorption (Kim and Palomino 2011). The final type of composite, exfoliated, is formed when the clay particles completely separate and are thus completely surrounded with polymers. This type of structure normally occurs with high polymer contents (Fu and Qutubuddin 2001).

The individual behaviors of clay and PAM both affect the overall behavior of a clay-polymer composite. The specific results of using these materials in this study

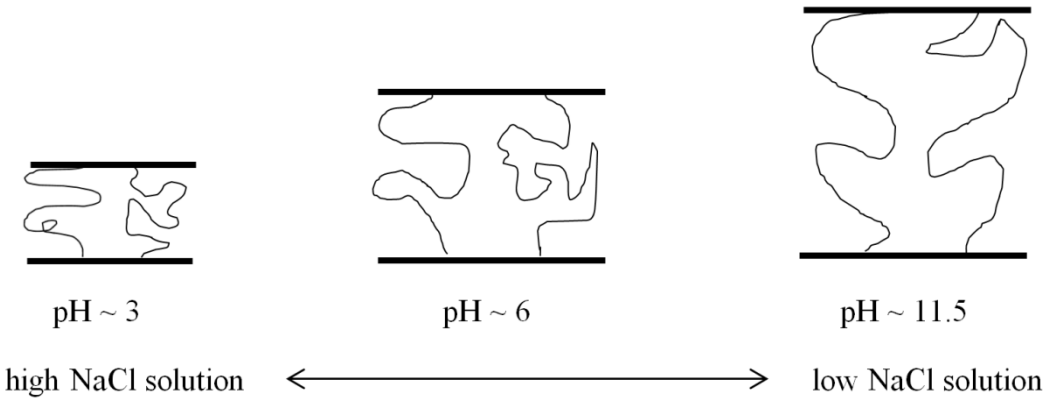


FIG. 2.8: Behavior of clay-polymer composite due to different pH and ionic concentration conditions (after Kim and Palomino 2011)

are shown in Figure 2.8. The composite schematics show the relationship between clay particles and PAM molecules. The figure shows how the interparticle spacing changes in the clay-polymer composite due to changing pore fluid conditions. The interlayer thickness is affected at the micro-level due to the change in conformation of the polymers. This fundamental behavior at the particle level has been shown through prior research (Kim and Palomino 2009; Kim and Palomino 2011). **The purpose of this study is to investigate the meso-scale behavior of the developed clay-polymer composites and determine if the "tunability" of these composites is observed at the meso-scale using laboratory testing.**

2.6 Previous Studies

The effects of polymers on the shear strength and compressibility of clays have been explored in similar ways. In one study, exopolymers were added to samples of kaolinite, and the shear strength and compressibility were compared to control samples (Nugent 2011). Exopolymers are different than the PAM used in this study, as they are biopolymers that are much larger in size. This study concluded that the shear strength of kaolinite could be increased depending on the concentration and type of exopolymer that was used. Also, the compressibility was shown to either increase or decrease depending on the concentration and type of exopolymer that was used. These tests confirmed that the clay's engineering properties could be changed with the addition of exopolymers. However, these polymers are much different in

size and behavior than PAM. Thus, this study will focus on the same concept, but with different polymers that exhibit a "responsive" behavior.

Additional studies have also already determined specific behaviors of PAM, kaolinite-PAM micro-composites, and montmorillonite-PAM nano-composites. This thesis will build upon these predetermined conclusions, so a discussion of these findings follows.

In one study, kaolinite-PAM composites were created in order to determine how the fabric of the material is affected by different variables (Kim and Palomino 2009). A wide variation of variables as related to the polymer was considered, such as polymer charge type, molecular weight, and concentration. Nonionic and cationic PAM were used to highlight charge type, while high molecular weight and low molecular weight PAM were used to highlight the impact of different chain lengths. The PAM concentrations also ranged from 20 mg/L to 500 mg/L, in order to determine at optimum composite mixture. Test methods included viscosity measurements, sedimentation tests, and liquid limit tests. Results showed that the composite floc density and sizes tended to increase with higher PAM concentrations, but composites with a higher molecular mass PAM tended to have a more open flocculated fabric. Also, the polymer charge was shown to only impact the composite fabric above a specific polymer concentration. This study showed that kaolinite-PAM fabric formation could be altered by using different combinations of variables.

In addition, another study evaluated similar parameters and developed a procedure to optimize the synthesis of montmorillonite-PAM composites (Kim and

Palomino 2011). As before, polymer molecular weight and concentration were considered, but the solution intercalation technique was also analyzed to determine the most appropriate method for composite synthesis. Several variables for optimizing the solution intercalation technique were considered including clay content, mixing temperature, drying temperature, polymer concentration, and polymer molecular weight. An optimized solution intercalation technique was developed, in which mixing and drying temperatures above room temperature were insignificant to composite synthesis. This was an important finding, in that excess energy in the form of high temperatures are unnecessary for the formation of clay-polymer composites at a large scale.

Finally, studies were also performed to understand if the conformation of PAM molecules in aqueous solution was also expected when the polymers were adsorbed onto the composite structure. In studies using dissipative particle dynamics (DPD) and spectroscopic ellipsometry, polymer interactions were studied in aqueous solutions, on clay surfaces, and between two clay surfaces (Kim et al. 2012; Kim et al. 2012). Through comparison of these different scenarios, it was determined that polymers exhibited extended conformation at high pH, and coiled conformation at low pH, irrespective of which scenario was considered. These studies showed that the changing conformation of PAM in aqueous solutions was also seen when bonded to a clay surface, as well as between two clay surfaces. This research showed that the micro-scale properties of polymers influenced the micro-scale properties of clay-

polymer composites. However, it is still not known if these properties translate to meso-scale composite specimens.

2.7 Shear Strength of Clays

With an understanding of the concepts that describe behaviors of clays and polymers, the engineering properties of these materials can be analyzed. There are many ways to analyze engineering properties in the clays kaolinite and montmorillonite, such as Atterberg limits, hydraulic conductivity, shear strength, compressibility, swelling and shrinkage, and time-dependent behavior (Mitchell and Soga 2005). Many of these properties describe strength and water interactions of these materials, but of great importance in this study is that of shear strength.

The shear strength of a soil refers to the ability of its particles to resist sliding laterally past one another upon application of an applied shear stress (Lambe and Whitman 1969). Because the shear strength of a soil is determined by its ability to withstand the forces of an applied load, this fundamental engineering property is very important in foundation design, lateral earth pressure calculations, slope stability analysis, slurry trenches, and other geotechnical problems (Fox 2004; Liu and Evett 2004; McCarthy 2002). Shear strength is also of great importance when clays or clay-polymer composites are used as a landfill liner. Adding certain liquids to soils, a practice usually performed under pressure to increase the moisture distribution in municipal solid waste landfills, can potentially negatively affect the slope stability due to the increase in the pore water pressure (and decrease of shear strength) of the

landfill materials (Xu et al. 2012). Because the shear strength of a soil has so many applications in geotechnical engineering, it is important to understand how to characterize and measure this engineering property.

There are multiple methods to test and analyze the shear strength of a soil, including laboratory methods and in-situ methods. Laboratory methods include the (1) unconfined compression test, (2) direct shear test, and (3) triaxial compression test. The unconfined compression test can be used to investigate fine-grained soils, whereas the direct shear test and the triaxial compression test can be used to investigate both fine-grained and coarse-grained soils. In these test methods, the equation that describes the relationship of the soil's shear strength to other factors is as follows:

$$\tau = \sigma \tan(\phi) + c \tag{2.1}$$

where τ is the shear strength, σ is the normal stress applied, □ is the angle of internal friction, and c is the cohesion between the particles. This equation is known as Mohr-Coulomb, and it shows that as the angle of internal friction within the material increases, so does the shear strength of the specimen (White et al. 1992).

There are different mechanisms that contribute to shear strength in montmorillonite and kaolinite, respectively. For low overburden pressures such as near the surface, the shear behavior of kaolinite and montmorillonite is dependent primarily on two things: the anisotropy of the clay particles as well as their net negative charge. The intergranular friction of the particles is the mechanism that primarily contributes to kaolinite's relatively higher shear strength, whereas

montmorillonite's shear strength is determined more from the actual electrical forces that hold the layers together (Müller-Vonmoos and Løken 1989). Also, because montmorillonite contains much more water at its different limit states (plastic, liquid), the interactions between the soil and water particles greatly influence its capability to resist shear forces. For example, in undrained conditions, kaolinite's strength is attributed to the specific type of particle arrangement as determined by the interparticle forces, whereas montmorillonite's strength is determined by the viscous shear resistance that is developed within the double-layer water (Sridharan and Prakash 1999). Whereas kaolinite contains less water than montmorillonite at its liquid and plastic limits, the effect of particle arrangement and interparticle forces is more heavily influenced. These fundamental differences in clay mineralogy have distinct implications for how the soil behaves with respect to shear strength.

In regards to shear strength, polymers can also be used to improve this engineering property for many materials. For example, the use of fiber reinforced polymer (FRP) materials in fields such as the precast concrete industry can lead to an increase in strength of structural members when used as a shear transfer mechanism for thermally efficient composite and partially-composite load bearing walls, flange reinforcement for double tee members, as reinforcement for precast architectural cladding panels, etc. (Rizkalla et al. 2012). In shear walls materials such as Carbon Fiber Polymers (CFRP) can be used to increase elastic stiffness, overall strength values, and shear capacity, which leads to an increase in stress distribution over the surface of walls (Hatami et al. 2012). Polymers are already used in structural

applications, but they are also utilized in the field of soil mechanics. It has been shown that increased shear strength can be realized through soil-polymer interactions, as compared to the shear strength of the soil itself. In tests involving sands and polymer interfaces, sands that were in contact with geomembranes, plastic piping, soil strip reinforcement, and other soil-polymer systems showed an increase in frictional strength (O'Rourke et al. 1990). The use of polypropylene fiber in backfill soils for reinforced walls has also been shown to increase its soil strength and stability (Park and Tan 2005). In addition, polymers are often used in the form of slurry walls, where the addition of the polymer during drilling increases the shear strength of the material around the wall (Day et al. 1999). However, this engineering property is currently being explored for the "tunable" clay-polymer composite materials investigated here. This presents a gap in current research that this study aims to fill.

Finally, shear strength in a soil can be affected by other factors as well. In particular, the shear strength is influenced by the ionic concentration levels and the pH of the pore fluid in the clays. The ionic concentration of the pore fluid has different effects for both kaolinitic and montmorillonitic soils. The primary source of interaction in kaolinitic soils is from net interparticle attractive forces, while in montmorillonitic soils this interaction is from the viscous nature of the double layer water (Müller-Vonmoos and Løken 1989). For kaolinitic soils, increases in salt concentration increases the undrained shear strength at any moisture content. However, the opposite is true for montmorillonitic soils. As salt concentration

decreases, the undrained strength increases at any moisture content. This is attributed to the expansion of the diffuse double-layer thickness, thus resulting in a higher viscous resistance and higher undrained shear strength (Sridharan et al. 2002).

Clays may also be exposed to environmental acidic or basic conditions, and changes in shear strength can occur with these changing conditions. The pore water pH of a clay is a determining factor for both the chemical and physical properties of a soil, as varying pH levels can affect the diffuse double layer thickness (Liaki et al. 2008). With regards to pH variations, it has been shown that clays that contain a pore fluid with a high or low pH have a considerable change in their undrained shear resistance (Spagnoli et al. 2012). In tests involving kaolinite, this variation of strengths due to the solution pH was shown to be related to changes in basal surface properties, mostly being attributed to acid-base reactions on the surfaces of the clay particles. This leads to a lower residual friction angle for solutions containing high amounts of hydrochloric acid and a larger residual friction angle for solutions containing high amounts of potassium hydroxide (Wahid et al. 2011). In other tests involving a Na-bentonite that was exposed to a low pH solution, results showed a higher stiffness and residual strength. In contrast, when exposing Na-bentonite to a high pH solution, results showed almost no change in strength at NaOH concentration up to about 0.1M. However, at higher NaOH concentrations, results showed a higher stiffness and residual strength (Gajo and Maines 2007). Thus far, no studies have been conducted on the effects of solution ionic concentration and pH on the shear strength of “tunable” clay-polymer composites.

2.8 Compressibility of Clays

In addition to shear strength, there are many other engineering properties in the field of soil mechanics that can describe the behavior of clays. Compressibility is another measure of a clay's behavior, and it is also of great importance in predicting how it will behave under applied loads. It is well known that when a force or load is applied to a material that it will undergo stress, thus also resulting in strain (Hibbeler 2003). Compressibility, also referred to as consolidation, demonstrates this concept as the time-dependent process by which a soil experiences a simultaneous compression of the actual soil skeleton and expulsion of pore fluid, leading to a change in volume under load, also known as settlement (Shroff and Shah 2003).

There can be several other causes of settlement, such as changes in the groundwater table, dynamic forces, adjacent excavation, etc., but the major cause is due to the compressive deformation of soil resulting from an applied force or loading. The cause of this deformation is usually due to a decrease in void volume, accompanied by a rearrangement of soil grains and compression of the material in the voids of the soil (Liu and Evett 2004). The voids between soil particles can be filled with either air or water, and the behavior of the soil under load depends heavily upon this condition. If it is assumed that the soil is at a saturation level of 100% and that both the water in the voids as well as the soil particles are incompressible, the overall change in volume can only take place if a portion of the water is expulsed from the voids (Ranjan and Rao 2000). This basic theory of compressibility is also related to the permeability of the soil. Soils that are highly permeable, such as coarse-grained

soils, require a relatively short time for settlement to take place as opposed to soils that have a low permeability, such as fine-grained soils, because the water filling the voids can be expelled at a much faster rate in coarser materials (Liu and Evett 2004). Therefore, foundations bearing on coarse-grained soils experience most of the settlement upon application of the load, whereas foundations bearing on fine-grained soils may take months or years to completely settle. For these fine-grained soils, the immediate settlement can be attributed to volume distortion of the sample. However, most of the total settlement extends for a much longer period of time, and is known as consolidation, or primary compression settlement (McCarthy 2002).

Soil compressibility is measured in a specific device called a consolidometer, or oedometer, in which an undisturbed sample, with porous stones inserted above and below the sample, is placed within a cylindrical ring (Liu and Evett 2004). According to ASTM D2435, normal stresses are then applied to the soil in increments that approximately double with each new loading (load increment ratio = 1), and the deformation of the sample with respect to time is recorded. Along with measurements of water content, sample density, height, and specific gravity, the void ratio can be calculated at various stages of loading as shown by

$$e = {}^{V_v}/_{V_s} \tag{2.2}$$

where e is the void ratio, V_v is the volume of the voids in the soil, and V_s is the volume of solids in the soil. This engineering property is normally in the range of about 0.5 for sands to about 4.0 or higher for some clays. The void ratio is a metric that is used to show the volume change of the soil over a period of time, which in turn

relates to the compressibility and loading capacity (Mitchell and Soga 2005). The compressibility is measured through a parameter known as the compression index (C_c), which is determined by taking the slope of the linear portion of data (after the preconsolidation pressure) obtained on the void ratio versus log effective stress plot. This C_c factor helps estimate settlement, which is important for the building of structures on different types of soil.

Mechanisms such as particle size, stress history, pore water chemistry, and others can contribute to soil compressibility in clayey soils. Assuming that the soil grains and pore fluid are incompressible, any changes in the soil volume are related to changes in the void ratio. The soil particle sizes and shapes, which in turn influence the specific surface area of the particles, are the most important factors influencing compressibility in clays. The specific surface area of these soil particles influences the void ratio at any normal stress and also affects the mechanical and physiochemical factors that contribute to consolidation (Meade 1964). There are many factors controlling this resistance to volume change such as: the chemical and organic environment, mineralogical detail, stress history, physical interactions between particles, stress paths of the soil, physicochemical interactions between particles, temperature, soil fabric and structure, and pore water chemistry (Mitchell and Soga 2005). Knowledge of how soils can change volume is important and can help to determine how that soil will behave under a given load.

When comparing kaolinite and montmorillonite, each has notably different mechanisms that contribute to the consolidation of the specific material. The

compressibility in montmorillonite is determined by the effects of the double-layer between the particles, which also determined its shear strength (Chen et al. 2000; Tiwari and Ajmera 2011). In contrast to montmorillonite's compressibility, which is controlled by the double-layer, the compressibility of kaolinitic clays is controlled by the electrical attractive forces and fabric of the soil. Typically, the behavior of montmorillonitic clay is affected most heavily by physicochemical factors, and behavior of kaolin is affected most heavily by mechanical factors such as soil fabric and structure and physical interactions between particles (Di Maio et al. 2002; Mitchell 1960).

In addition to the fundamental compressibility properties of these soils, ionic concentration and pH level can possibly affect how they behave. For kaolinite, increasing ionic concentration of the pore fluid results in decreasing compressibility for the same void ratio. On the other hand, for montmorillonite, increasing ionic concentration of the pore fluid results in increasing compressibility for the same void ratio (Horpibulsuk et al. 2011). The effect of ionic concentration on kaolinitic soils is also different depending on the level of consolidation pressure. At low vertical stress (below 300 kPa), van der Waals attractive forces contribute to the physicochemical effects on compressibility. However, pore fluid composition has virtually no effect on this engineering property at higher vertical stresses, as the mechanical interactions between the particles become more important (Chen et al. 2000; Wahid et al. 2011).

The pH, however, has little effect on the compressibility for kaolinite and montmorillonite. Whereas kaolinite is affected by the ionic concentration of the pore

fluid, the changes to 1-D compressibility are negligible when the sample is saturated with high or low pH pore water solutions (Wahid et al. 2011). Also, based on results from tests on montmorillonite, the pH of the pore fluid from which the soil was sedimented was almost independent of any changes to the consolidation curves (Mesri and Olson 1971).

With information on how the compressibility of these clays is affected by soil type, ionic concentration, and pH, knowledge of how "tunable" clay-polymer composites react under these conditions is also needed. The influence of the polymer interactions with both the clay surface and various pore fluid environments have yet to be investigated. The tests conducted in this research are meant to determine how the compressibility is affected for clay-polymer composites containing polymers that are responsive to pH and ionic concentrations.

Furthermore, the stiffness of the clay-polymer composite materials can be investigated through shear wave velocity measurements. Shear wave velocity can be measured using bender elements, which are made of a piezoceramic crystalline material that can transmit shear waves through a soil specimen (Dyvik and Madshus 1985). A typical test setup includes both a source and receiver bender element on opposite ends of a soil sample. The source bender element converts electrical voltage to mechanical energy as shear waves, while the receiver bender element captures the wave propagation and converts the mechanical energy back to electrical voltage. These bender elements can be used to measure the shear wave velocity of a soil in order to further characterize the engineering properties of the material (Alvarado and

Coop 2012; Lee 2003). This technique will be utilized in this study and will be further described in Chapter 5.

CHAPTER 3: SAMPLE PREPARATION

The purpose of this chapter is to outline the materials used for testing and the procedures used to prepare the specimens. These procedures are followed for the materials of interest in this study. Topics discussed in this chapter include an overview of: (1) materials; (2) Na-kaolinite process; (3) solution intercalation; (4) preconsolidation; and (5) test matrix.

3.1 Materials

3.1.1 Kaolinite

Kaolinite (Kt) was chosen for this study to maintain consistency with previous studies and due to its clay-polymer composite behavior. Because of its strong hydrogen bonding between the layers of its particles, kaolinite-polymer composites form phase-separated structures, in which the polymer molecules are unable to penetrate between the particle layers (Kim and Palomino 2009). Polymer adsorption is limited to the particle faces and edges. Thus, changes in the polymer's conformation can only affect the interparticle spacing of kaolinite-polymer composites, as there is no polymer absorption within the particle layers.

The specific type of kaolinite used in this study is known by the trade name Acti-Min SA-1, which is manufactured by the company Active Minerals International (Gordon, GA). This material is used in soft rubber applications, which consist of computer mouse pads, toilet plungers, floor mats, floor tiles, and various gaskets. Its

composition is nearly the same as pure kaolinite with a small amount of impurities. Its chemical composition is shown in Table 3.1. In previous studies (Kim and Palomino 2009), tests were conducted to determine specific properties of this material, and these results are shown in Table 3.2.

3.1.2 Montmorillonite

Montmorillonite (Mt) is the second clay mineral chosen for this study due to its differing behavior as compared to kaolinite and to maintain consistency with previous work. Since montmorillonite has relatively weak van der Waals forces that bond the particle layers together, it has a high swelling potential. This allows the polymer adsorption to occur not only on the outside of particles, but also within the interlayer spaces (Kim and Palomino 2011). Thus, changes in the polymer's conformation can affect the both the interparticle and interlayer spacing of

TABLE 3.1: Elemental Composition of kaolinite (Supplier data)

Compound	% Composition
SiO_2	45.6%
Al_2O_3	38.4%
Fe_2O_3	0.4%
TiO_2	1.5%
CaO	0.06%
MgO	Trace
K_2O	0.18%
Na_2O	Trace
LOI	13.82%

TABLE 3.2: Properties of the kaolinite used in this study (Kim and Palomino 2009)

Property	Value	Method/Reference
Median particle diameter, D_{50} (μm)	1.68	Particle size distribution test (ASTM D422)
Specific gravity	2.60	Supplier data
Specific surface (m^2/g)	40.37	Modified methylene blue European spot test (Santamarina et al. 2002)
pH (at solids content of 2%)	7.5	Determined with pH meter
Isoelectric point (pH)	2.3	Determined from zeta potential measurements using a PALS zeta potential analyzer (Brookhaven Instruments Co.)
Cationic exchange capacity (cmol/kg)	2.3	Ammonia-electrode method (Borden and Giese 2001)

montmorillonite-polymer composites, as polymer absorption can occur along both surface types.

The specific type of montmorillonite used in this study is known by the trade name Volclay SPV 200, manufactured by the American Colloid Company (Hoffman Estates, IL). Its functional use is as a multi-purpose suspending, emulsifying, and binding agent for industrial applications that require a dry 200 mesh particle size. It is mostly pure, but contains small of amounts of feldspar, calcite, and quartz. It is a dioctrahedral smectite, and its chemical formula is denoted as $(Na,Ca)_{0.33}(Al_{1.67}Mg_{0.33})Si_4O_{10}(OH)_2 \cdot nH_2O$. The elemental composition of this material is shown in Table 3.3. Measurements of selected properties were conducted in a previous study (Kim and Palomino 2011) and are listed in Table 3.4.

TABLE 3.3: Elemental Composition of montmorillonite (Supplier data)

Compound	% Composition
SiO_2	63.02%
Al_2O_3	21.08%
Fe_2O_3	3.25%
FeO	0.35%
MgO	2.67%
Na_2O	2.57%
CaO	0.65%
Trace	0.72%
LOI	5.64%

TABLE 3.4: Properties of the montmorillonite used in this study (Kim and Palomino 2011)

Property	Value	Method/Reference
Median particle diameter, D_{50} (μm)	2.72	Particle size distribution test (ASTM D422)
Specific gravity	2.50	Supplier data
Specific surface (m^2/g)	706	Modified methylene blue European spot test (Santamarina et al. 2002)
pH (at solids content of 2%)	8.5	Determined with pH meter
Isoelectric point (pH)	0.03	Determined from zeta potential measurements using a PALS zeta potential analyzer (Brookhaven Instruments Co.)
Cationic exchange capacity (cmol/kg)	80.8	Ammonia-electrode method (Borden and Giese 2001)

3.1.3 Polyacrylamide

The polymer used to form the composites is a form of polyacrylamide (PAM), as described in Section 2.4. The form of PAM used here is a high molecular weight

(HMW), nonionic type that is manufactured by the company Kemira (Lakeland, FL) and distributed under the brand name of Superfloc N-300. The polymer has a molecular weight of approximately 6 x 10^6 g/mol (Kim and Palomino 2009; Kim and Palomino 2011).

The HMW, nonionic PAM was chosen to maximize the amount of composite formed and to remain consistent with previous studies. First, a nonionic PAM was chosen over a cationic PAM due to their differing effects on the flocculation of the composite. A nonionic PAM was shown to flocculate the composite material more readily than a cationic PAM, thus allowing the composite to form with a lower concentration of PAM (Kim and Palomino 2009). Also, a high molecular weight (HMW) polymer was chosen over a low molecular weight (LMW) polymer for similar reasons. Composites formed with HMW polymer were shown to form larger intercalated structures than those with LMW polymer. This allows for easier penetration of the polymer molecules into the interparticle and interlayer spaces (Kim and Palomino 2011).

3.2 Na-Kaolinite Process

Before samples were prepared and tested, an extra step was taken for the kaolinite specimens in this study. In their natural state, kaolinite may have many different counterions (Na^+, Ca^{2+}, Al^{3+}, etc.) that are bonded to the clay particles, thus making the clay polyionic (Mitchell and Soga 2005). A washing procedure developed by Palomino and Santamarina (2005), was performed based on a concept

from van Olphen (1977) that would render the clay monoionic, with Na^+ being the major counterion in the system. The reason for this process is to reduce variability from one kaolinite specimen to the next. Even though these specimens are mined from the same location, their behavior may change due to differences in their distribution of counterions.

The Na-kaolinite rendering procedure involves taking a sample of dry kaolinite, mixing it with a 2 M NaCl solution, allowing it to settle for 48 hours, and then draining the supernatant. The specimen is then mixed with a 1 M NaCl solution, allowing it to settle for 24 hours, the supernatant is drained, and this step is repeated. Finally, the specimen is mixed with distilled water, allowed to settle for 24 hours, the supernatant is drained, and this process is repeated until the excess salt solution is removed. This point is reached when the supernatant conductivity is less than 100 µS/cm. When this condition occurs, the specimens are oven dried, and then ground with a pestle and mortar to prepare them for testing or composite preparation.

The concept behind this method is to simply flood the clay sample with a large amount of excess Na^+ ions in order to replace most of the counterions on the clay particles. These excess ions will replace most of the existing counterions on the clay surface (Na^+, Ca^{2+}, Al^{3+}, etc.), thus rendering the material monoionic. This process requires between 1-2 months for completion on the kaolinite clay. These procedures were not performed on the montmorillonite clay, however, due to montmorillonite's much lower permeability when compared to kaolinite. With such a low permeability, montmorillonite would take several more months to complete this

process. The time required to complete this process for montmorillonite makes this procedure impractical to perform on this clay.

3.3 Solution Intercalation

There are different methods in which to synthesize clay-polymer composites. Of those methods, they can be divided into three different approaches (Sinha Ray and Okamoto 2003): (1) solution intercalation, (2) in-situ polymerization, and (3) melt intercalation. Solution intercalation is based on the use of a solvent system where the polymer is soluble and the clay particles and/or layers swell. Solution intercalation involves the mixing of polymer and clay solutions, which result in an intercalated structure. In-situ polymerization involves the formation of polymer chains from a liquid monomer solution within the clay pore fluid. This process requires the use of heat, radiation, diffusion of an initiator, or some type of catalyst to promote the reaction. Finally, melt intercalation involves the process of annealing, the mixture of clay and polymer above the melting point of the polymer. This allows for a more thorough mixing of the clay and polymer than the other processes, but is used to improve the polymer's properties by adding the clay mineral, instead of improving properties of the clay by adding the polymer (Kim and Palomino 2011; Sinha Ray and Okamoto 2003; Zeng et al. 2005). The solution intercalation technique was used for this study due to its ease of implementation and significantly lower energy costs. Because this technique does not require added heat, a significant environmental impact can be realized when transferred to the macro-scale. The solution

intercalation process requires 4 main steps: (1) determine mass of clay to use, (2) determine mass of polymer to use, (3) separately mix clay and polymer in distilled water, and (4) mix the two solutions together. All mixing in this process is performed with an Arrow Engineering JR4000 paddle mixer at 350 rpm, shown in Figure 3.1.

The first step in this procedure is to determine the mass of dry clay to use for the specific clay-polymer composite (Kt-PAM or Mt-PAM). In this step, the clay content, which is the volume of clay per volume of total solution, is first determined for each composite. The optimum clay content used for Kt-PAM and Mt-PAM was



FIG. 3.1: Mixer used to prepare the clay-polymer composites

determined from previous studies (Kim and Palomino 2009; Kim and Palomino 2011), and is 0.05 and 0.02, respectively. These values are then used to calculate the mass of clay to use for different volumes of water as given by:

$$mass\ of\ clay = clay\ content \times water\ volume \times G_s \times \frac{1\ g\ water}{1\ mL\ water} \qquad (3.1)$$

For example, using when preparing a sample of Kt-PAM for a 2000 mL solution, the mass of Kt to use is calculated by:

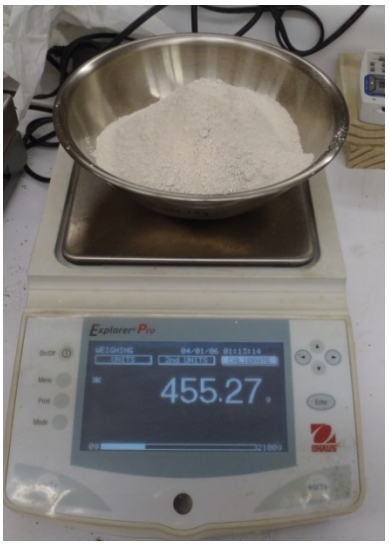
$$mass\ of\ Kt = .05 \times 2000\ mL \times 2.6 \times \frac{1\ g}{1\ mL} = 260\ g$$

Results for these calculations are shown in Table 3.5 for different volumes of water typically used to prepare composites. A sample of dry Kt being prepared during this step can also be seen in Figure 3.2a.

The second step in this procedure is to determine the mass of PAM to use for each type of composite. This step is achieved by using the calculation of the optimum clay-polymer volume ratio of 62.5 for Kt and 8 for Mt, also determined from previous studies (Kim and Palomino 2009; Kim and Palomino 2011). The clay-

TABLE 3.5: Mass of each clay and polymer to use for solution intercalation technique based on a batch of 2000 mL or 3500 mL

Volume of water	2000 mL	3500 mL
Mass of **Kt** for Kt-PAM (g)	260	455
Mass of **Mt** for Mt-PAM (g)	100	175
Mass of **PAM** for Kt-PAM (g)	1.200	2.100
Mass of **PAM** for Mt-PAM (g)	3.750	6.563

(a) 

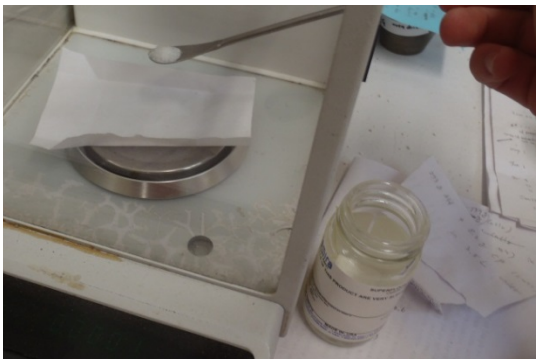
(b) 

FIG. 3.2: Materials used for Kt-PAM composites consist of (a) Kaolinite and (b) PAM

polymer volume ratio is represented as the proportion of clay volume per the proportion of polymer volume in the composite:

$$clay\ polymer\ volume\ ratio = \frac{clay\ mass / G_s\ of\ clay}{polymer\ mass / G_s\ of\ polymer} \quad (3.2)$$

For example, in the case of Kt-PAM with a clay-polymer volume ratio of 62.5, there is 62.5 times more volume of clay in the composite than that of the polymer. Results for the mass of polymer to be used can also be found in Table 3.5. A sample of dry PAM being prepared during this step can also be seen in Figure 3.2b.

The third step of this procedure is to mix and hydrate the clay mineral and the polymer in separate containers of distilled water. For Kt, 1 hour of mixing time is sufficient for hydration at the water content of 770%, but for Mt, 4 hours of mixing

time is needed for complete hydration at the water content of 2000%. Water contents were calculated based on the weights shown in Table 3.5. For PAM, 1 hour of mixing time is sufficient for hydration for the very high water contents used.

The fourth and final step in this procedure is to combine the clay mixture and PAM mixture into a final container and mix for 2 hours. At this point, the clay-polymer composite is complete and ready for the next steps of the testing. Further detail into the water content of the materials at each step can be found in Table 3.6.

3.4 Pre-Consolidation

The materials used in this testing were pre-consolidated under the same conditions in order to simulate an in-situ condition. While many samples were pre-consolidated in this manner, each consisted of one of four different specimens (kaolinite, kaolinite-PAM composite, montmorillonite, or montmorillonite-PAM composite). This setup is shown in Figure 3.3. In order to pre-consolidate the

TABLE 3.6: Sample calculations showing the resulting water contents for both Kt-PAM and Mt-PAM composites mixed to a total volume of 3500 mL.

	Material	Mass of water (g)	Mass of material (g)	Water content (%)
Kt-PAM	clay	3000	455	659
	polymer	500	2.1	23810
	composite	3500	457.1	766
Mt-PAM	clay	3000	175	1714
	polymer	500	6.563	7618
	composite	3500	181.563	1928



FIG. 3.3: Pre-consolidation setup showing samples prepared in PVC tubes and consolidated with weights

materials, perforated PVC tubes of diameter 3" were placed into a wooden frame, and a porous stone was placed at the bottom of each tube. Then, the clays or clay-polymer composites were taken in slurry form and placed inside the tube until the tube was full of the sample. A loading block, with a diameter slightly smaller than 3" was then placed at the top of the sample, and 23.3 kg of weight were applied to the tube. This amount of weight resulted in a normal stress of 50 kPa for each sample. Water was also added into the top of the tube periodically to ensure that the samples remained saturated during the pre-consolidation process. The tubes were consolidated for one month under this normal stress, and the specimens were removed from the tubes for testing.

Perforated PVC tubes were used for this procedure to allow for drainage during loading. However, filter paper was not used to line the inside of the tubes, allowing for the perforations to become clogged with the soil sample. Therefore, water was only allowed to escape from the samples through the bottom porous stone and around the top loading block.

In order to determine the water content distribution throughout the tubes, tests were performed to evaluate these conditions. To perform this study, extra tubes of each material were assembled, following the same procedures as before for composite preparation and preconsolidation. The resulting consolidated material was cut into a minimum of 10 layers of height ¾" throughout the height of the tube, from the top to the bottom. The samples were weighed after removal from the tube in order to obtain the wet weight and weighed after oven drying at 110 ± 5°C to obtain the dry weight. With these values, the water content with specimen height was determined throughout the tube. The void ratio was also calculated at these same points based on the volume of each sample. This data is shown in Figure 3.4, with the four specimens of a) kaolinite; b) kaolinite-PAM composite; c) montmorillonite; and d) montmorillonite-PAM composite.

Figure 3.4 shows that the samples used in this test could have varying initial void ratios when extracted from the pre-consolidation tubes. However, the samples were also saturated at varying pore fluid conditions upon removal from the tubes, which can lead to fabric changes of the material. This additional step was performed in order to prepare the samples for the different test conditions listed in Section 3.5.

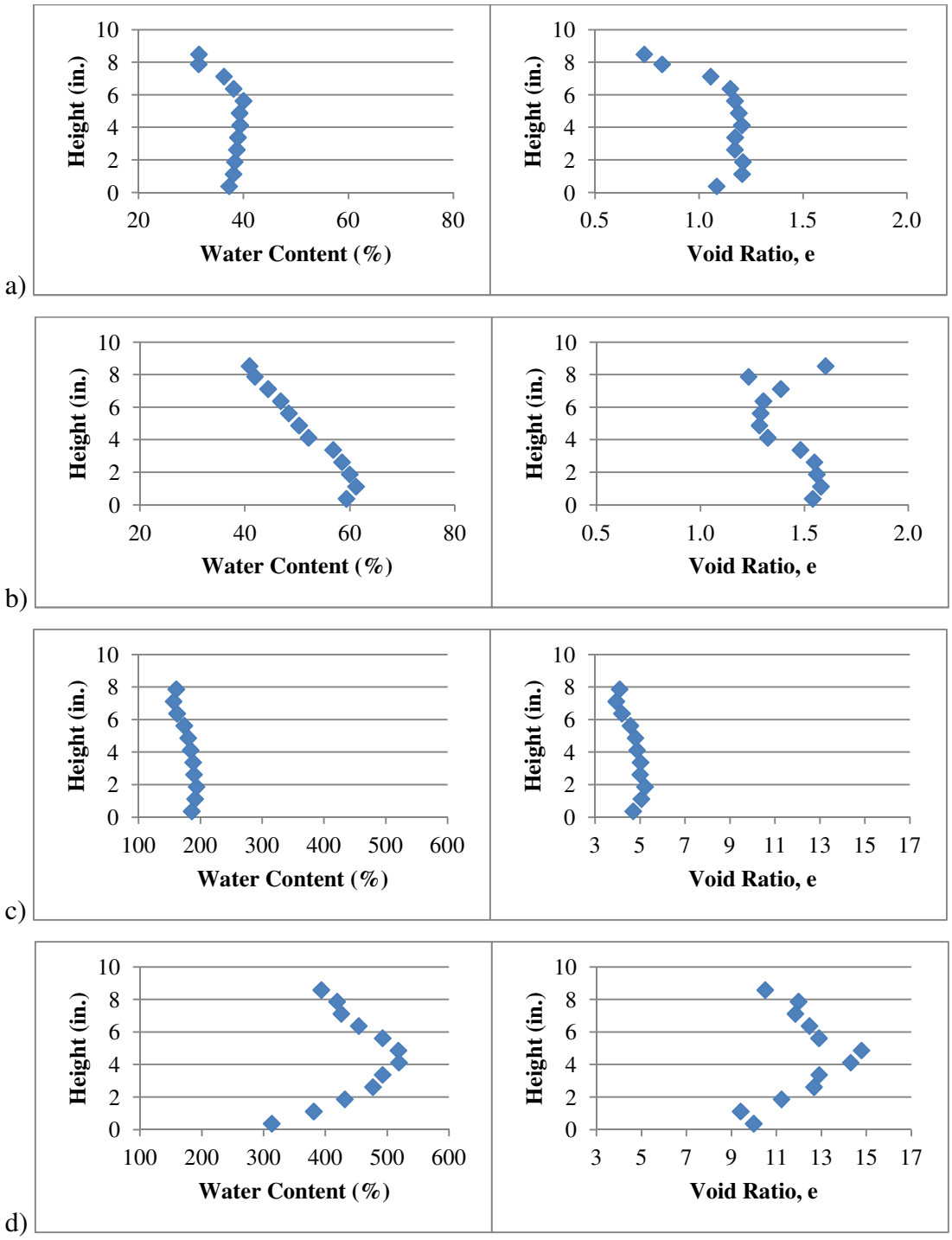


FIG. 3.4: Water content and void ratio results for the materials: a) kaolinite; b) kaolinite-PAM composite; c) montmorillonite; and d) montmorillonite-PAM composite

Due to the fabric changes instigated by the different pH levels and ionic concentrations of the saturating fluid, further void ratio changes are likely to occur within the materials before the test is started. Therefore, the samples are expected to have different void ratios at the start of the test due to the variations in void ratios seen throughout the tube and the fabric changes instigated by the specific saturating fluid. These findings will be discussed further in Section 5.3.

3.5 Test Matrix

A key aspect of this study is to highlight the effects of changing pore fluid conditions on the behavior of these "responsive" clay-polymer composites. Because the polymer of interest, PAM, is affected by changing pH levels and ionic concentrations, those factors will be adjusted in this study. For each type of clay (kaolinite and montmorillonite), there are 8 different test conditions, shown in Table 3.7. These conditions were chosen carefully based on previous studies to maximize the potential response (Kim and Palomino 2009; Kim and Palomino 2011). The first variable investigated was the type of sample, which refers to either a control sample or clay-PAM composite sample. The control material is the pure clay mineral phase, kaolinite or montmorillonite, without polymer. The second variable is the pore fluid chemistry, specifically pH and ionic concentration. The pH conditions investigated are pH 3, pH 6 (distilled water), and pH 11.5. pH 3 solutions were created by adding a 1M solution of HCL to a container of distilled water. pH 11.5 solutions were created by adding a 2M solution of NaOH to a container of distilled water. The ionic

concentration conditions investigated are 0.3M NaCl and 0M NaCl (distilled water). 0.3M NaCl solutions were created by adding NaCl crystals to a container of distilled water. These pore fluid conditions were chosen based on the knowledge of PAM conformation shown previously (Section 2.4). Therefore, these materials will be compared across the spectrum of pH (3 < 6 < 11.5) and ionic concentration (distilled water < 0.3M NaCl), which are known to induce coiled, intermediate, and extended polymer molecule conformations. Because distilled water has an ionic concentration of approximately 0M NaCl and a pH of 6, it should be noted that the distilled water case was used as both the pH 6 variable and the 0M NaCl concentration variable.

TABLE 3.7: Test Matrix

Kaolinite (Kt)				Kaolinite-PAM composite (Kt-PAM)			
pH 3	pH 6 (dist wtr)	pH 11.5	0.3M NaCl	pH 3	pH 6 (dist wtr)	pH 11.5	0.3M NaCl
Montmorillonite (Mt)				Montmorillonite-PAM composite (Mt-PAM)			
pH 3	pH 6 (dist wtr)	pH 11.5	0.3M NaCl	pH 3	pH 6 (dist wtr)	pH 11.5	0.3M NaCl

CHAPTER 4: SHEAR STRENGTH

The content of this chapter will outline the research conducted in order to determine the shear strength of the different materials. The direct shear test was performed in accordance with ASTM standards and the results are evaluated. Topics discussed in this chapter include: (1) the direct shear procedure; (2) results; (3) discussion of results; and (4) conclusions.

4.1 Direct Shear Procedure

4.1.1 Procedure

The direct shear test was performed by referencing ASTM D3080, "Standard Test Method for Direct Shear Test of Soils Under Consolidated Drained Conditions" as a basis for the procedures. However, in the interest of time, the samples were sheared at a displacement rate that resulted in undrained conditions, as will be described subsequently. Therefore, it must be noted that while this standard is for drained conditions, the modified displacement rate used resulted in undrained behaviors.

In this procedure, three or more direct shear tests are completed on each sample using different normal loads in order to analyze their effects upon deformation and shear resistance. Normal loadings were applied to 3 different specimens from one sample of the materials shown in Table 3.7 (ex. Kt-PAM at pH

3). These different loadings resulted in normal stresses of 50 kPa, 100 kPa, and 200 kPa.

According to ASTM D3080, this test is conducted in a direct shear machine, in which an undisturbed sample is placed inside a shear box with porous stones inserted above and below the sample. The normal load is applied directly to the top of the specimen, and the two halves of the shear box are pulled apart under a strain-controlled condition. Along with measurements such as the vertical deformation, the shear resistance of the material is measured during the test. The shear stress can be calculated using the shear resistance and the cross-sectional area of the specimen in order to determine the maximum value during the test.

Specimens were placed in the direct shear machine and the normal load was applied before the start of the shearing phase. During this time, the samples remained saturated at the desired pore fluid condition (e.g. pH 11.5). In order for the specimens to be fully consolidated under the normal load prior to shearing, this load was applied for a minimum of 20 hours depending on the material. Deformation vs. log time curves were constructed during this loading in order to determine when the end of primary consolidation had been reached.

However, additional steps were taken for samples containing montmorillonite (Mt & Mt-PAM). Due to their relatively large amount of deformation during the consolidation stage, the sample heights decreased to a point to where the test could not proceed without the addition of more material. Therefore, these samples were initially consolidated for 1 day, then removed from the machine, and more material

was added into the direct shear box. The normal load was then restarted, and the samples were allowed to reach the end of primary consolidation.

At this point, the shear box halves were separated at a distance of 0.025 in. according to the standard, and the shearing phase could begin. ASTM D3080 states that for fine-grained materials, the specimen shearing must occur over a long timeframe in order to prevent the buildup of excess pore water pressure. This rate must be determined by first calculating the total elapsed time to failure:

$$t_f = 50 \times t_{50} \tag{4.1}$$

where t_f is the total elapsed time to failure and t_{50} is the time required for the specimen to achieve 50% consolidation as determined by a consolidation test. The displacement rate can then be calculated by:

$$R_d = \frac{d_f}{t_f} \tag{4.2}$$

where R_d is the displacement rate and d_f is the estimated relative lateral displacement. Values for d_f are given as 0.5 in. if the material is a normally consolidated fine-grained soil. For example, a typical t_{50} value for a Mt-PAM sample in this test is approximately 1500 min. Using this value, the total elapsed time to failure (t_f) was found to be about 52 days.

Because of this large timeframe for shearing these materials, direct shear tests were performed in a manner in which the samples were undrained, instead of drained. In this case, the development of the undrained shear strength could be calculated for each normal loading. All samples were sheared at a displacement rate (R_d) of .0079

in./min. over a lateral displacement (d_f) of 0.59 in (15 mm). With these parameters, the resulting total elapsed time to failure (t_f) was 75 min.

4.1.2 Test Setup

After the procedures outlined in Chapter 3 have been performed to prepare the composite materials for testing, the samples must be removed from the preconsolidation tubes and inserted into the direct shear setup. This procedure begins with extruding the sample from the 76.2 mm (3") diameter pre-consolidation tube to a height of approximately 29.2 mm (1.15") as shown in Figure 4.1(a). The sample is then removed from the tube using a sample trimmer shown in Figure 4.1(b). Next, the sample diameter is trimmed to 63.5 mm (2.5") in order to fit into the direct shear box in Figure 4.1(c). The trimmed sample is inserted into the direct shear box with a porous stone at both the top and bottom of the sample, shown in Figure 4.1(d). The box, porous stones, and sample are then placed into the direct shear cell, and the desired pore fluid (pH 3, 6, 11.5, or 0.3M NaCl) is added to saturate the sample, shown in Figure 4.1(e). Samples were allowed to saturate in this cell at the desired pore fluid condition for 1 day prior to the commencement of the direct shear test. Note that 1 day is not likely long enough for the saturating fluid to completely permeate the sample. However, this is a reasonable model of anticipated field conditions.

At this point, the testing can proceed in the direct shear device. This device consists of the aforementioned direct shear box and cell, a loading arm, a load transferring ring, two GeoJacs, two load cells, and one LVDT. This device is shown

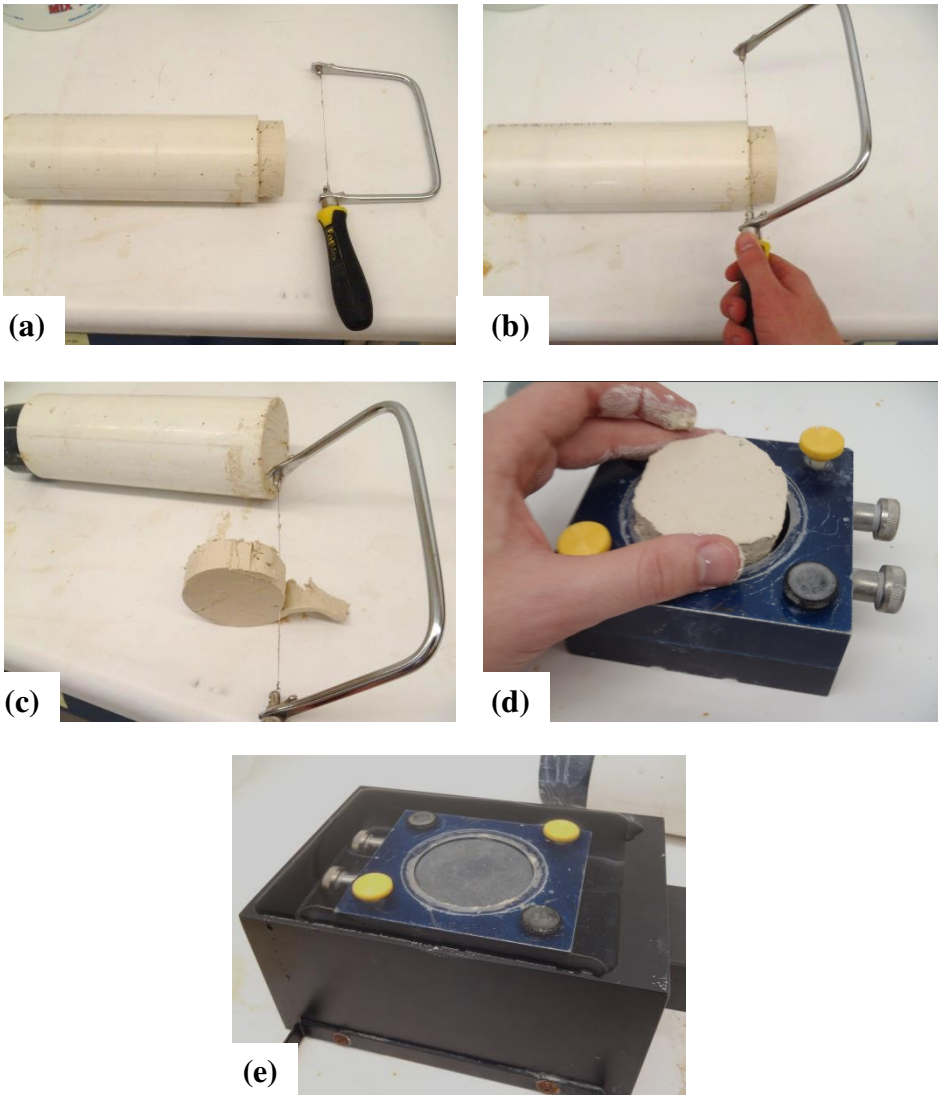


FIG. 4.1: Procedure showing the steps for extruding each sample from the preconsolidation tube, trimming, and placing into the direct shear box and cell: (a) extruding, (b) trimming from tube, (c) trimming the diameter, (d) inserting into direct shear box, (e) saturating

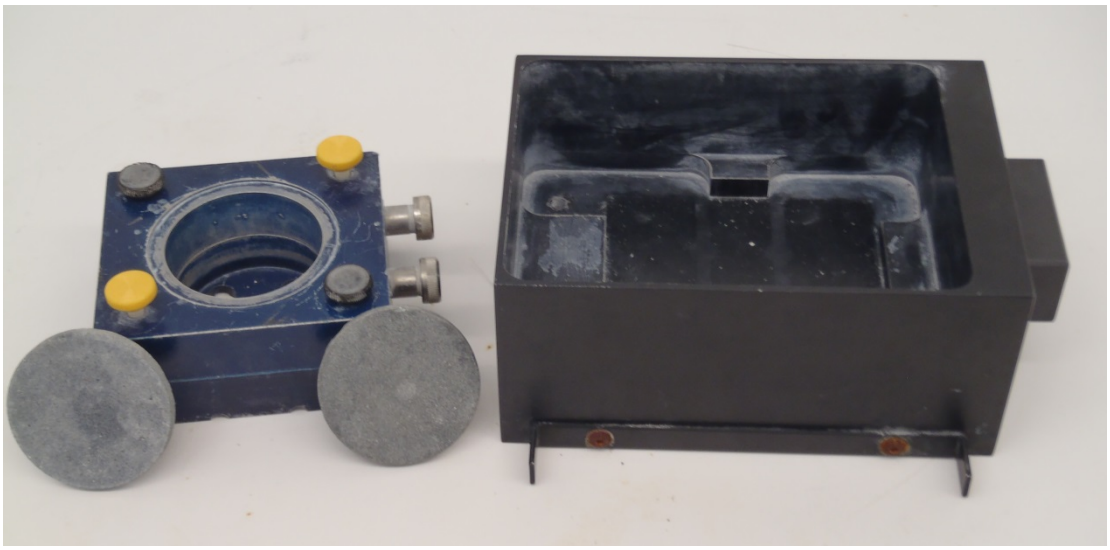


FIG. 4.2: Direct shear box and cell before the start of a test

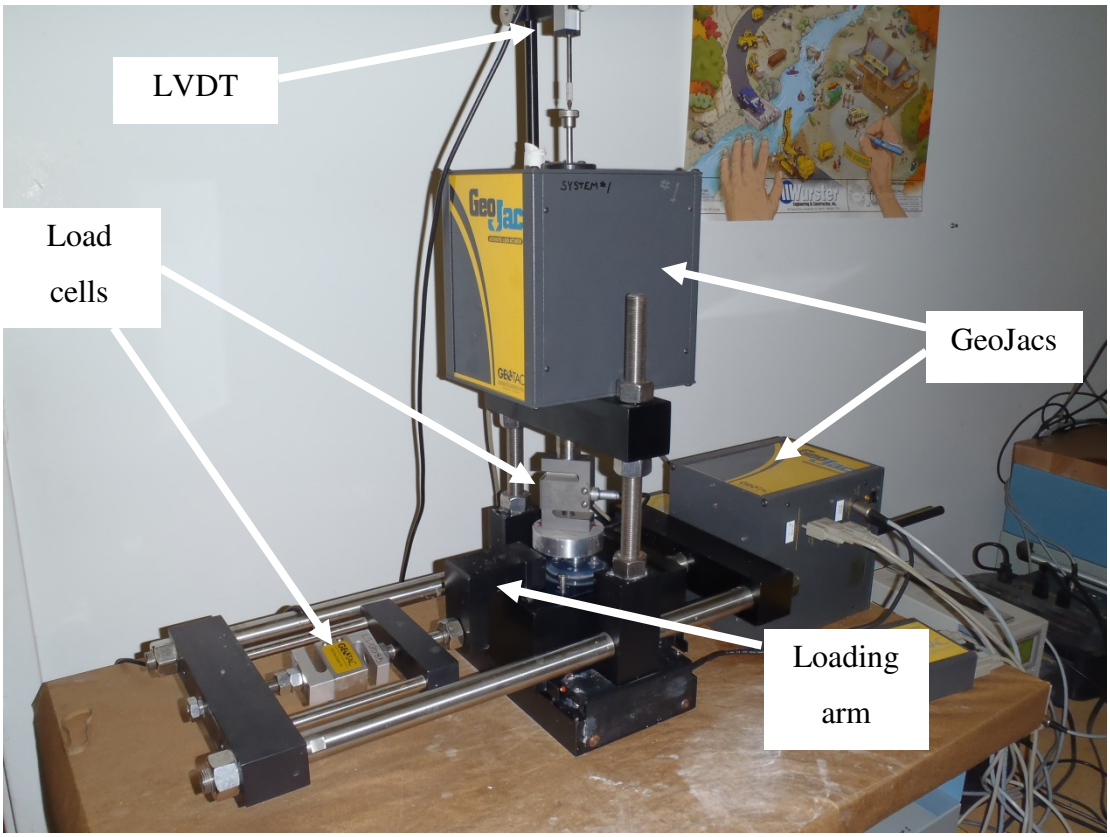


FIG. 4.3: Direct shear device showing the various components of the test setup

in Figures 4.2 and 4.3. The computer program DigiShear was used to control the equipment by sending the signals through a DC regulated power supply. Settings were loaded into the program to apply the required vertical load, shear rate, and maximum displacement during the test.

4.1.3 Measurements

During the direct shear test, measurements were recorded throughout the consolidation phase and shearing phase, as well as at the end of the test. These measurements were recorded with the program DigiShear. With this program, measurements such as DCDT displacement, GeoJac speed and displacement, and load cell force are displayed and recorded. A screenshot of this program is shown in Figure 4.4. For all samples studied, the following key measurements were recorded: (1) vertical deformation during the consolidation and shearing phases, (2) shear displacement during the shearing phase, (3) vertical load during the consolidation and shearing phases, (4) shear load during the shearing phase, (5) wet weight after test completion, and (6) dry weight after test completion.

Measurements 1-4 were used to determine the undrained shear strength. Measurements 5-6 were used to calculate the water content of the samples at the end of the test according to:

$$w\ (\%) = \frac{M_w - M_d}{M_d} \times 100\% \tag{4.3}$$

where w is the water content, M_w is the weight (or mass) after the test, and M_d is the dry weight (or mass) after the test. These values are given in Appendix A.

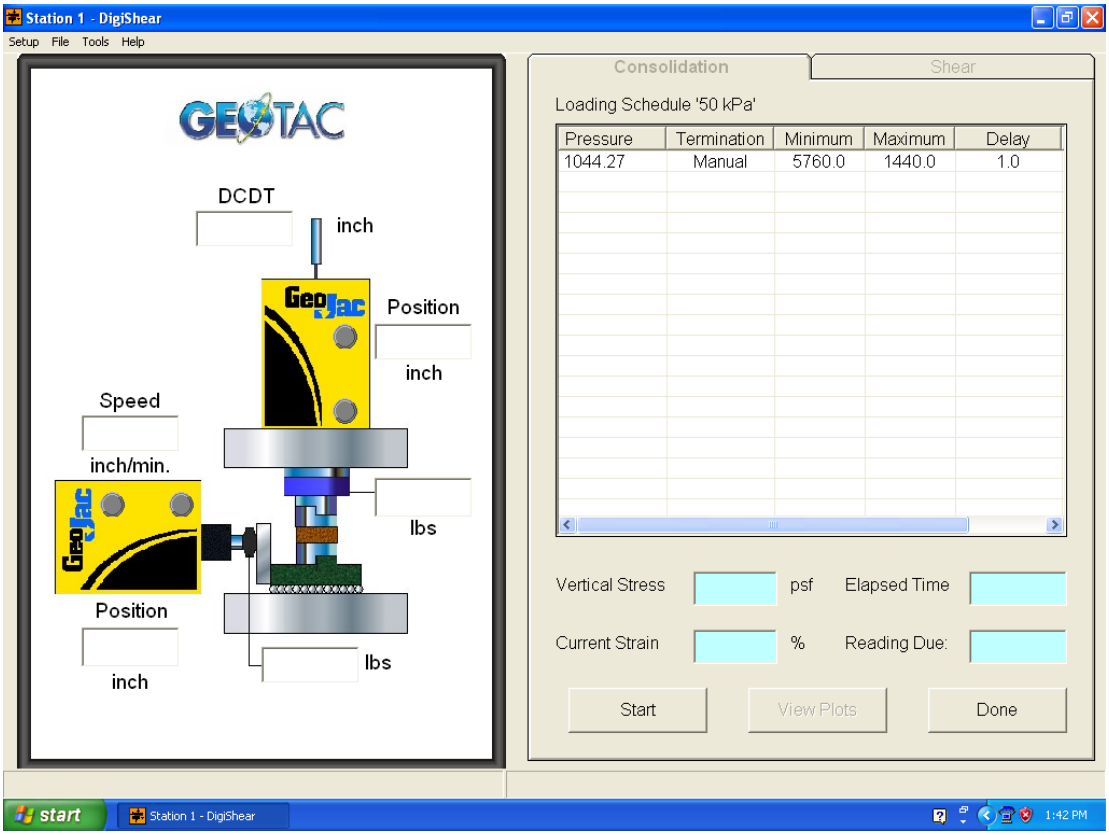


FIG. 4.4: Screenshot of the DigiShear program

4.1.3 Undrained Shear Strength

The shear displacement and shear load during the shearing phase were then used to calculate the undrained shear strength (S_u) of the materials. According to ASTM D3080, the shear stress acting on the specimen during the test is given by:

$$\tau = \frac{F_s}{A} \tag{4.4}$$

where τ is the shear stress, F_s is the shear force, and A is the area of the shear box. Therefore, the shear stress at any time during the test can be calculated with this equation. However, the contact area of the shear plane is constantly changing

throughout the test. As the two halves of the shear box are separated, the cross-sectional area of the specimen is decreasing. It is necessary to correct the cross-sectional area of the sample by first obtaining the area correction factor using the following equation obtained from the DigiShear manual:

$$F = \frac{2}{\pi}\left\{cos^{-1}\left[\frac{\Delta d_f}{D}\right] - \frac{\Delta d_f}{D}\sqrt{1-\left(\frac{\Delta d_f}{D}\right)^2}\right\} \tag{4.5}$$

where F is the area correction factor, Δd_f is the lateral displacement, and D is the sample diameter. This equation is valid for determining the area correction factor at a specific lateral displacement for circular samples. The corrected area was then determined using the area correction factor by:

$$A = F \times A_0 \tag{4.6}$$

where A is the corrected area and A_0 is the initial area.

The shear stress at any time during the test was then plotted with respect to the lateral displacement. The undrained shear strength was determined using these plots. Two examples of this are shown in Figure 4.5; all control samples developed a peak shear stress as in Figure 4.5(a), and most composite samples did not develop a peak shear stress as in Figure 4.5(b). In order to compare the shear responses between the control and composite samples, the undrained shear strengths were determined using the following procedure.

Figure 4.5 shows both the control and composite samples at the same saturating fluid and normal stress. As shown in Figure 4.5(a), S_u was first defined based on the response of the control samples as the shear stress value when the

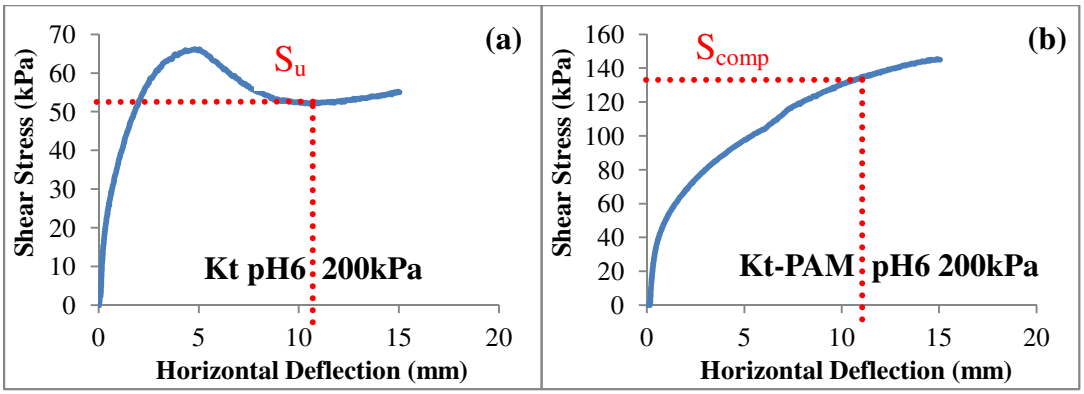


FIG. 4.5: Direct shear tests showing the determination of the undrained shear stresses (S_u, S_{comp}) for: (a) Kt at pH 6 pore fluid and 200 kPa normal stress, and (b) Kt-PAM at pH 6 pore fluid and 200 kPa normal stress

residual state is just reached. The displacement corresponding to this shear strength is noted. In this example (Figure 4.5(a)), the horizontal deflection when the specimen just reaches residual state is 11 mm. The comparable shear strength value of the composite was determined using this same displacement (e.g. 11 mm in Figure 4.5(a)). The shear strength of the composite at this displacement is defined as S_{comp} (e.g. Figure 4.5(b)). Note that each control case will likely result in a different displacement at which the residual state is reached. In other words, the displacement at which S_{comp} is defined can vary. The shear stress-lateral displacement graphs corresponding to all the direct shear tests performed in this study are included in Appendix A.

Finally, S_u and S_{comp} were then normalized with respect to the normal stress. This step was undertaken in order to compare the relative shear stress under any normal stress. This calculation was performed by dividing either S_u or S_{comp} by the

normal stress for the particular test (S_u/σ_v or S_{comp}/σ_v). Values for this calculation are also included in Appendix A.

4.2 Results

The direct shear test results will be compared with respect to the variables of clay type and type of saturating fluid. The clay types of interest are kaolinitic and montmorillonitic clays, and the saturating fluids include distilled water (serves as both pH 6 and 0M NaCl solutions), pH-modified distilled water (pH 3 and 11.5), and a NaCl electrolyte (0.3M NaCl).

4.2.1 Kaolinite (Kt) and Kaolinite Composite (Kt-PAM)

The results for tests on kaolinitic soil and composite are shown in Figure 4.6, which highlights the effects of different pH levels of the saturating fluid, and Figure 4.7, which highlights the effects of different ionic concentrations. As shown in both figures, with the addition of PAM to the samples, there is a significant increase in the normalized shear stresses ($S_{comp}/\sigma_v > S_u/\sigma_v$). The strength for the composite material is greater than that of the kaolinite material at the tested pore fluid conditions. Also, the normalized shear stress tends to decrease with increasing vertical stresses, likely due to the undrained testing conditions.

In Figure 4.6, the effects of pH can be seen on the individual materials. For the Kt samples, the pH 3 condition results in the lowest strengths. Depending on the normal stress applied, either the pH 6 condition or the pH 11.5 condition results in the

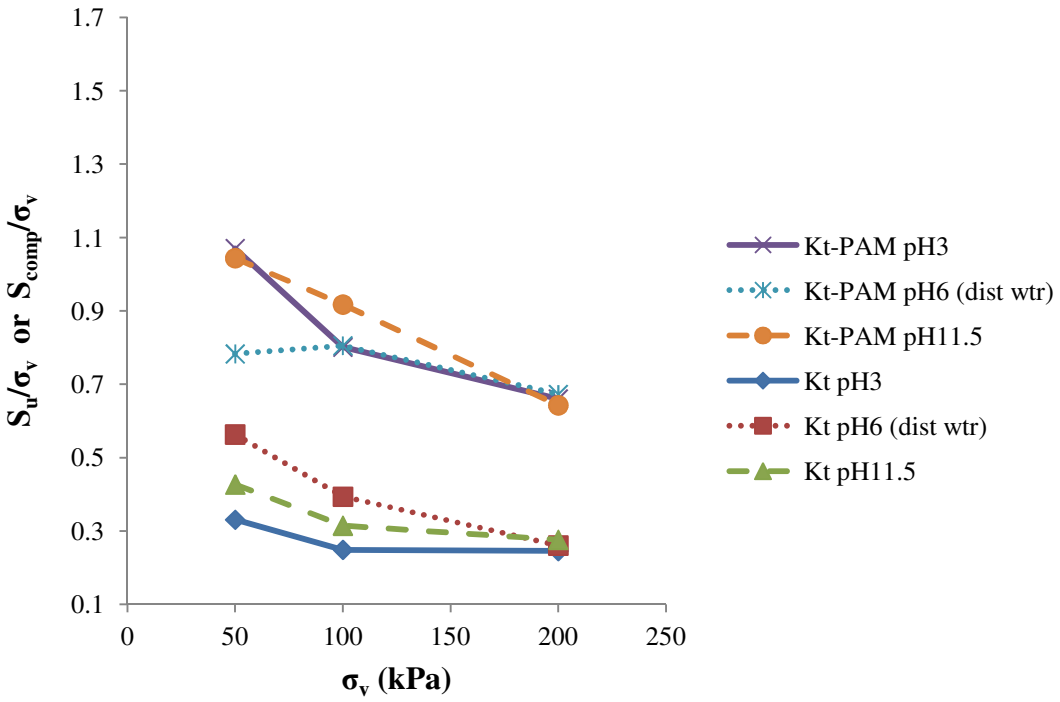


FIG. 4.6: Normalized shear stress values (S_u/σ_v or S_{comp}/σ_v) of Kt and Kt-PAM at various pH levels

highest normalized shear stress. The overall observed trend is increasing pH level results in higher strengths. For the Kt-PAM samples, the pH 3 condition also results in the lowest strengths with the exception of the outlier at 50 kPa normal stress. The pH 11.5 condition results in among the highest normalized shear stresses when compared to the other conditions; however, the pH 3 condition is higher at 50 kPa normal stress. Thus, there is not a clear trend that high pH or low pH results in greater values of normalized shear stress.

In Figure 4.7, the effects of ionic concentration can be seen on the individual materials. For Kt, the distilled water (0M NaCl) pore fluid condition results in the

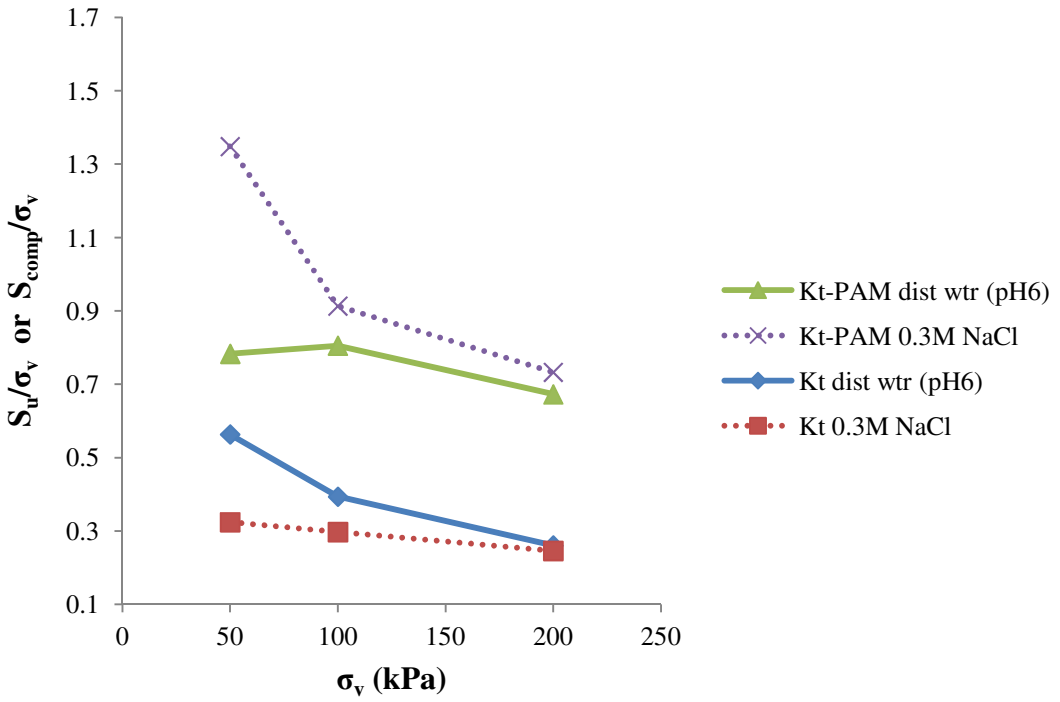


FIG. 4.7: Normalized shear stress values (S_u/σ_v or S_{comp}/σ_v) of Kt and Kt-PAM at various ionic concentrations

higher normalized shear stresses. However, the opposite is true for Kt-PAM samples. In the latter case, a pore fluid condition of 0.3M NaCl produces higher normalized shear stresses.

The soil fabric can greatly affect the shear strength of the material, as a flocculated soil fabric is known to have a higher shear resistance than a dispersed fabric (Mitchell and Soga 2005; Sridharan and Rao 1979). An additional test on kaolinitic samples was conducted in order to infer the particle arrangements of the samples tested in Figure 4.7. Tests on montmorillonitic samples were not conducted in the interest of time. A simple sedimentation test was performed on samples of Kt

at distilled water (pH6), Kt-PAM at distilled water (pH6), Kt at 0.3M NaCl, and Kt-PAM at 0.3M NaCl, as shown in Figure 4.8. Sedimentation tests were performed at low solids content in order to allow particle interactions to occur freely without being inhibited by additional stresses. All samples were prepared at a solids content of 0.01, resulting in a mass of 2.61 g for Kt samples and 2.51 g for Kt-PAM samples. Each of the four samples tested were placed in separate 100 mL graduated cylinders and hydrated with 100 mL of the desired pore fluid solution (distilled water, 0.3M NaCl) for 1 hour. The suspensions were then shaken vigorously in the cylinder, and the particles were allowed to settle. The supernatant-suspension and suspension-sediment interfaces were recorded with time and are shown in Figure 4.9.

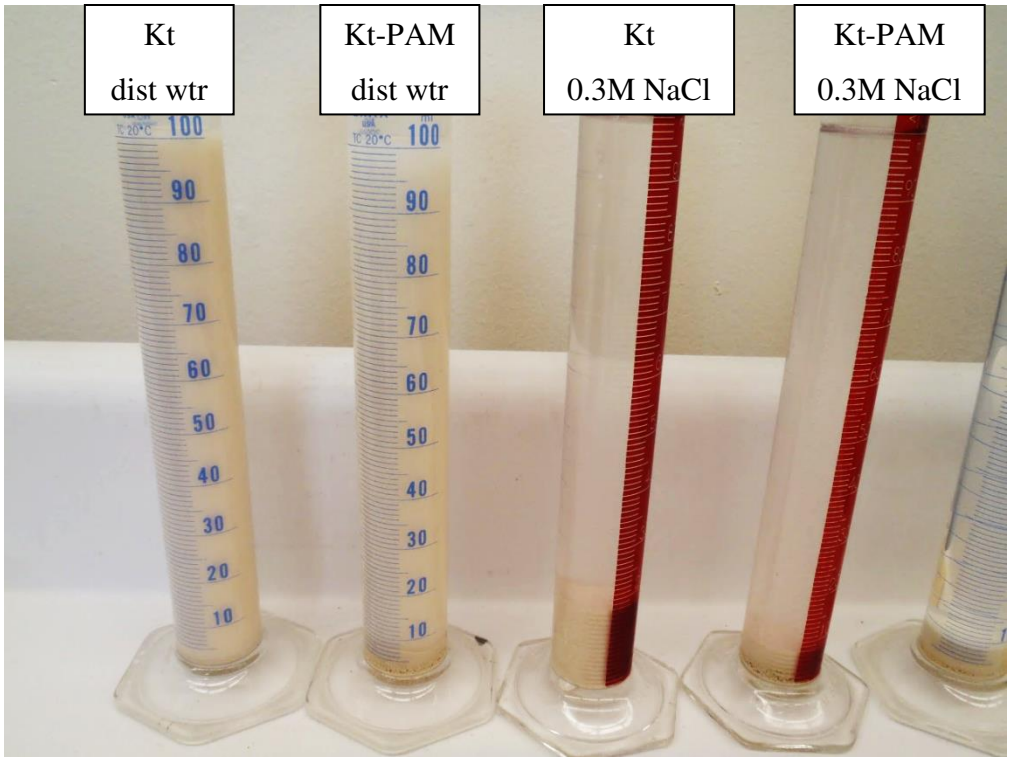


FIG. 4.8: Test setup for conducting the sedimentation test

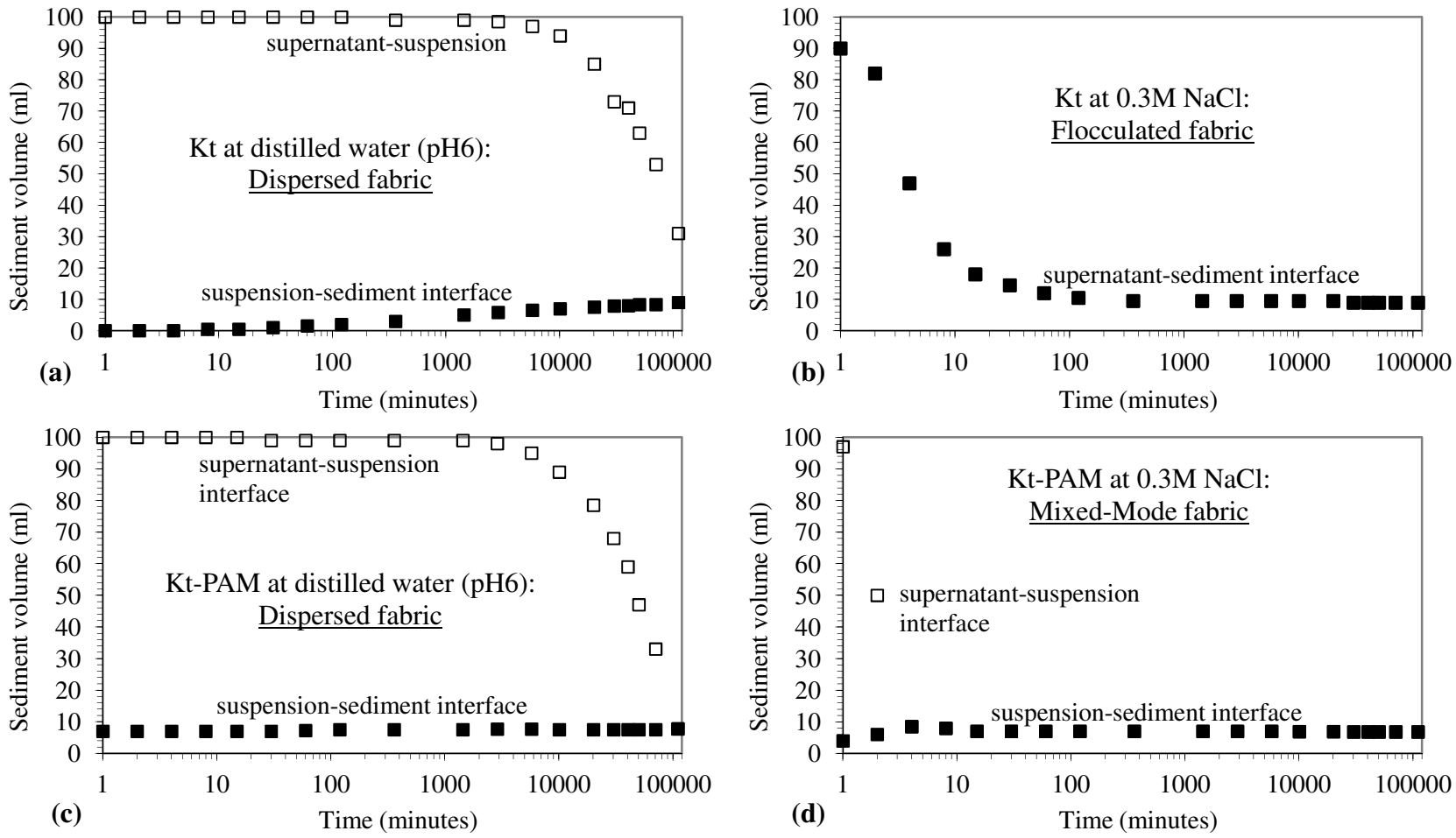


FIG. 4.9: Sedimentation curves showing inferred fabrics for: (a) Kt at distilled water, (b) Kt at 0.3M NaCl, (c) Kt-PAM at distilled water, and (d) Kt-PAM at 0.3M NaCl

When comparing the Kt samples in Figures 4.9(a) and 4.9(b), it can be seen that the distilled water sample took much longer to settle to its final sediment height, and a large volume of suspension remained until the end of the test. In contrast, the 0.3M NaCl sample settled very quickly and had a clear supernatant throughout the test. These results were similar to previous studies on kaolin clay (Palomino and Santamarina 2005). In this previous study, the dispersed fabrics took a long time to settle and the suspension remained cloudy until the end of the test. Also, the flocculated fabrics settled very quickly and had a clear supernatant. Therefore, settling characteristics of the Kt sample at 0.3M NaCl are consistent with those of a flocculated fabric, and the settling characteristics of the distilled water sample are consistent with a dispersed fabric. When comparing the Kt-PAM samples in Figure 4.9(c) and 4.9(d), similar trends are shown. In the distilled water sample, a large volume of suspension remained until the end of the test, indicating a dispersed fabric. In the 0.3M NaCl sample, the suspension-sediment interface formed quickly, and the supernatant was clear throughout the test. According to the suspension settlement modes outlined in Palomino and Santamarina (2005), this behavior is most indicative of a mixed-mode fabric, which is similar in nature to the flocculated fabric as before. Therefore, the sedimentation test showed that for both Kt and Kt-PAM samples, the fabric at 0.3M NaCl is more flocculated than the fabric at distilled water, implying that this condition would likely result in a higher shear strength. However, the results from the direct shear test showed that for Kt samples, the normalized shear stress was higher at the distilled water condition, contrary to the results of the sedimentation

test. Thus, the flocculated fabric of the Kt sample at 0.3M NaCl exhibited lower strengths than the dispersed fabric of the Kt sample at distilled water.

4.2.2 Montmorillonite (Mt) and Montmorillonite Composite (Mt-PAM)

The results for the normalized shear stress of montmorillonitic soil and composite are shown in Figure 4.10, which highlights the effects of different pH levels of the saturating fluid, and Figure 4.11, which highlights the effects of different ionic concentrations. As is shown in both figures, the addition of PAM causes a significant increase in the normalized shear stress as seen with the kaolinitic soils. Also similar to kaolinitic samples, the normalized shear stress tends to decrease with increasing vertical stresses.

In Figure 4.10, Mt and Mt-PAM are compared with respect to changes in the pore fluid pH. For the Mt samples, the pH 3 condition results in the lowest strengths, the pH 6 condition has the highest strengths, and the strengths at pH 11.5 are in between. For the Mt-PAM samples, the pH 11.5 condition results in the highest strengths with the exception of the outlier at 50 kPa normal stress. The pH 3 and pH 6 conditions show the lowest normalized shear stresses, again with the exception of the previous outlier. As in Figure 4.6, there is not a clear trend that high pH or low pH results in greater values of normalized shear stress for the composite samples, and there is not a clear link between the trends shown in the control and composite samples.

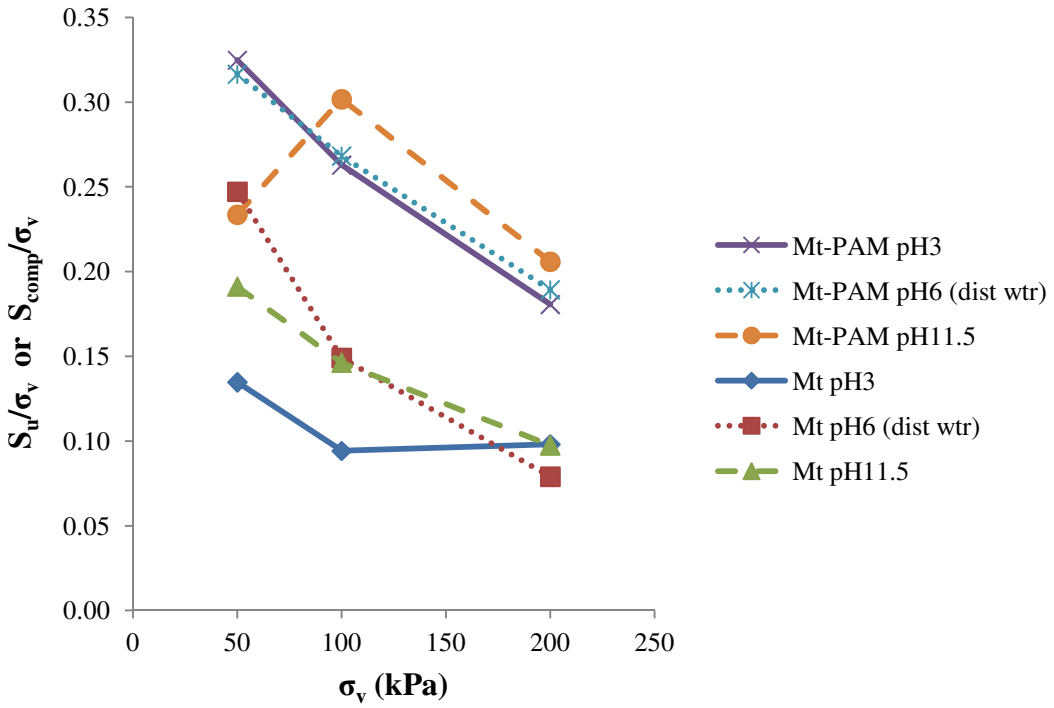


FIG. 4.10: Normalized shear stress values (S_u/σ_v or S_{comp}/σ_v) of Mt and Mt-PAM at various pH levels

In Figure 4.11, the effects of ionic concentration are shown for Mt and Mt-PAM samples. Mt saturated with distilled water (0M NaCl) resulted in higher strengths than when saturated with 0.3M NaCl. For Mt-PAM, the normalized shear stress for samples saturated at 0.3M NaCl showed higher values than those saturated with distilled water. The relationship with Mt and Mt-PAM saturated at these ionic concentrations is consistent with the results for Kt and Kt-PAM at the same saturating fluid conditions.

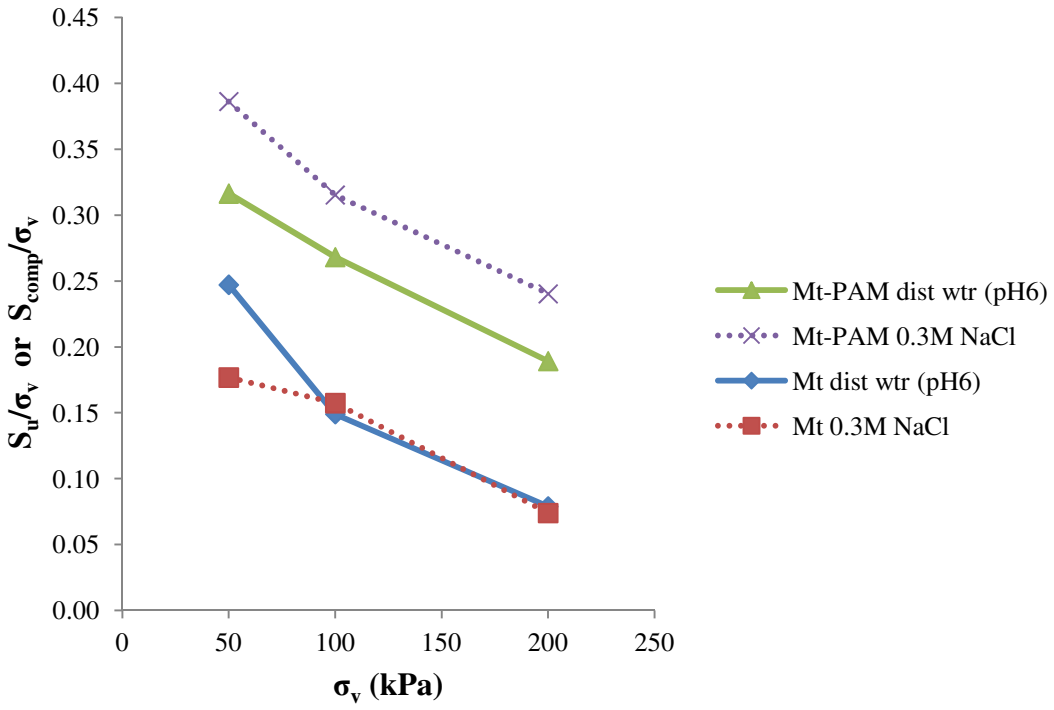


FIG. 4.11: Normalized shear stress values (S_u/σ_v or S_{comp}/σ_v) of Mt and Mt-PAM at various ionic concentrations

4.3 Discussion of Results

In a direct shear test, one expects to observe an increase in shear stress when the vertical stress is increased (Budhu 2011; Coduto 1999; Lambe and Whitman 1969). Thus, shear stress values were normalized with respect to the vertical stress, in order to construct the plots shown in Figures 4.6, 4.7, 4.10, and 4.11. Using this procedure, typically the slope of the lines connecting the normalized shear stresses is zero, i.e. a horizontal line. However, the trendlines in the stated figures have negative slopes. These results are most likely consistent with changing excess pore water pressure as a result of different vertical stresses. Samples tested at 50 kPa vertical

stress could be exhibiting a lower increase in excess pore water pressure throughout the test than samples tested at 200 kPa. Because of the increase in excess pore water pressure with increasing vertical stress, the effective stress of the soil would decrease, thus resulting in a lower shear strength. When these values were normalized and shown in the preceding figures, the results are consistent with this explanation.

Even though the testing procedure produced samples with changing pore water pressures, all samples were tested in the same manner. Based on this fact, comparisons were made between the samples. The most important observation gathered from this testing is the increase in normalized shear stress from a control specimen to a PAM-treated specimen, such that the strength of the PAM-treated material can be much greater than that of the untreated clay, depending on the specific conditions. The addition of PAM to a kaolinitic or montmorillonitic soil in accordance with the procedures outlined in this test leads to an increased shear stress.

Sedimentation tests were conducted in order to determine the differing behaviors of Kt and Kt-PAM under the tested ionic concentrations. The sedimentation test results showed that both Kt and Kt-PAM had more flocculated structures at the ionic concentration of 0.3M NaCl, which typically indicates an increase in shear stress. Yet, the distilled water condition produced higher normalized shear stresses in Kt, while the 0.3M NaCl condition produced higher stresses in Kt-PAM. In other words, the predicted trend of S_u did not manifest in the observed trend of S_u.

These results were compared to a previous study in which kaolin samples were tested using a fall cone liquid limit test (Palomino and Santamarina 2005). The liquid limit can be used to indirectly measure the shear strength of a soil, as a soil at its liquid limit has a shear strength of approximately 2 kPa (Wood and Wroth 1978). Hence, in a fall cone liquid limit test, a higher liquid limit indicates a higher shear strength at a given water content. Fall cone liquid limit measurements were performed on kaolin samples at differing ionic concentrations, and the samples were prepared at a much higher solids content than that of the sedimentation test. At this higher solids content, this study determined that at high ionic concentrations (> 0.1M NaCl), there was a significant decrease in liquid limit compared to the low ionic concentration (10^{-5}M NaCl). This is likely due to two reasons. First, high ionic concentrations (> 0.1M NaCl) induces FF aggregated systems in kaolin. This reduces the pore volume and thus decreases the volume of water needed to reach the liquid limit. Second, the effects of a high solids content system may somewhat counter the influence of the pore fluid chemistry on the particle interactions. Therefore, the high ionic concentration and the solids content of the kaolin samples were shown to have a great influence on the shear resistance (Palomino and Santamarina 2005).

The results of this study are consistent with the behavior of the kaolin material investigated in Palomino and Santamarina (2005). The samples tested under the distilled water condition have higher shear strengths than the samples at 0.3M NaCl. Therefore, the ionic concentration and solids content of the Kt samples in this test were more influential than fabric alone in determining their shear resistance.

However, the opposite result is seen with Kt-PAM samples. Kt-PAM at 0.3M NaCl results in a higher shear resistance than Kt-PAM at distilled water. Therefore, the fabric of Kt-PAM samples has a greater effect than the solids content and ionic concentration on their shear resistance.

PAM's conformation is known (Section 2.4) to change between coiled and extended based upon the pore fluid conditions. PAM has an extended conformation at high pH and low ionic concentration, and it has a coiled conformation at low pH and high ionic concentration. For the composite samples (Kt-PAM, Mt-PAM), the normalized shear stress was shown to be highest at both high pH levels (extended polymer) and high ionic concentration (coiled polymers). In other words, the composites exhibited higher strengths at both extended and coiled polymer conformations. Therefore, the data did not show a strong link between polymer conformation and increases in shear strength. Also, when comparing the effects of pH, the composite samples of Kt-PAM and Mt-PAM did not show similar changes in normalized shear stress as the control samples of Kt and Mt. While the control samples showed increases in strength with increasing pH, there was not a clear trend with the composite samples under these same conditions. Therefore, "tunability" was not evident in the composites based on the known conformational changes of PAM.

4.4 Conclusions

The direct shear test showed some unexpected results based on excess pore water pressure. Because the direct shear test is best for a drained test on clays,

performing this test in undrained conditions produced differing levels of excess pore water pressure. Without the measurement of these pressures, the resulting effective stresses in the soil during shearing could not be calculated. However, the results that were obtained showed important relationships between the samples.

The direct shear data collected was important for determining the effects of PAM on the clay minerals of interest. It was shown that the shear strength of the clay-PAM composites is greater than the shear strength of the control samples depending on the pore fluid conditions. However, both the Kt-PAM and Mt-PAM composites exhibited higher strengths at both extended and coiled polymer conformations. Thus, the data did not show a strong link between polymer conformation and increases in shear strength. Therefore, the "tunability" of the clay-polymer composites was not evident based on the direct shear test results.

It is also concluded that for Kt samples, the fabric alone was not the most influential factor for determining their shear strength. For this material, the particle interactions as well as solids content was shown to be more influential than the fabric alone in determining shear strength. With the addition of PAM, however, it was shown that the soil fabric was the most influential factor for determining the shear strength of the composites. An increasingly flocculated fabric with increasing ionic concentration led to a higher normalized shear stress for the composites. While these conclusions were based on previous tests as well as tests in this study on Kt, the same results were seen in Mt samples in this study.

CHAPTER 5: COMPRESSIBILITY AND SHEAR WAVE VELOCITY

The purpose of this chapter is to study the compressibility and shear wave velocity of the different samples. Typical 1D consolidation tests were performed, and shear wave velocities were determined with the assistance of bender elements. Topics discussed in this chapter include: (1) the 1D consolidation procedure; (2) shear wave velocity measurement; (3) results; (4) discussion of results; and (5) conclusions.

5.1 1D Consolidation

5.1.1 Procedure

The materials of interest were subjected to 1D consolidation tests according to the ASTM D2435 standard with some modifications. In this testing, a larger, modified consolidation cell was used in order to accommodate bender element testing, which will be described in detail in Section 5.2. This test is conducted using an oedometer, in which an undisturbed sample is placed inside a cylindrical ring, or consolidation cell, with porous stones inserted above and below the sample. According to ASTM D2435, the soil is then applied with successive normal stresses that are approximately doubled at each stage, and the deformation with respect to time is recorded. Along with measurements such as the sample density, water content, specific gravity, and height, the void ratio can be calculated at various stages

of loading. The void ratio can be used to track the volume changes of the soil over time, which can then be used to determine the compressibility and loading capacity of the material (Mitchell and Soga 2005).

According to ASTM D2435, the standard loading schedule consists of approximately doubling the normal effective stress with each loading (load increment ratio = 1). Due to the non-standard diameter of the modified consolidation cell and loading stones, limited availability of standard weight sizes, and time limitations, modifications were made to the loading schedule. In addition, the loading schedule was altered for samples containing kaolinite (Kt and Kt-PAM) and samples containing montmorillonite (Mt and Mt-PAM). This was due to the different consolidation behaviors of these materials, as montmorillonite samples experienced a much greater amount of consolidation. These observations will be discussed further in Section 5.3. The general loading schedule used for these tests is shown in Table 5.1.

In addition, ASTM D2435 specifies that deformation readings are to be taken at time intervals that are approximately doubled with each step. These readings are to be taken for a minimum of 24 hours or longer, depending on when the end of primary consolidation has been reached. For all samples, deformation readings were taken at the following time steps:

6 sec, 15 sec, 30 sec, 1 min, 2 min, 4 min, 8 min, 15 min, 30 min, 1 hour, 2 hours, 4 hours, 8 hours, and 24 hours.

TABLE 5.1: General loading schedule for 1D consolidation testing

Loading No.	Normal Stress (kPa)	Load Increment Ratio
1	15	
2	38	1.5
3	87	1.3
4	136	0.6
5	439	2.2
6	841	0.9
7	1643	1.0
8	841	-0.5
9	439	-0.5
10	136	-0.7
11	87	-0.4
12	38	-0.6
13	15	-0.6

Note: A negative Load Increment Ratio denotes unloading stages

This 24 hour span of deformation readings was a sufficient amount of time for all of the kaolinite samples to reach the end of primary consolidation. However, because of montmorillonite's consolidation behavior, additional deformation readings were recorded for all Mt and Mt-PAM samples. At least one additional reading was taken each day following the initial reading schedule, until the end of primary consolidation was reached.

5.1.2 Test Setup

The pure clay minerals and composite specimens were placed in PVC tubes and preconsolidated according to the procedures outlined in Chapter 3. Samples of each material were then removed from the preconsolidation tubes and inserted into

the consolidation ring. This procedure began by carefully extruding the sample from the tube to a height of approximately 50 mm, shown in Figure 5.1(a). The sample was then trimmed from the tube, and its diameter was trimmed from 76.2 mm (3" – PVC tube diameter) to a diameter of approximately 74.9 mm in order to fit into the consolidation ring. This step is shown in Figure 5.1(b). The sample was placed into the consolidation ring shown in Figure 5.1(c) and saturated in a container filled with the desired pore fluid (pH 3, 6, 11.5, or 0.3M NaCl). Shown in Figure 5.1(d), the samples were then saturated for a minimum of 3 days prior to the commencement of the consolidation test. Note that 3 days is not likely long enough for the saturating

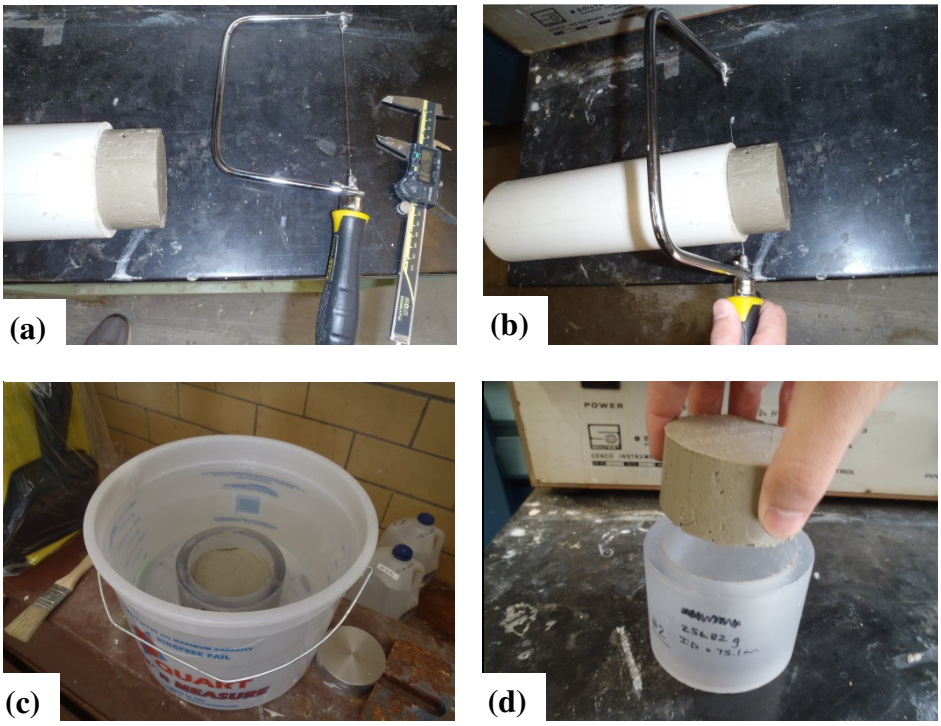


FIG. 5.1: Procedure showing the steps for extruding each sample from the preconsolidation tube and placing into the consolidation ring: (a) extruding, (b) trimming from tube, (c) inserting into consolidation ring, (d) saturating

fluid to completely permeate the sample. However, this is a reasonable amount of time to observe material response to the fluid.

The consolidation ring and sample were then removed from the container at the end of the saturation time. Porous stones, modified to accommodate bender elements, were also added at the top and bottom of the sample to allow for a doubly drained condition. The consolidation ring, sample, and porous stones were then placed into a modified consolidation cell, shown in Figure 5.2. The desired pore fluid condition was then added again into the consolidation cell in order to saturate the sample for the duration of the test. A larger, modified consolidation cell was required

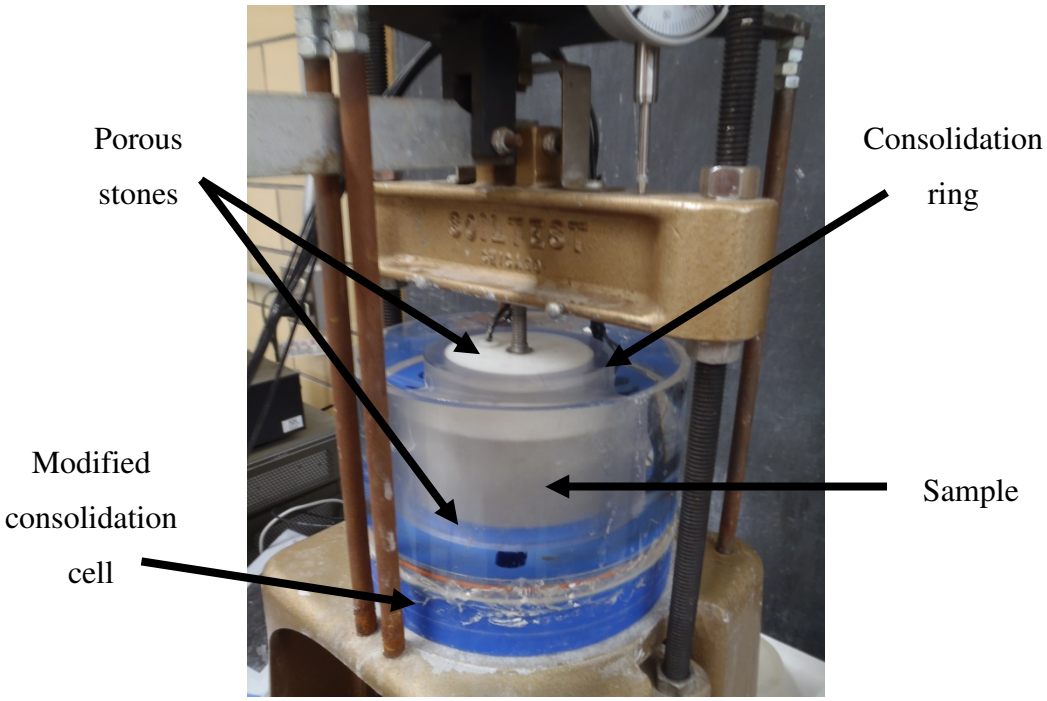


FIG. 5.2: Modified consolidation cell containing the sample and desired pore fluid condition

in order to accommodate the use of bender elements, as will be discussed in detail in Section 5.2.2.

A Soiltest C-220 oedometer, fitted with a dial gauge to track deformation, was used to perform the 1D consolidation tests. According to the manufacturer's specifications, effective normal stresses are applied to the sample with an accuracy of ½% to 1% of the target stress. As shown in Figure 5.3, weights are applied onto the end of the loading arm. This load is then transferred to the loading frame, at the top of the device. The loading frame directly applies the load to the sample. This device

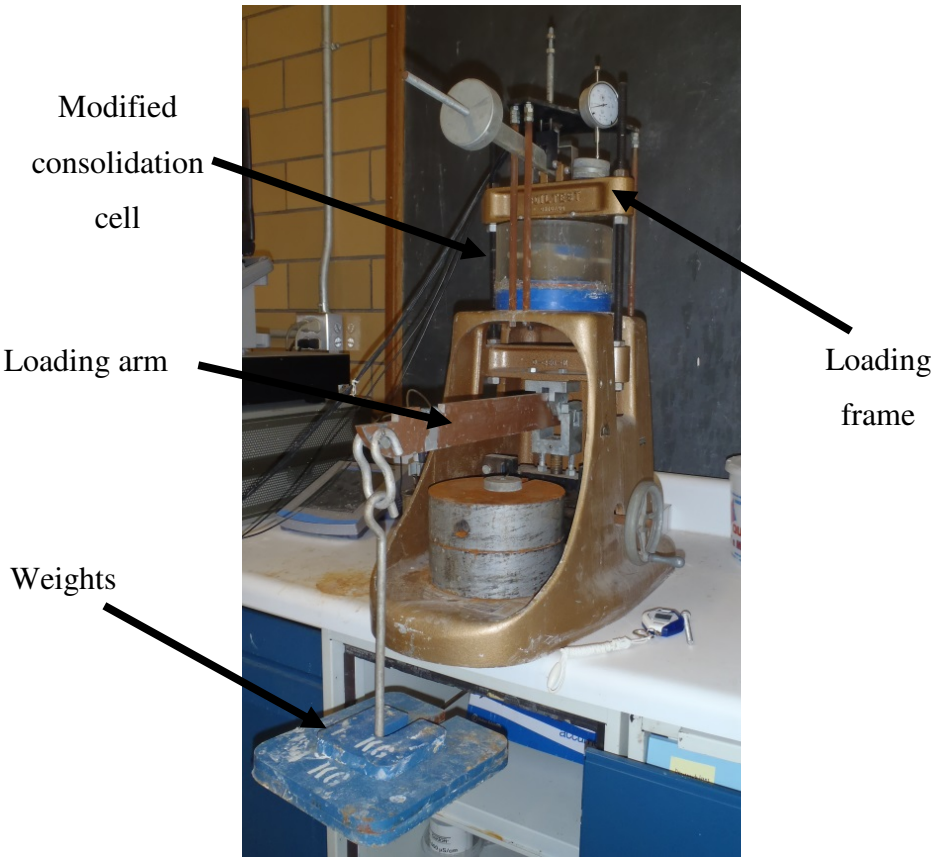


FIG. 5.3: Soiltest C-220 oedometer used for consolidation testing

allows for a 20:1 multiplying ratio. For example, if 1 kg of weights are applied to the device, the sample will experience a load of 20 kg.

5.1.3 Measurements

When running the 1D consolidation test, measurements were recorded at predetermined stages of the procedure in order to track the material deformation and calculate several key parameters. For all samples studied, the following key measurements were recorded (Appendix B): (1) initial height before first loading (immediately after saturation), (2) height at every stage of the test, (3) final height after test completion, (4) wet weight after test completion, and (5) dry weight after test completion. For a few samples, additional measurements were also taken which included: (1) sample height before saturation, (2) wet weight before saturation, and (3) wet weight after saturation. The latter set of measurements is included for observation, however, and no comparisons will be made based on these values in the Results section.

5.1.4 Void Ratio

Void ratio is defined as the ratio of the volume of voids to the volume of solids in a given sample (Budhu 2011; Lambe and Whitman 1969; Mitchell and Soga 2005). Throughout each test, sample height and water content measurements were taken in order to calculate the change in void ratio. The void ratio is important in order to note changes within the material as well as compared to other materials. To

calculate void ratio, the procedures in ASTM D2435 were followed by first determining the volume of solids as:

$$V_s = \frac{M_d}{G\rho_w} \tag{5.1}$$

where V_s is the volume of solids, M_d is the dry mass of the sample at the end of the test, G is the specific gravity of the material, and ρ_w is the density of water.

Next the height of solids was determined as:

$$H_s = \frac{V_s}{A} \tag{5.2}$$

where H_s is the height of solids, and A is the cross-sectional area of the sample.

Finally, the void ratio could be calculated at any time during the test using the equation:

$$e_x = \frac{H_x - H_s}{H_s} \tag{5.3}$$

where e_x is the void ratio at any time x, and H_x is the height of the sample at any time x.

5.1.5 Coefficient of Consolidation

The time rate in which the material experiences consolidation due to an applied load can be represented by the coefficient of consolidation. This parameter is usually denoted in units of cm^2/sec (Budhu 2011; Coduto 1999). In accordance with ASTM D2435, the coefficient of consolidation was determined according to "Alternative Interpretation Procedure 1." This method involves plotting the strain vs. log time curves for each loading. According to this procedure, these curves are then

used to extract the strain at the end of primary consolidation (ε_{100}), the strain at the beginning of primary consolidation (ε_0), and the strain at 50% of primary consolidation (ε_{50}). ε_{50} is then used to determine the time at 50% of primary consolidation (t_{50}), and the coefficient of consolidation (c_v). An example of this procedure applied to the data from one of the tests in this study is shown in Figure 5.4.

The coefficient of consolidation, C_v, can then be calculated based on t_{50}:

$$C_v = \frac{0.197 H_{dr}^2}{t_{50}} \tag{5.4}$$

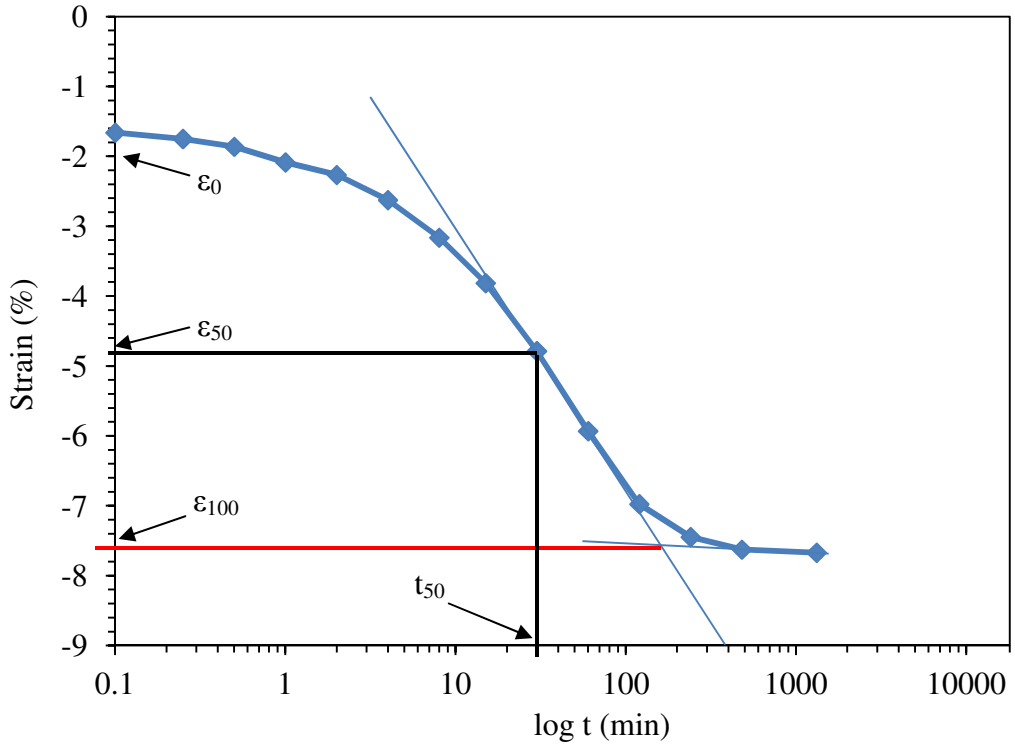


FIG. 5.4: Example data from a stain vs. log time curve showing the locations of ε_0, ε_{50}, ε_{100}, and t_{50}

where C_v is the coefficient of consolidation and H_{dr} is the length of the drainage path at 50% consolidation. Because this calculation was performed for each loading (87 kPa, 136 kPa, etc.) of the sample being tested, an average value was taken for each sample and recorded (Appendix B).

5.1.6 Compression Index and Recompression Index

In addition to loading conditions, it is also important to observe the material response to unloading in order to determine if the material demonstrates recoverable strain. In the plot of vertical effective stress vs. void ratio, the slope of the normal compression line is known as the compression index, or C_c. In the same plot, the slope of the unloading line is known as the recompression index, or C_r. These values are important because they show the relative amount of consolidation or rebound throughout the test, with higher slopes denoting larger variations in the void ratio with load (Budhu 2011; Coduto 1999; Lambe and Whitman 1969). As shown in Figure 5.5, a sample effective stress vs. void ratio curve is shown, with logarithmic trendlines added for the loading and unloading portions, respectively. The slope of the initial loading curve (C_c) is 0.180, and the slope of the rebound (C_r) is 0.079. Plots containing these values for each sample are shown in Appendix B.

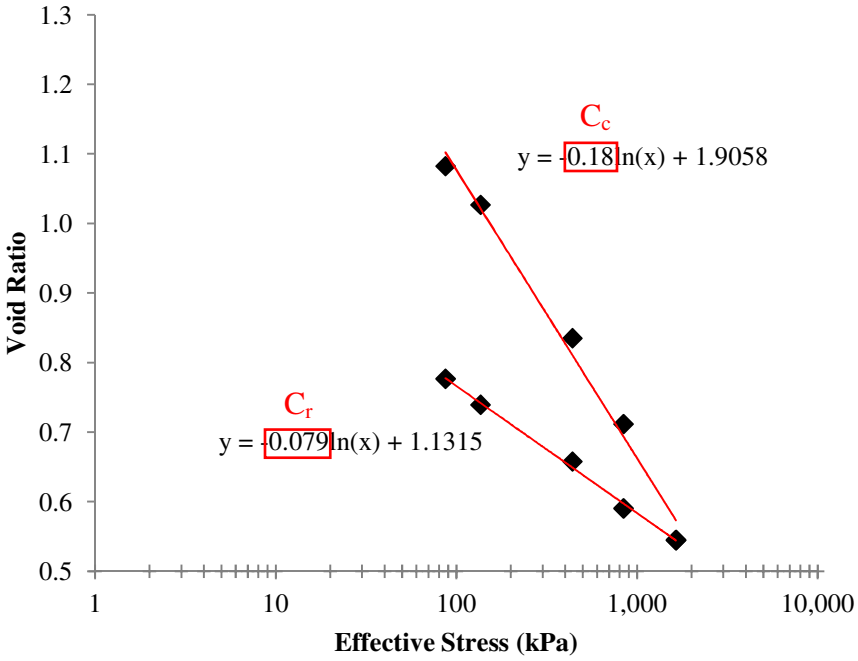


FIG. 5.5: Sample data from a void ratio vs. effective stress curve showing values for C_c and C_r

5.2 Shear Wave Velocity Measurement

5.2.1 Procedure

The 1D consolidation test is used to determine the compressibility of the material, but the stiffness of the material is also of interest. The stiffness of a soil is defined as a measure of its resistance to compressibility (Mitchell and Soga 2005). Bender elements can be used to infer the stiffness of a soil, but do not measure the stiffness directly. These elements transmit shear waves into the sample and directly measure the shear wave velocity of the material. The shear wave velocity is an indicator of the stiffness of the material, as the two are directly related (Lee and Santamarina 2005). The use of bender elements is a fairly common technique in

laboratory soil testing. However, what is fairly uncommon about this technique is using them in conjunction with a 1D consolidation test.

The bender elements were fabricated for this study. Small (approximately 0.8x0.5 cm), rectangular elements were cut from a larger piezoceramic sheet (Piezo Systems, Inc.). Coaxial cables were then soldered to the piezoceramic elements to form parallel type bender elements. Bender elements were used in this study to determine the shear wave velocity of the materials as calculated at each normal stress by the following equation:

$$SWV = \frac{Distance\ between\ two\ bender\ elements}{(t_2 - t_1)} \tag{5.5}$$

where SWV is the shear wave velocity, t_2 is the arrival time of the output signal and t_1 is the arrival time of the input signal as shown in Figure 5.6 (Lee 2003). Average shear wave velocities for several types of soil and rock are also included in Table 5.2.

5.2.2 Test Setup

The testing system for measuring shear wave velocity consists of several components: (1) modified consolidation cell with bender elements, (2) waveform

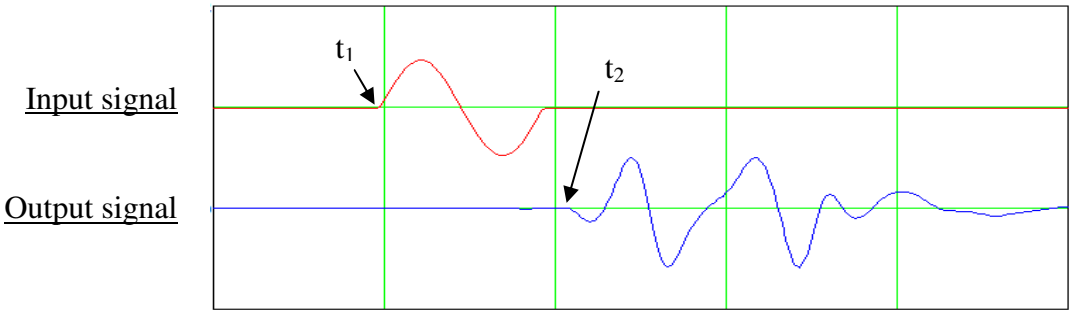


FIG 5.6: Input and output shear wave signals (Lee 2003)

TABLE 5.2: Typical shear wave velocities of different materials (Ashland 2013)

Material	SWV (m/s)
Lacustrine and alluvial silt and clay	199
Lacustrine sand	301
Lacustrine and alluvial gravel	387
Pre-Bonneville alluvial-fan deposits	437
Glacial deposits including till and outwash	486
Tertiary sedimentary and volcanic rocks	1023
Mesozoic sedimentary rocks	1449
Tertiary intrusive (igneous) rocks	2197

generator, (3) filter/amplifier, (4) oscilloscope, and (5) laptop. First, the consolidation cell was modified in order to accept the use of the bender elements. The modified cell, which includes modified porous stones, was constructed after Lee (2003), who designed the cell for the specific purpose of measuring shear wave velocities of soil samples during 1D consolidation testing. The materials used to construct the cell and porous stones were selected so that the shear waves would preferentially pass through the soil and not the consolidation cell walls. This selection allows for an accurate determination of shear wave signals that are penetrating through the sample, and not reflecting off of the cell walls. The modified consolidation cell, bender element, and modified porous stones used in this testing are shown in Figure 5.7.

In the modified consolidation cell, a source and receiver bender element protrudes into each end of the sample through the porous stones and is connected to

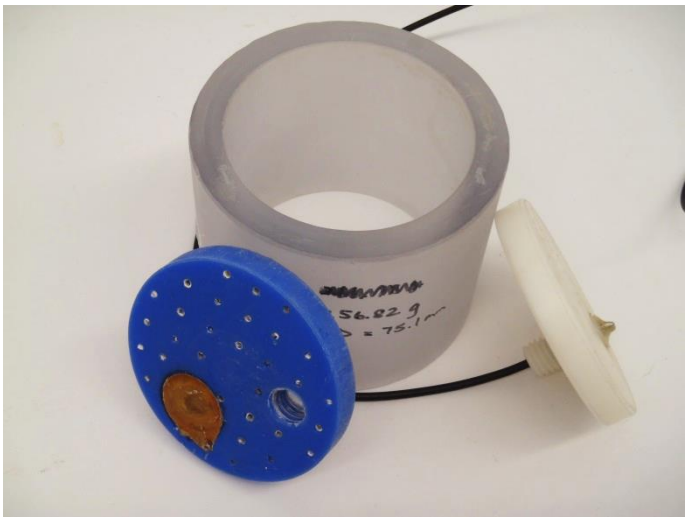


FIG 5.7: Modified consolidation cell, bender element, and modified porous stones

electronic equipment through coaxial cables. A signal is sent to the source bender element through a waveform generator (Agilent 33220A) and is received by the opposite bender element. The signal is then transmitted through a frequency filtering device (Krohn-Hite Model 3944) and displayed on an oscilloscope (Agilent 54624A). A laptop that is connected to the oscilloscope was used as a data acquisition device to record the input and output signals for analysis. A supporting program (IntuiLink Connectivity Software) was installed on the laptop and was used to capture the signals. The shear wave velocity measurement system is shown in Figure 5.8, with the arrows connecting the devices representing the coaxial cable connections. The input and output signals are displayed on the oscilloscope in such a way that a time difference can be seen between the two signals. At each time interval in the test, the distance between the two bender elements is also known. Therefore, shear wave

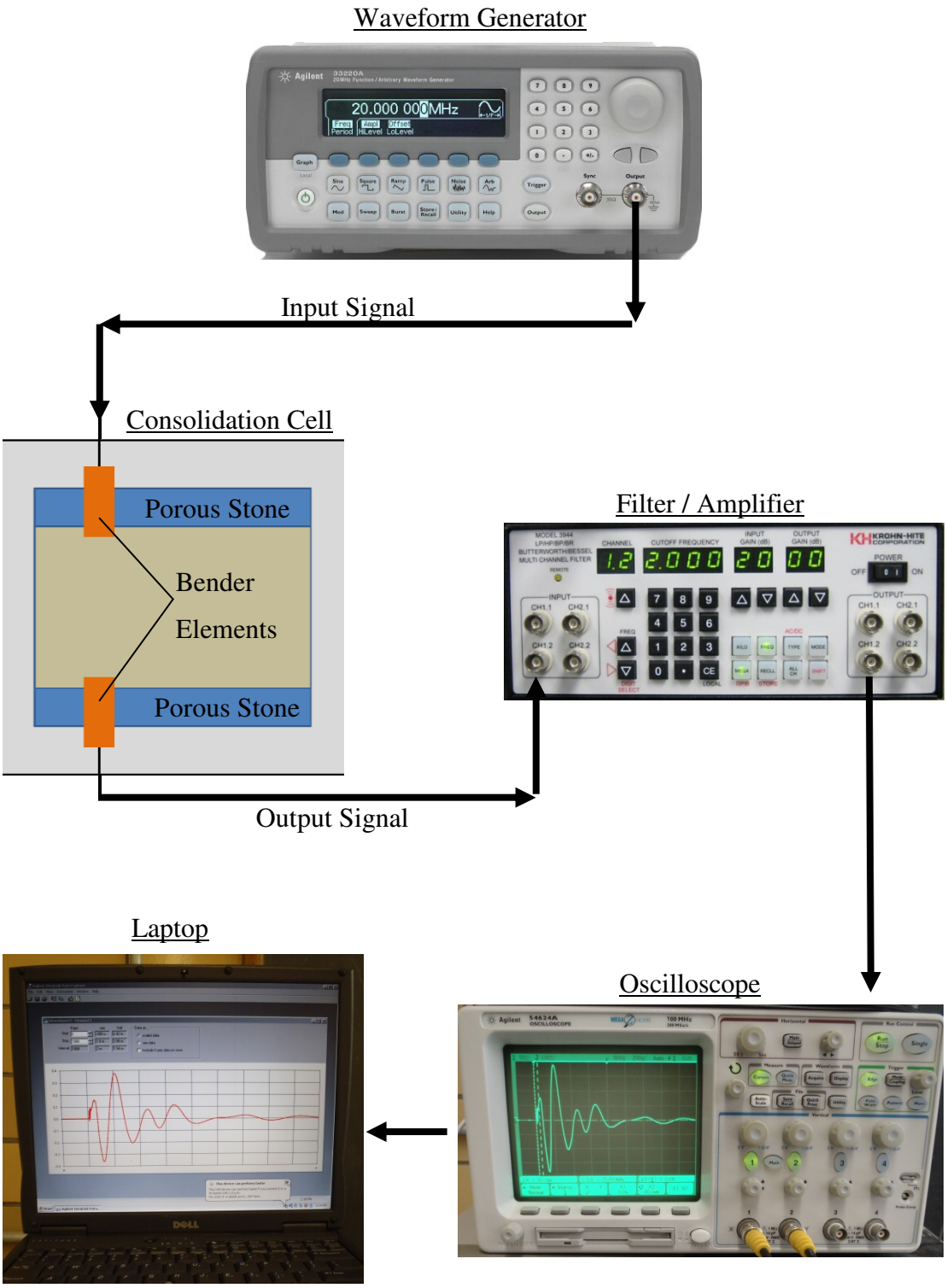


FIG 5.8: Shear wave velocity measurement system: waveform generator, consolidation cell, filter/amplifier, oscilloscope, and laptop

velocity of the material can be calculated by knowing the relationship between these two values (Fernandez 2000; Lee and Santamarina 2005).

5.2.3 Measurements

At the final load increment (24 hours or later, depending on the material of each sample), the shear wave data was recorded with the use of sine waves and square waves as input waves at a display resolution of 500 μs. Each data file output was in the format of a .txt file and included discretized points for an amplitude vs. time relationship. To capture these signals, specific guidelines were used to program the equipment. Several inputs were required for the signal generator and filter/amplifier, including but not limited to: square wave frequency, sine wave frequency, amplitude, and scale. These guidelines were developed in correspondence with Jong-Sub Lee, and were based on previous research (Lee 2003; Lee 2012).

5.2.4 Shear Wave Velocity

The data files obtained from test measurements were then analyzed using Mathcad in order to calculate the first arrival times of the shear waves. The output signals generated often contain complex waveforms, and thus must be broken down into a superposition of simple waveforms through the use of a Fast Fourier Transform (FFT). Through the use of FFT, high frequency noise can be removed, and an Inverse Fast Fourier Transform (IFFT) was used to return the signals to the time domain. Finally, the signals were then normalized with respect to their maximum amplitude to make comparison easier. The end result of these calculations is an

output similar to the example shown in Figure 5.9. In this example, the first signal is a sine input wave, and the remaining signals are the output waves for the entire consolidation test. As shown, the time differential between the input wave and any output wave is proportional to the vertical effective stress being applied. As the stress increases, the time between input and output waves ($t_2 - t_1$) decreases.

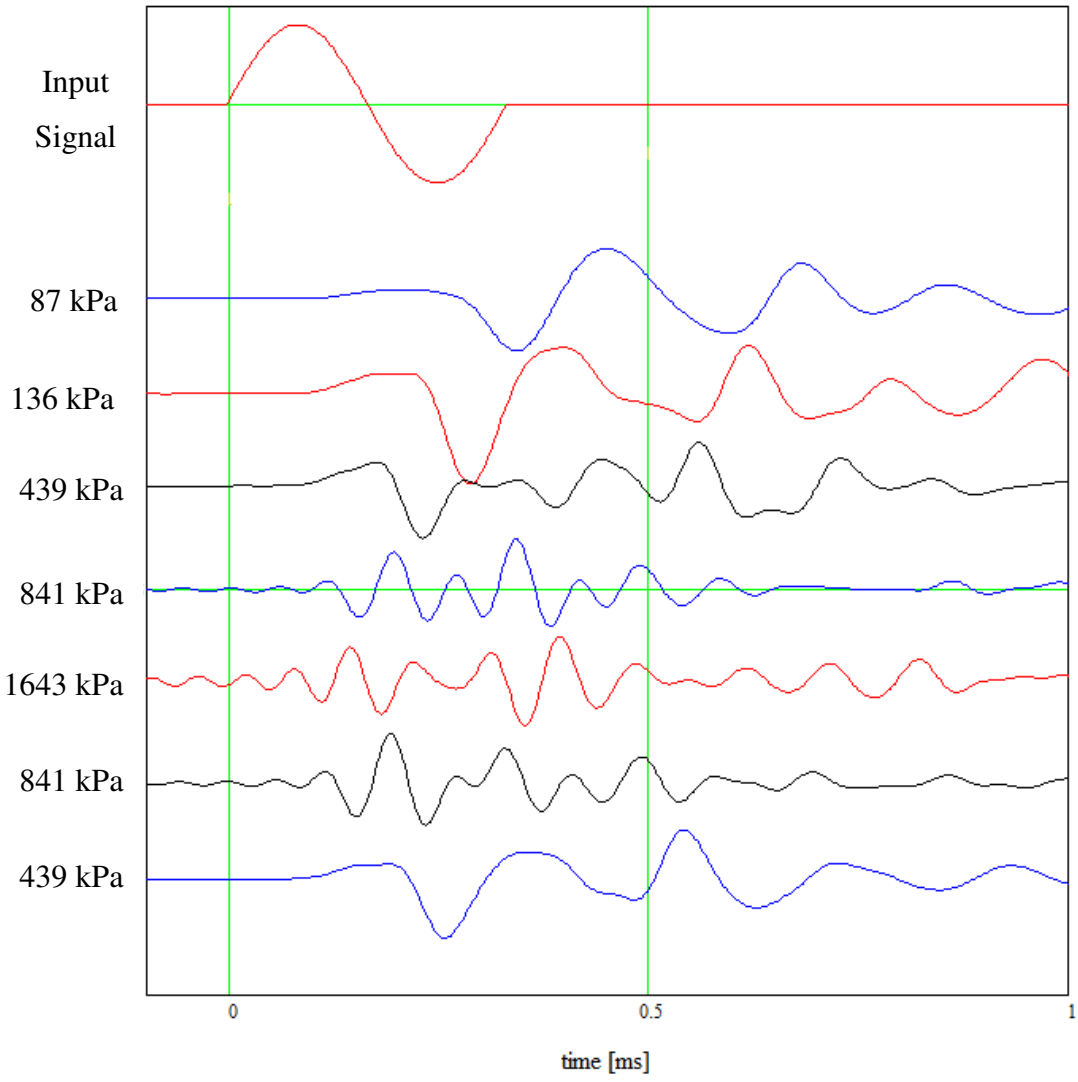


FIG 5.9: Input sine wave and the resulting output signals for each loading of a consolidation test

In addition to the previous example, square waves were also used to calculate the first arrival times of the shear waves. However, the need to use square waves in addition to sine waves was not realized until later in the testing. Therefore, not all samples were analyzed with both sine and square waves. This technique is shown in Figure 5.10, in which the output waves generated from both a sine wave and square wave are used to calculate the first arrival time. Using the output files from both sine and square waves, point 1 is found as the first "dip" in the square wave and the first "peak" in the sine wave. Point 2 is then found at the point where the output from the square wave crosses the x-axis (Amplitude = 0) again. Finally, the blue star denotes the actual first arrival time as an average between points 1 and 2.

The distance between the bender elements can be calculated based on the deformation of the sample and the lengths of the bender elements into the sample.

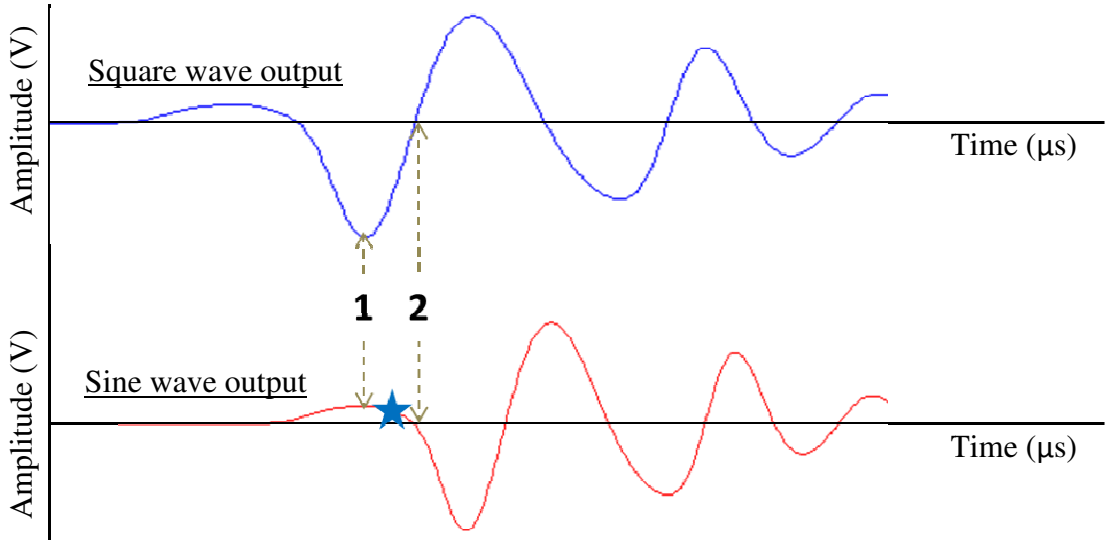


FIG 5.10: First arrival time calculated using both square and sine waves. The resulting first arrival time is denoted using the blue star (Lee 2003; Lee 2012).

The shear wave velocity is calculated based on the first arrival time and the distance between bender elements using Equation 5.5.

5.3 Results

Due to the differing compressibility of kaolinitic and montmorillonitic samples, alternate loading schedules were formulated based upon the general loading schedule found in Table 5.1. Generally for Kt and Kt-PAM samples, loading steps 3-11 were followed, in which the samples were loaded from 87 kPa to 1643 kPa, and then unloaded back to 87 kPa. Some of the unloading steps were skipped to save time; however, at least 3 unloading steps were measured for every sample.

Generally for Mt and Mt-PAM samples, loading steps 1-4 and 12-13 were followed, where loading was applied from 15 kPa to 136 kPa, and then unloaded back to 15 kPa. Some Mt-PAM samples, however, were only loaded to a maximum effective stress of 87 kPa due to the large amount of deformation exhibited by these samples. Loadings greater than 87 kPa were not possible to perform, as the bender elements would approach each other too closely and cause interference with the measurement, i.e. near-field effects were induced. Therefore, comparison between Mt and Mt-PAM materials will be limited to 87 kPa in order to make consistent comparisons between the samples.

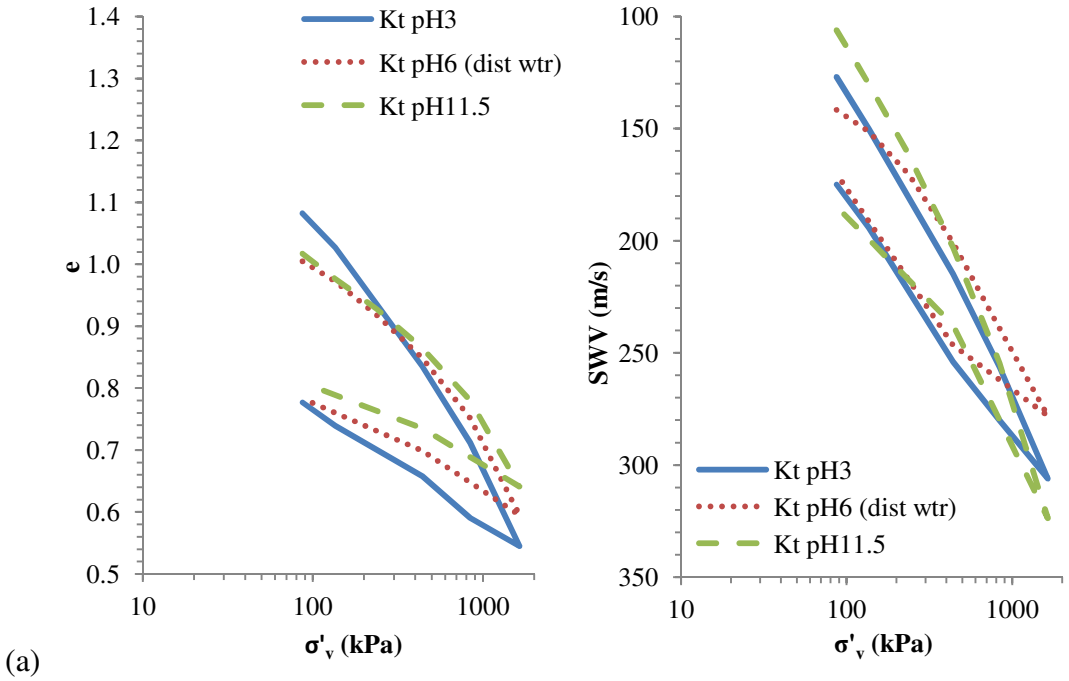
In addition, due to the results of the water content test outlined in Section 3.4, careful considerations must be used when analyzing the consolidation results. Figure 3.4 showed that the samples used in this test could have varying initial void ratios

when extracted from the pre-consolidation tubes. The samples were also saturated at varying pore fluid conditions. The different pH levels and ionic concentrations of the saturating fluid then initiate further void ratio changes to the materials before the test is started, depending on the type of saturating fluid. For these reasons, the samples in the consolidation tests are expected to have differing initial void ratios at the start of the test. Thus, the analysis of these results will take these findings into account, as the samples' initial void ratio will not be directly compared. Instead, changes in void ratio throughout the test will be analyzed.

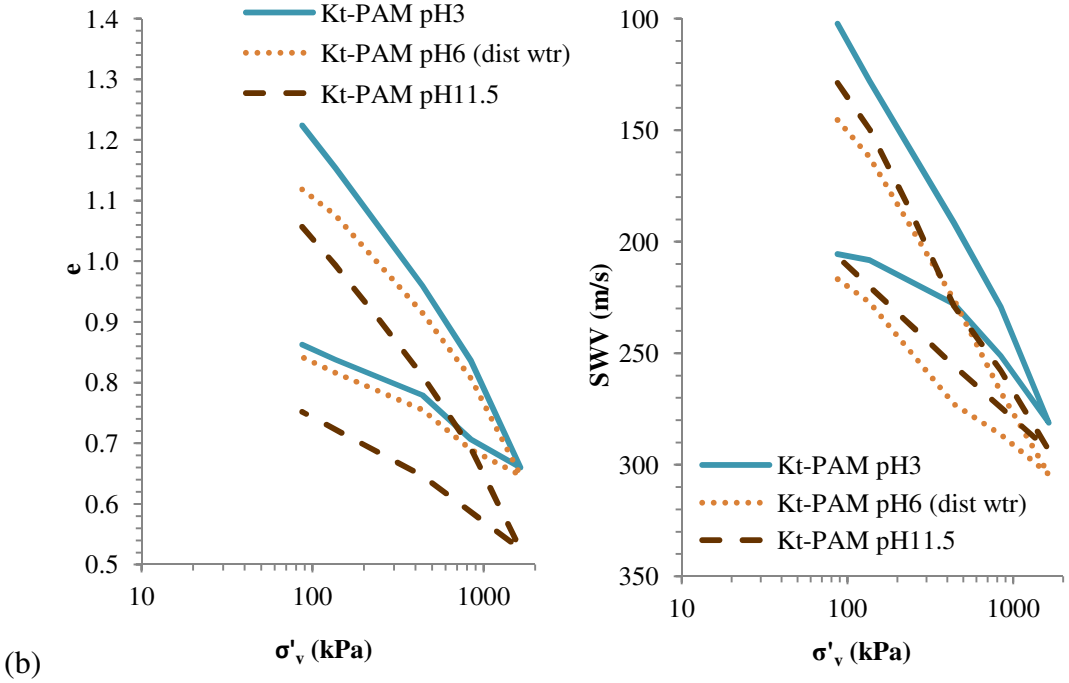
Sections 5.3.1 and 5.3.2 to follow contain notable data and figures extracted from the tests. Only the most relevant data is shown, but a full list of measurements is also included (Appendix B).

5.3.1 Kaolinite (Kt) and Kaolinite Composite (Kt-PAM)

The void ratio and shear wave velocity curves for Kt and Kt-PAM samples tested at varying pH levels (pH 3, 6, 11.5) are shown in Figure 5.11. Figure 5.11(a) highlights the effects that pH has on Kt samples, while Figure 5.11(b) highlights the effects that pH has on Kt-PAM samples. These curves show that depending on the material (Kt, Kt-PAM) or the pH level (3, 6, 11.5), the samples have variations in their void ratio and shear wave velocity. Also shown in Figure 5.12 are the void ratio and shear wave velocity curves for Kt and Kt-PAM samples tested at varying ionic concentrations (distilled water, 0.3M NaCl). Figure 5.12(a) highlights the effects that ionic concentration has on Kt samples, while Figure 5.12(b) highlights the effects that ionic concentration has on Kt-PAM samples. In these plots, variations in void ratio

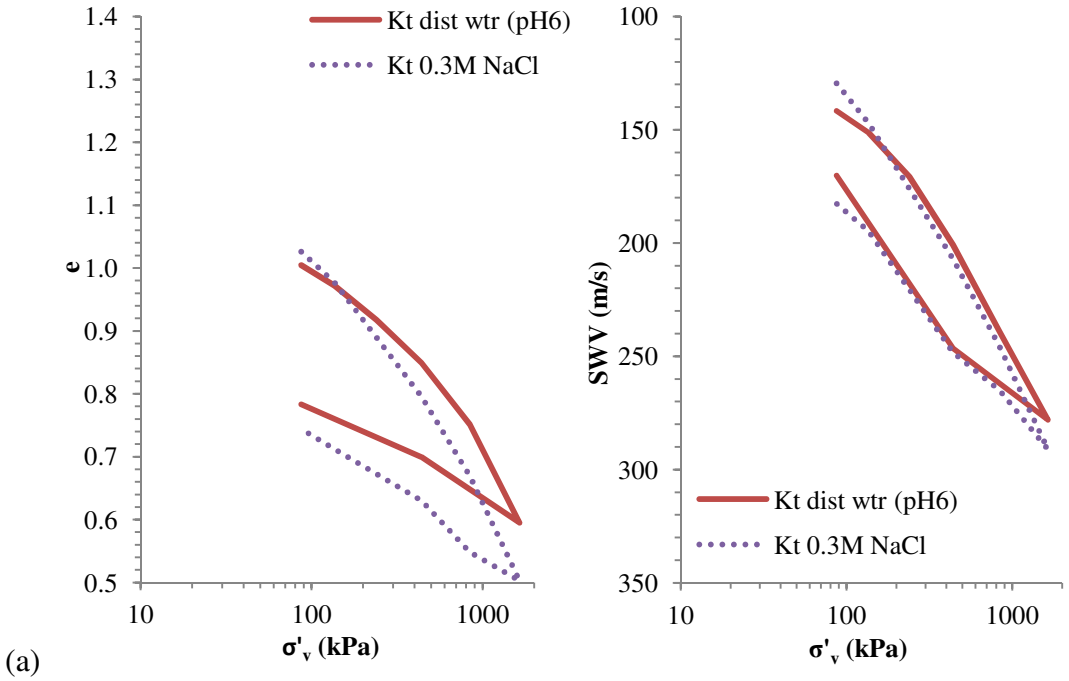


(a)

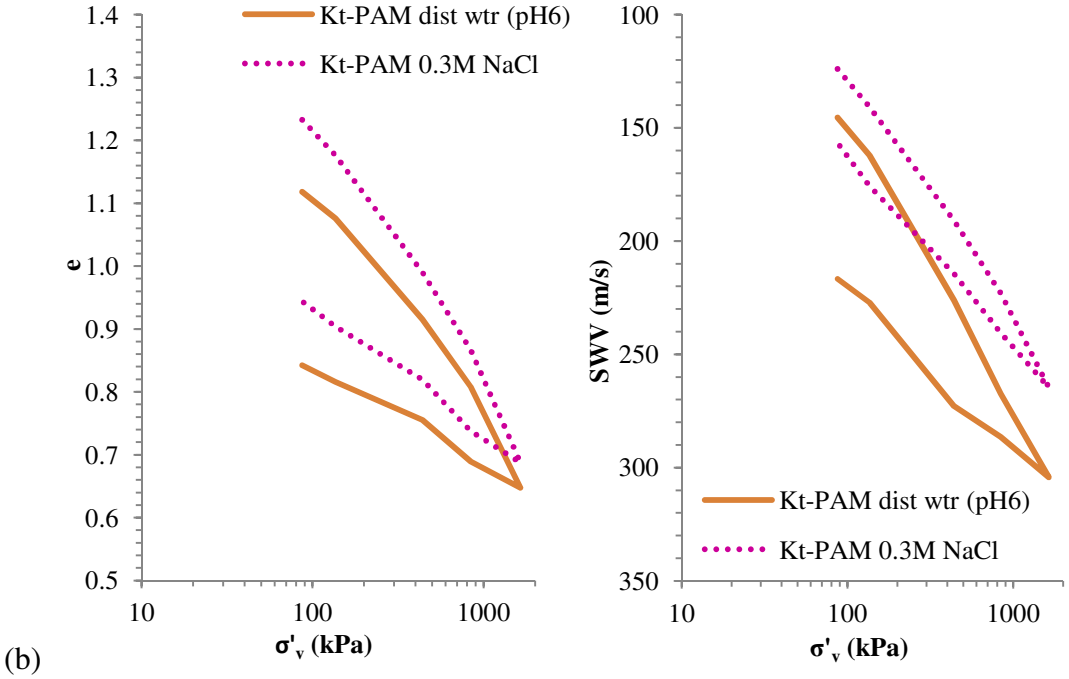


(b)

FIG 5.11: Void ratio and shear wave velocity curves showing the effects of pH for (a) Kt samples and (b) Kt-PAM samples



(a)



(b)

FIG 5.12: Void ratio and shear wave velocity curves showing the effects of ionic concentration for (a) Kt samples and (b) Kt-PAM samples

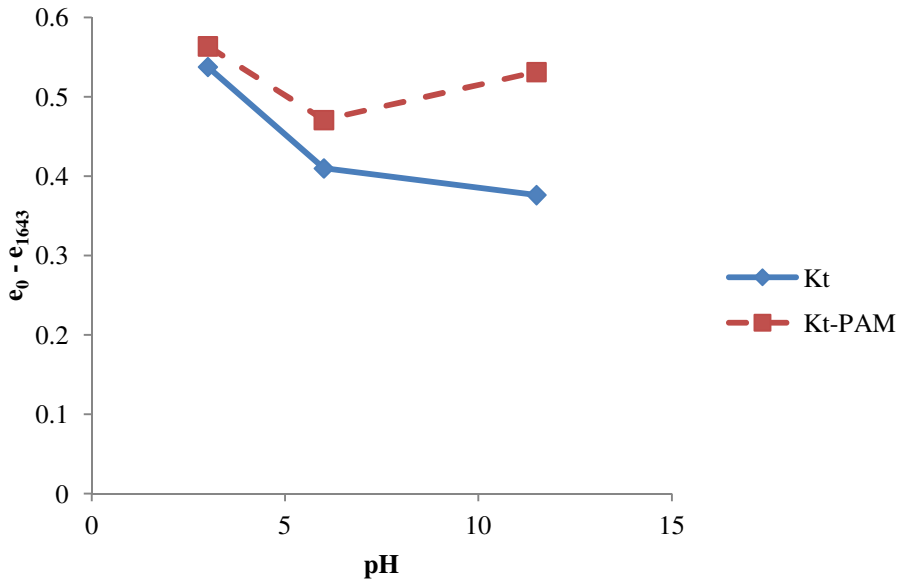
and shear wave velocity are again seen. Therefore, these plots also show that the samples behave differently depending on the material and ionic concentration.

Further detail into the consolidation and stiffness behavior of these materials can be seen when analyzing the void ratio and shear wave velocities throughout the test. These values for Kt and Kt-PAM samples throughout the test are shown in Table 5.3. In this table, e_0 is the void ratio before the first loading (after saturation), e_{1643} is the void ratio at the end of the maximum load of 1643 kPa, and e_f is the void ratio at end of the test (after the last unloading stage). Also, SWV_{87} is the shear wave velocity at the end of the 87kPa loading stage, SWV_{1643} is the shear wave velocity at the end of the maximum load of 1643 kPa, and SWV_f is the shear wave velocity at the end of the test (after the last unloading stage). These points were selected for comparison to show how void ratio and shear wave velocity change throughout the loading stages ($e_0 - e_{1643}$) and unloading stages ($e_{1643} - e_f$). Note that e_0 is a comparison before the first loading of 87 kPa and SWV_{87} is a comparison after the first loading of 87 kPa. The shear wave velocities were compared at this time, as the signals are not easily detected before this load.

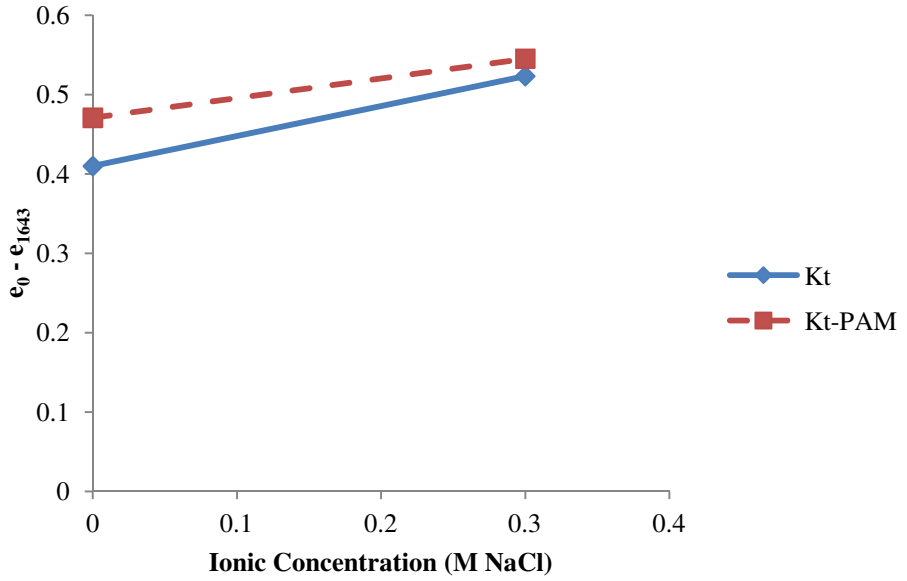
Corresponding figures show the change in void ratio up to the maximum load, change in void ratio during unloading, and shear wave velocities at different stages of the test in Figures 5.13, 5.14, and 5.15, respectively. In Figure 5.13, the effects of pH and ionic concentration on the change in void ratio up to the maximum load for Kt and Kt-PAM samples are shown. The Kt-PAM samples are shown to have a larger decrease in their void ratio during loading as compared to the Kt samples. Also,

TABLE 5.3: Void ratio and shear wave velocity results for Kt & Kt-PAM samples under varying pore fluid conditions

Sample	e_0	e_{1643}	e_f	$e_0 - e_{1643}$	$e_f - e_{1643}$	SWV_{87}	SWV_{1643}	SWV_f
Kt pH3	1.47	0.54	0.78	0.92	0.23	127.0	306.0	174.9
Kt pH6	1.17	0.59	0.78	0.58	0.19	141.7	278.1	170.2
Kt pH11.5	1.25	0.64	0.81	0.61	0.17	106.1	323.7	184.8
Kt 0.3M NaCl	1.36	0.50	0.74	0.86	0.24	129.5	291.0	182.7
Kt-PAM pH3	1.33	0.66	0.86	0.67	0.20	102.4	281.1	205.6
Kt-PAM pH6	1.28	0.65	0.84	0.64	0.19	145.4	304.2	216.7
Kt-PAM pH11.5	1.42	0.53	0.75	0.90	0.23	128.8	293.5	206.7
Kt-PAM 0.3M NaCl	1.42	0.69	0.94	0.73	0.26	124.0	264.5	156.7



(a)



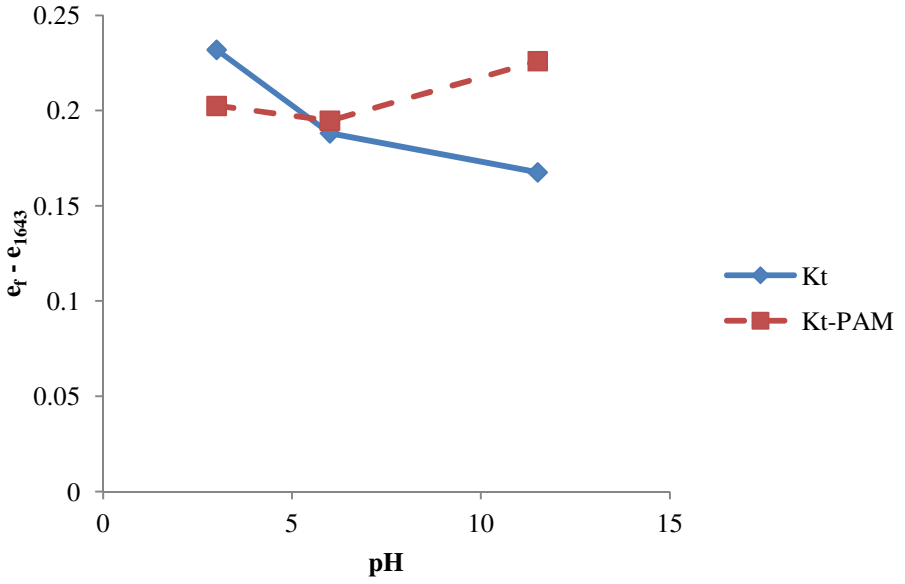
(b)

FIG 5.13: Change in void ratio from start of test to maximum loading of 1643 kPa for Kt and Kt-PAM under varying (a) pH levels and (b) ionic concentrations

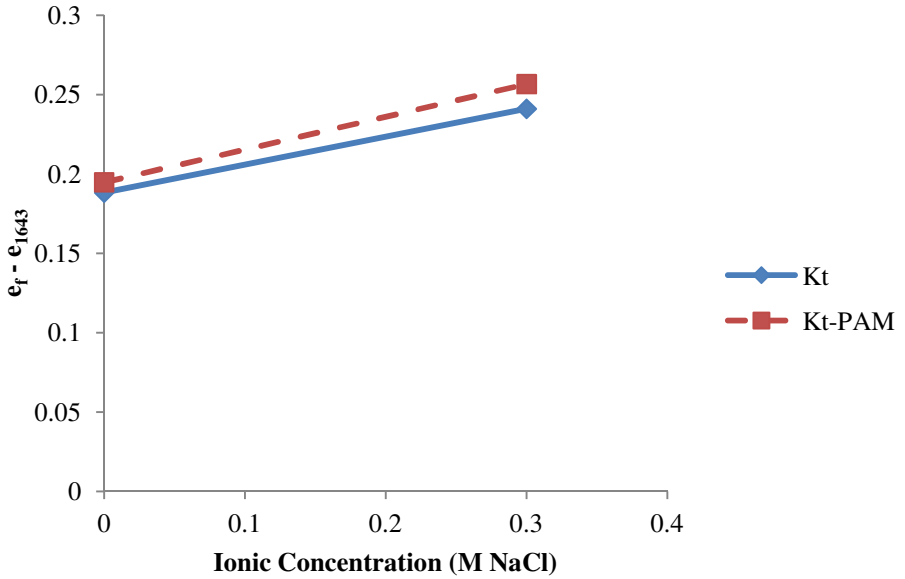
Figure 5.13(a) shows that with increasing pH level, the composites show larger changes in void ratio than the control samples. Figure 5.13(b) shows that with decreasing ionic concentration, the composites again show larger changes in void ratio than the control samples.

Figure 5.14 compares the same conditions but with respect to the change in void ratio during unloading. In these plots, the Kt-PAM samples do not always show a higher change in void ratio than the Kt samples. However, Figure 5.14(a) shows that with increasing pH level, the composite materials show increasingly greater changes in void ratio as compared to the control samples. This is the same trend shown in Figure 5.13(a). Figure 5.14(b) shows that the composites have greater changes in void ratio again, but only slightly more than the control samples.

Figure 5.15 shows the shear wave velocities of these materials throughout the test at the given loading conditions. Both Kt and Kt-PAM samples have lower shear wave velocities at the beginning of the test (load of 87 kPa). At the maximum load of 1643 kPa, the shear wave velocities are the highest. Upon the final unloading (87 kPa), the shear wave velocities rebound to values between the initial and maximum loadings of the test. This shows the plastic component of these materials, as their stiffness is shown to increase during the test but not fully recover to the initial values. Also, Figures 5.15(a) and 5.15(b) do not show any trends with regard to sample type or pore fluid condition. The addition of polymers or change in pore fluid is not shown to affect the stiffness of these materials in any significant way.

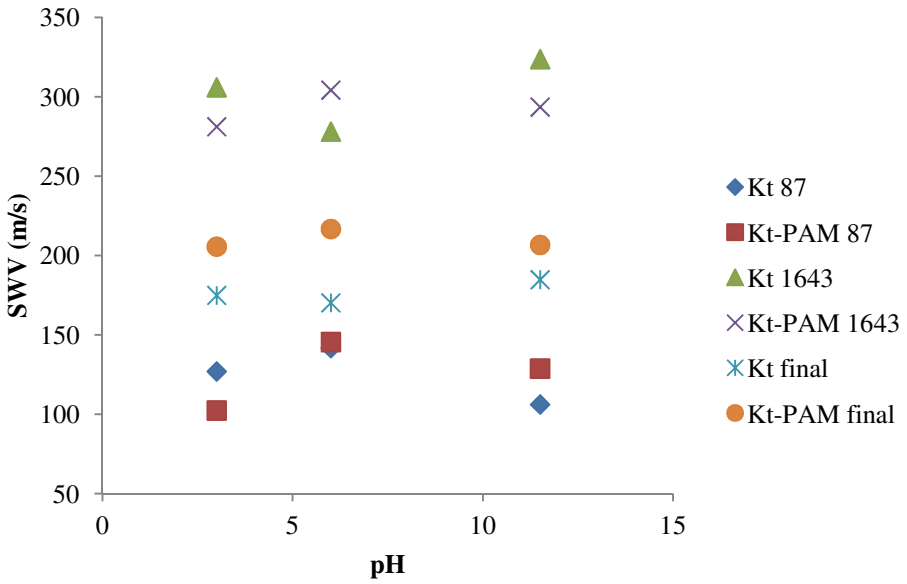


(a)

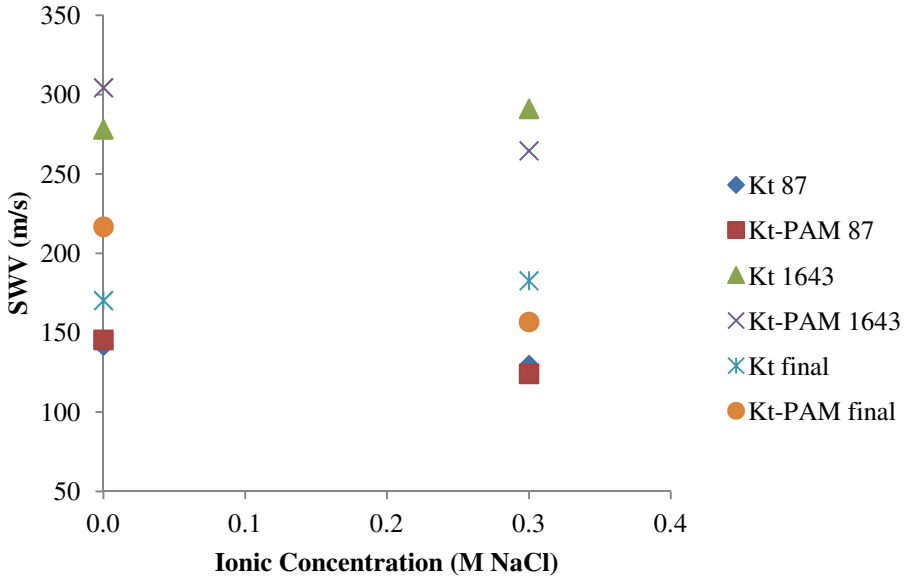


(b)

FIG 5.14: Change in void ratio from maximum loading of 1643 kPa to end of test (after final unloading of 87 kPa) for Kt and Kt-PAM under varying (a) pH levels and (b) ionic concentrations



(a)



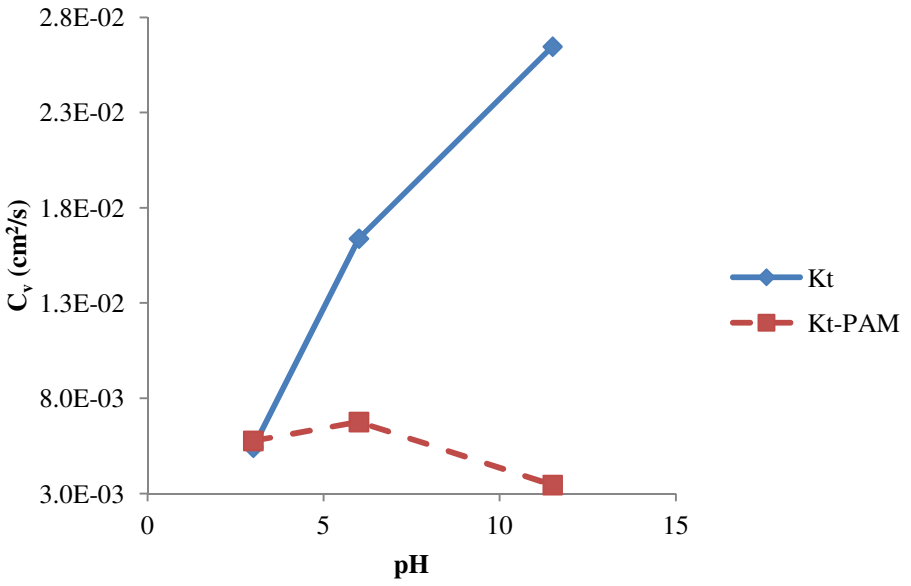
(b)

FIG 5.15: Shear wave velocities measured at the initial load of 87 kPa, maximum load of 1643 kPa, and at the end of the test (after final unloading of 87 kPa) for Kt and Kt-PAM under varying (a) pH levels and (b) ionic concentrations

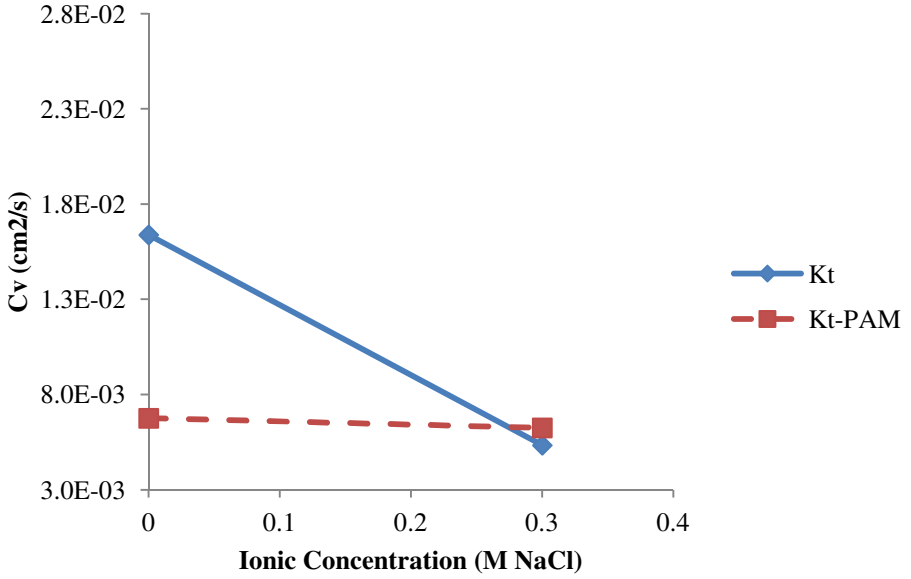
In addition, the coefficient of consolidation was calculated for each sample, and the values are plotted in Figure 5.16. (A complete list of these values is also included in Appendix B). Figure 5.16(a) shows the effects of pH on Kt and Kt-PAM samples, while Figure 5.16(b) shows the effects of ionic concentration on Kt and Kt-PAM samples. The Kt samples tend to exhibit a higher coefficient of consolidation, with minor exceptions. There is no significant difference between the Kt and Kt-PAM samples in this parameter at pH 3 and 0.3M NaCl. As seen previously in Figures 5.13 and 5.14, there is an observable trend. As the pH increases or as the ionic concentration decreases, the composite materials show larger changes in C_v when compared with the control samples.

The compression index and recompression index summary plots are shown in Figures 5.17 and 5.18, respectively. (A complete list of these values is also included in Appendix B). When comparing the Kt and Kt-PAM samples, it is observed that the Kt-PAM samples have higher values for C_c regardless of the pore fluid condition. Also, the same trends are seen as before, i.e. C_c values for Kt-PAM increase with increasing pH and decreasing ionic concentration relative to Kt.

Kt-PAM samples also have higher values for C_r, with the exception of the pH 3 condition. As the pH level increases, the composite materials show larger changes in C_r when compared with the control samples. Again, this is the same trend where increasing pH leads to higher values of C_r for the composite materials. However, this trend is not as clear when looking at the effects of ionic concentration shown in Figure 5.18(b). Kt-PAM samples have higher C_r values than Kt samples, but the 0M

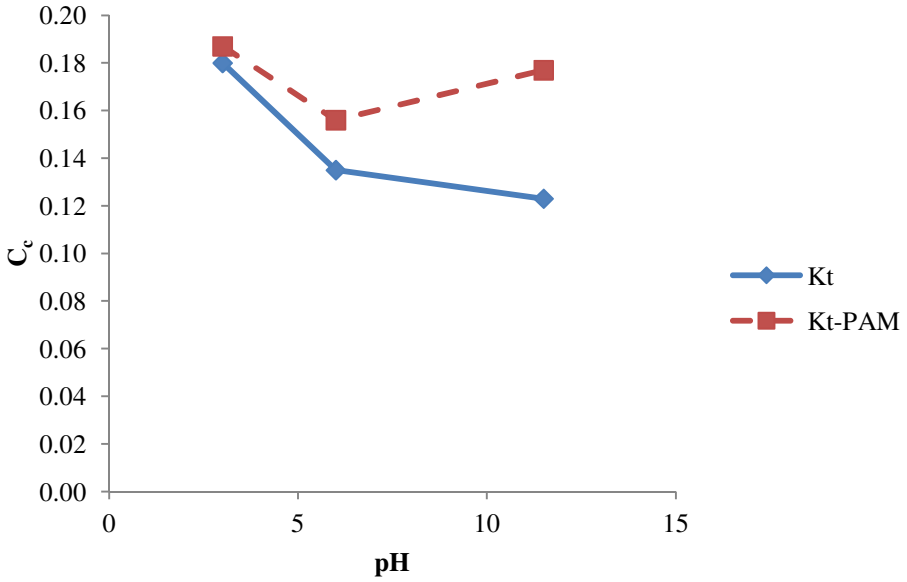


(a)

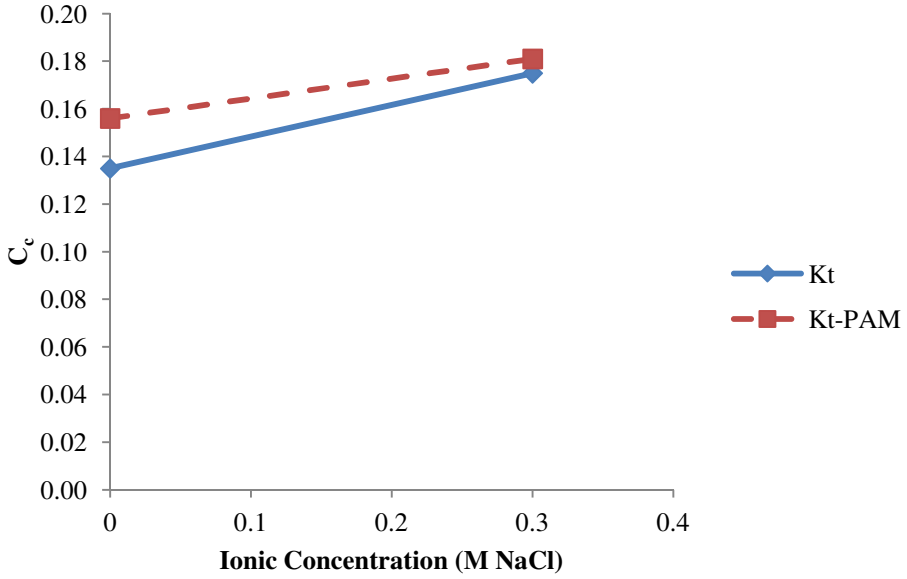


(b)

FIG 5.16: Coefficient of consolidation results for Kt and Kt-PAM under varying (a) pH levels and (b) ionic concentrations

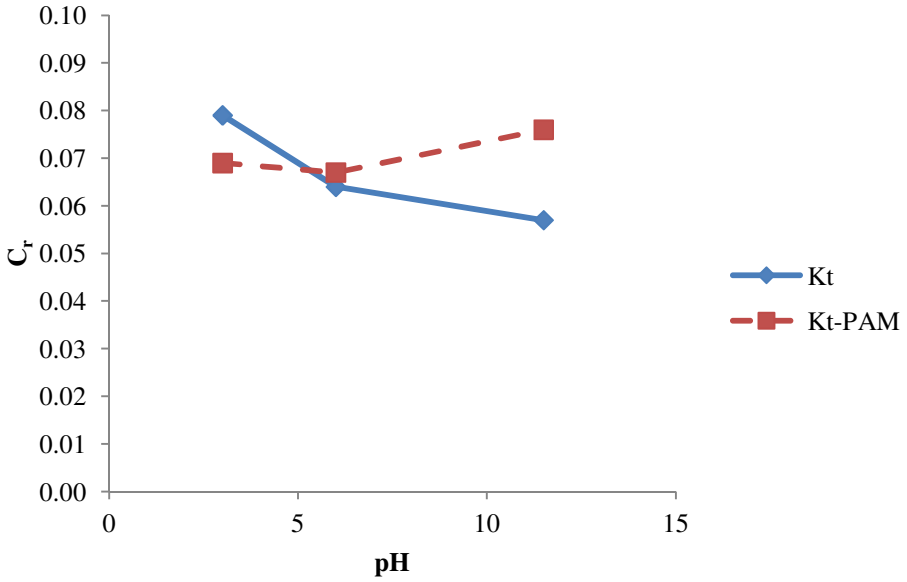


(a)

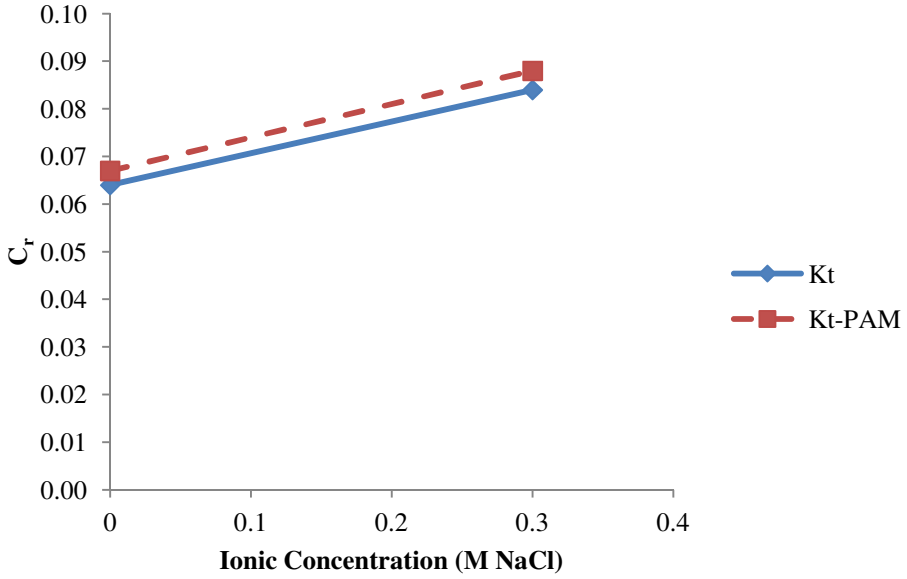


(b)

FIG 5.17: Compression index results for Kt and Kt-PAM under varying (a) pH levels and (b) ionic concentrations



(a)



(b)

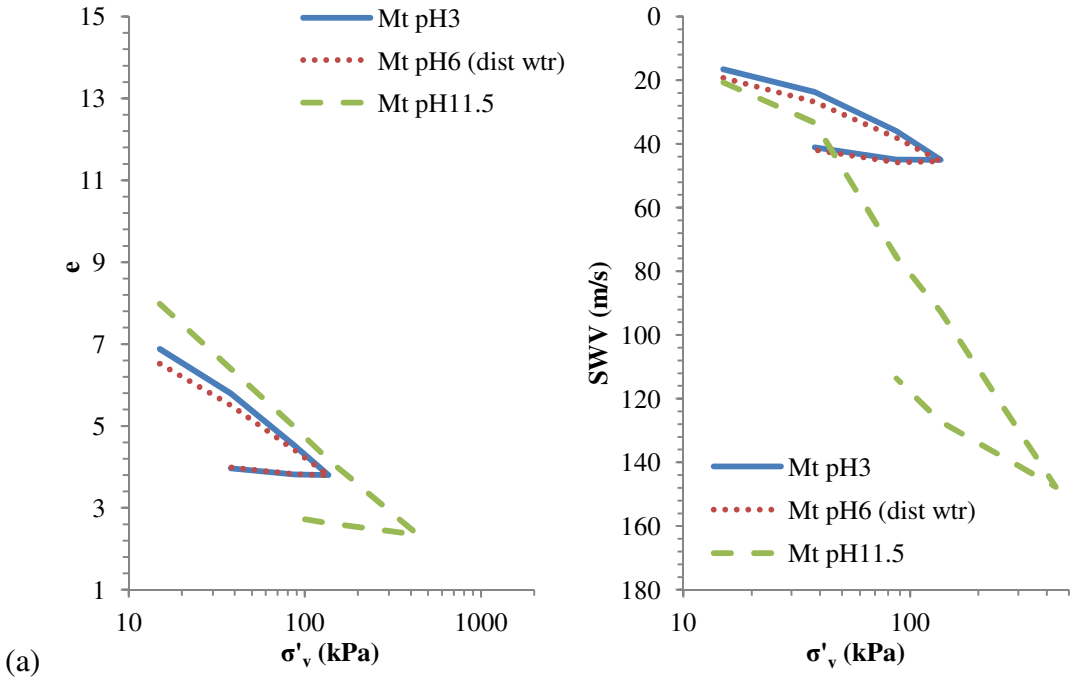
FIG 5.18: Recompression index results for Kt and Kt-PAM under varying (a) pH levels and (b) ionic concentrations

NaCl condition does not show a significantly greater change than the 0.3M NaCl condition.

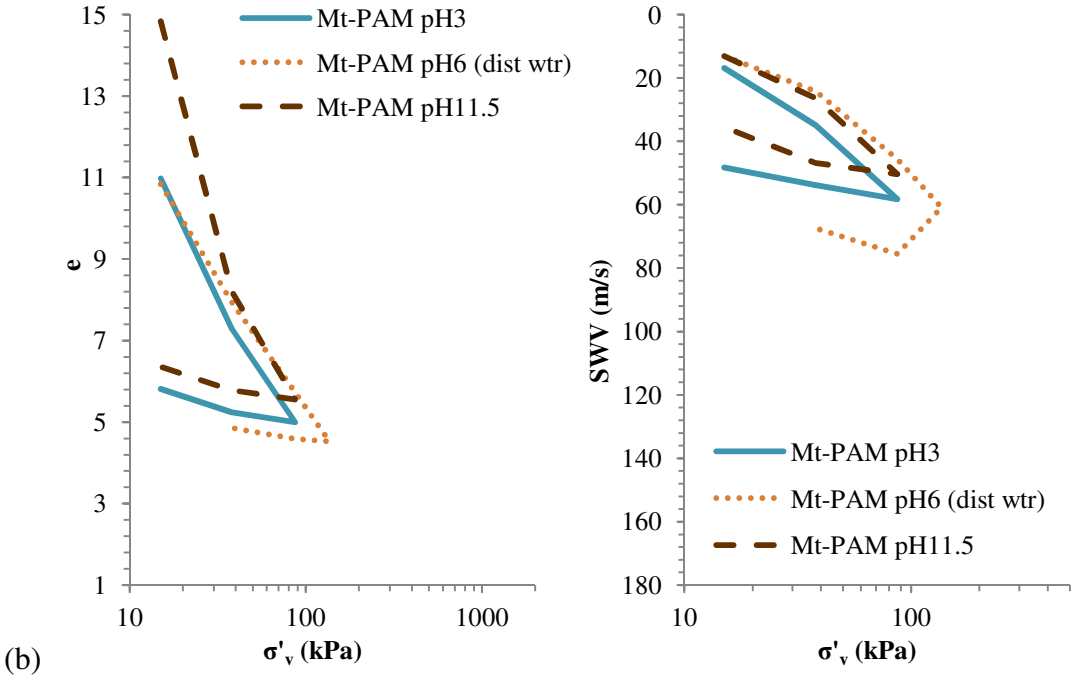
5.3.2 Montmorillonite (Mt) and Montmorillonite Composite (Mt-PAM)

The void ratio and shear wave velocity curves for Mt and Mt-PAM samples tested at varying pH levels (pH 3, 6, 11.5) are shown in Figure 5.19. Figure 5.19(a) highlights the effects that pH has on Mt samples, while Figure 5.19(b) highlights the effects that pH has on Mt-PAM samples. It must first be noted that two samples from this data (Mt pH11.5 and Mt 0.3M NaCl) were taken to much higher maximum effective stresses than the other samples. This led to a large amount of sample deformation, in which the bender elements became very close to one another during the test. This led to erratic measurements of shear wave velocity for these materials due to near-field effects, as can be seen in Figures 5.19 and 5.20. In the interest of time, these samples were unable to be retested, and the results will be presented with this fact in mind.

When comparing these samples to the plots as seen in Section 5.3.1, it can again be seen that these curves show that depending on the material (Mt, Mt-PAM) or the pH level (3, 6, 11.5), the samples have variations in their void ratio and shear wave velocity. In Figure 5.20, the void ratio and shear wave velocity curves for Mt and Mt-PAM samples tested at varying ionic concentrations (distilled water, 0.3M NaCl) are shown. Figure 5.20(a) highlights the effects that ionic concentration has on Mt samples, while Figure 5.20(b) highlights the effects that ionic concentration has on Mt-PAM samples. In these plots, variations in void ratio and shear wave velocity



(a)



(b)

FIG 5.19: Void ratio and shear wave velocity curves showing the effects of pH for (a) Mt samples and (b) Mt-PAM samples

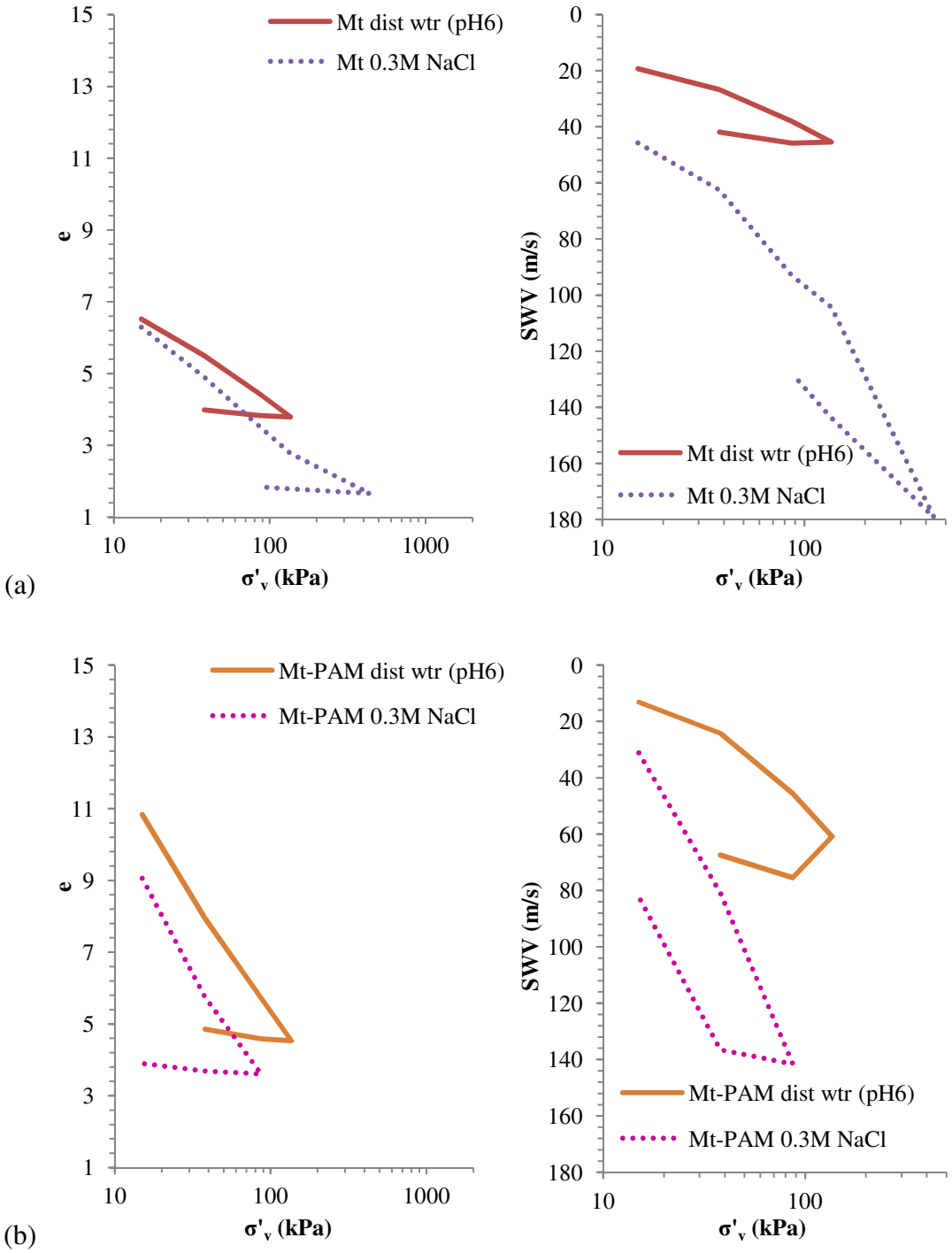


FIG 5.20: Void ratio and shear wave velocity curves showing the effects of ionic concentration for (a) Mt samples and (b) Mt-PAM samples

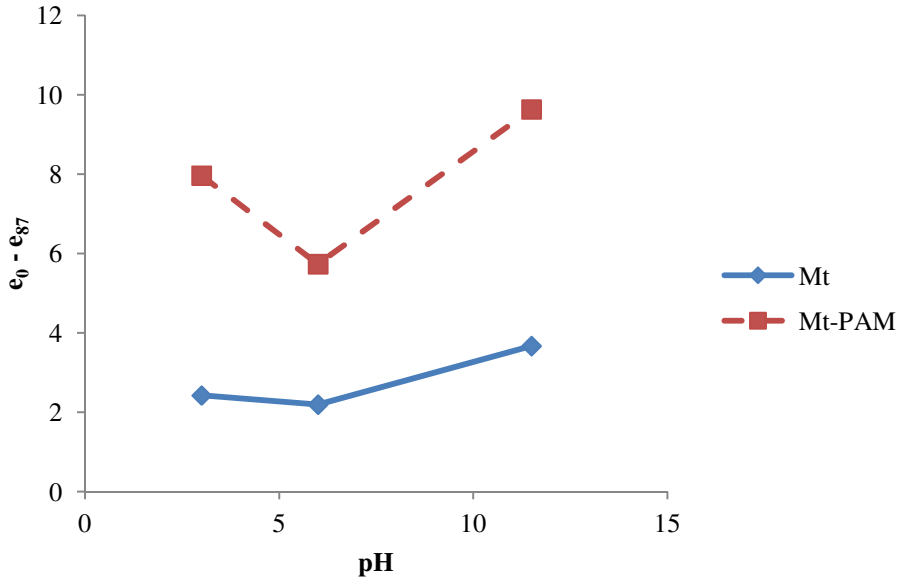
are again seen. Therefore, these plots also show that the samples behave differently depending on the material and ionic concentration.

The void ratios and shear wave velocities throughout the test are also included in Table 5.4. In this table, e_0 is the void ratio before the first loading (after saturation) and e_{87} is the void ratio at the end of the maximum load of 87 kPa. Note that the void ratio will not be compared at the end of the test, as the samples were loaded to different values of maximum effective stress. Therefore, only valid comparisons can be made up to the effective stress of 87 kPa. Also in Table 5.4, SWV_{15} is the shear wave velocity at the end of the 15 kPa loading stage and SWV_{87} is the shear wave velocity at the end of the maximum load of 87 kPa. These points were selected for comparison to illustrate the relationship between void ratio and shear wave velocity throughout a comparable portion of the loading stages ($e_0 - e_{87}$). Note that e_0 is a comparison before the first loading of 15 kPa and SWV_{15} is a comparison after the first loading of 15 kPa.

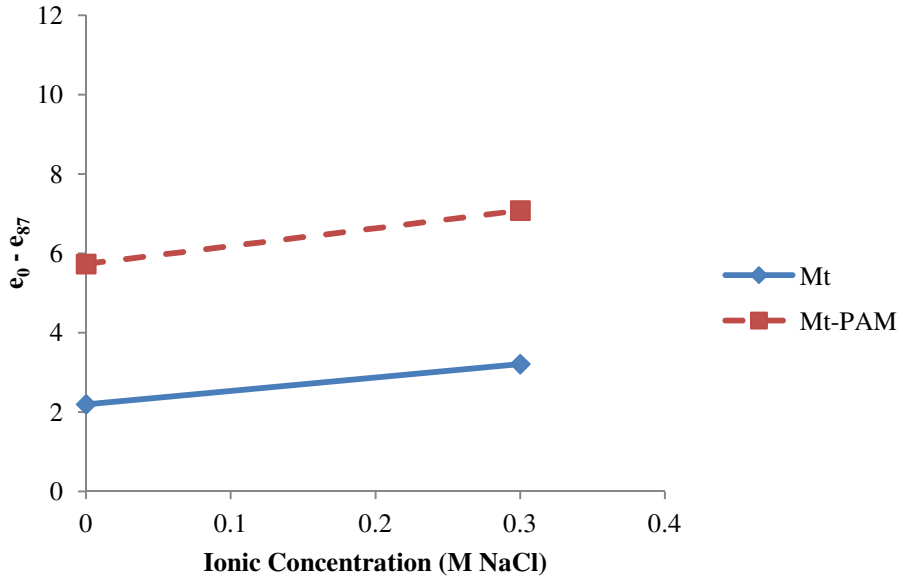
The change in void ratio up to the maximum load of 87 kPa and shear wave velocities up to this same load are presented in Figures 5.21 and 5.22, respectively. In Figure 5.21, the effects of pH and ionic concentration on the change in void ratio up to the maximum load for Mt and Mt-PAM samples are shown. The Mt-PAM samples are shown to have a much larger decrease in their void ratio during loading as compared to the Mt samples. Figure 5.21(a) shows that at a low or high pH level, the composites show larger changes in void ratio than at pH 6. Figure 5.21(b) does not show a significant trend between ionic concentration and changing void ratios.

TABLE 5.4: Void ratio and shear wave velocity results for Mt & Mt-PAM samples under varying pore fluid conditions

Sample	e_0	e_{87}	$e_0 - e_{87}$	SWV_{15}	SWV_{87}
Mt pH3	6.95	4.53	2.42	16.5	35.9
Mt pH6	6.61	4.42	2.19	19.3	38.1
Mt pH11.5	8.65	4.98	3.67	20.7	75.4
Mt 0.3M NaCl	6.71	3.50	3.21	45.7	93.1
Mt-PAM pH3	12.96	5.00	7.96	16.9	58.3
Mt-PAM pH6	11.46	5.72	5.73	13.1	45.6
Mt-PAM pH11.5	15.19	5.56	9.63	13.1	50.3
Mt-PAM 0.3M NaCl	10.69	3.61	7.07	31.1	141.6



(a)

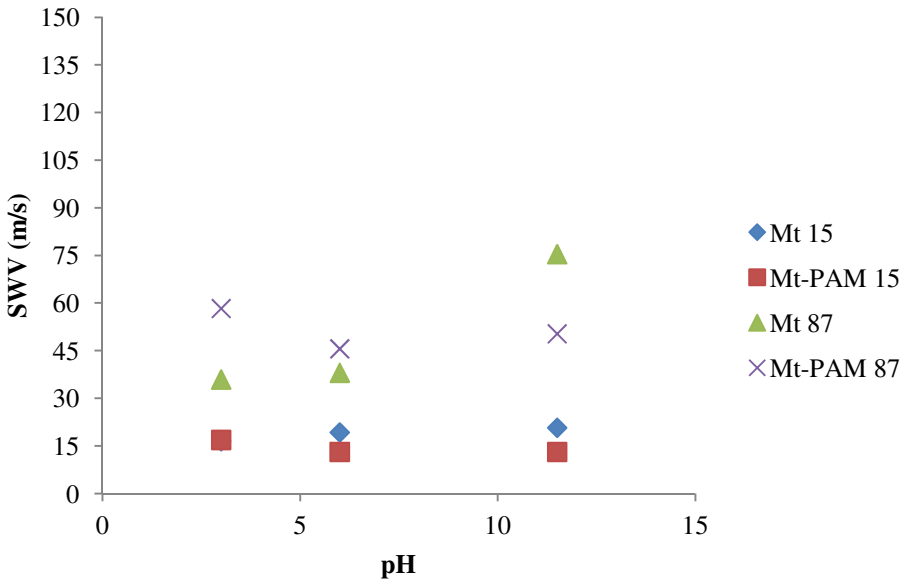


(b)

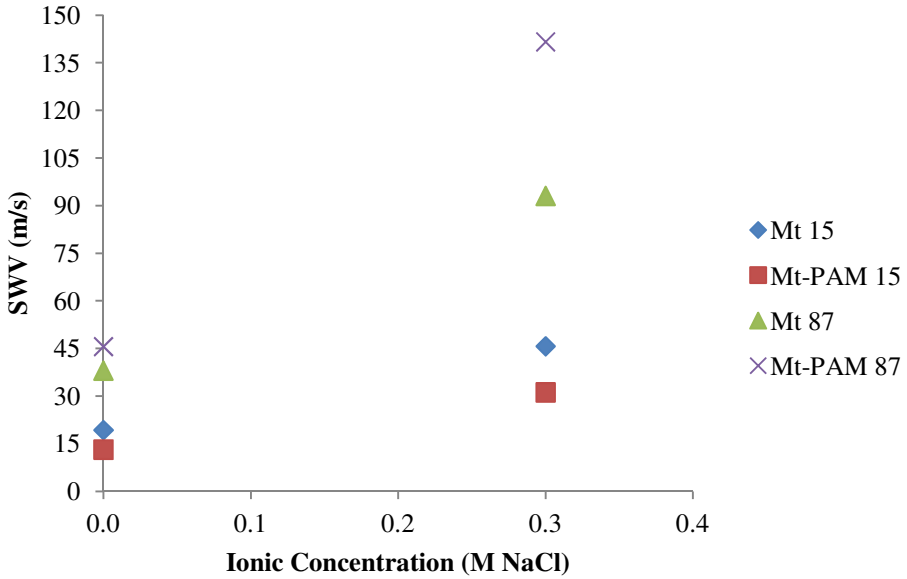
FIG 5.21: Change in void ratio from start of test to maximum loading of 87 kPa for Mt and Mt-PAM under varying (a) pH levels and (b) ionic concentrations

Figure 5.22 shows the shear wave velocities of these materials throughout the test. As seen before, the shear wave velocities are shown to be lower at 15 kPa effective stress than at 87 kPa effective stress. Also, the control samples have consistent shear wave velocity values as the composite samples at the same effective stress values. In Figure 5.22(a), there is no distinguishable trend between sample type or pH level. However, in Figure 5.22(b), it appears that with increasing ionic concentration there is an increase in shear wave velocity for both Mt and Mt-PAM samples.

The coefficient of consolidation results are shown in Figure 5.23. (A complete list of these values is given in Appendix B). Figure 5.23(a) shows the effects of pH on Mt and Mt-PAM samples, while Figure 5.23(b) shows the effects of ionic concentration on Mt and Mt-PAM samples. These results are in contrast to the results shown with the kaolinitic samples. In Section 5.3.1, the coefficient of consolidation was at least the same or higher for Kt samples versus Kt-PAM samples. Mt samples exhibit a higher coefficient of consolidation than that of Mt-PAM samples, but only at low pH and low ionic concentration. However, as shown in Figure 5.23(a), the coefficient of consolidation greatly increases with increasing pH for the Mt-PAM samples. Based on Figure 5.23(b), there appears to be no significant difference between Mt and Mt-PAM at varying ionic concentration.

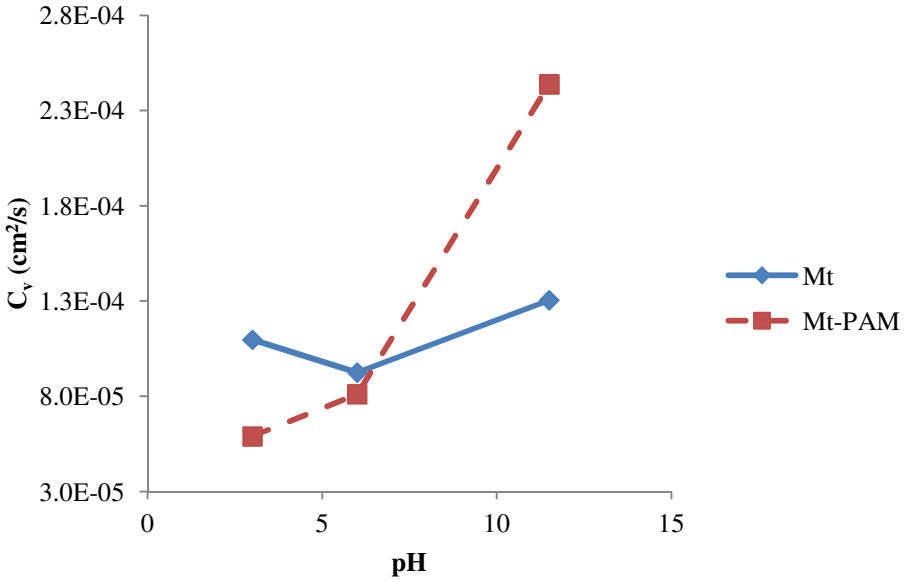


(a)

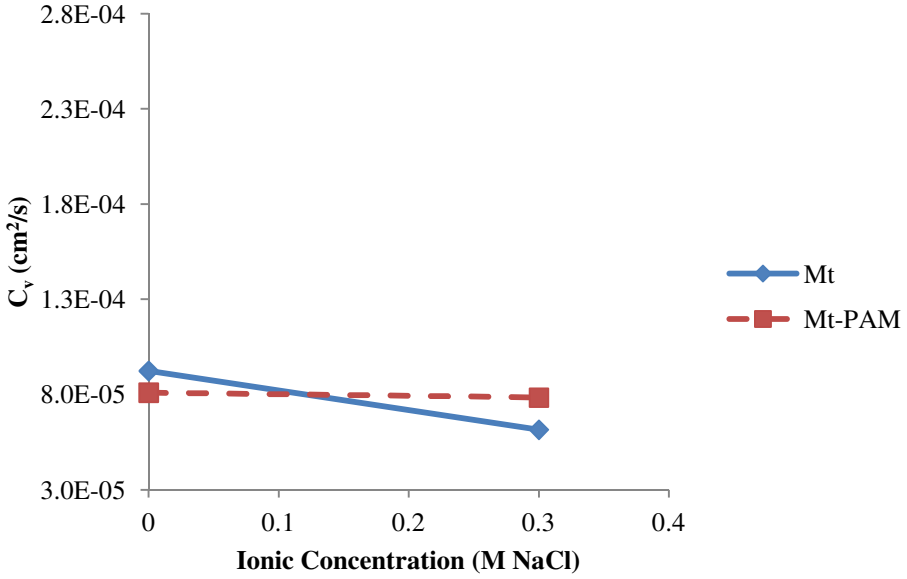


(b)

FIG 5.22: Shear wave velocities measured at the initial load of 15 kPa and maximum load of 87 kPa for Mt and Mt-PAM under varying (a) pH levels and (b) ionic concentrations



(a)



(b)

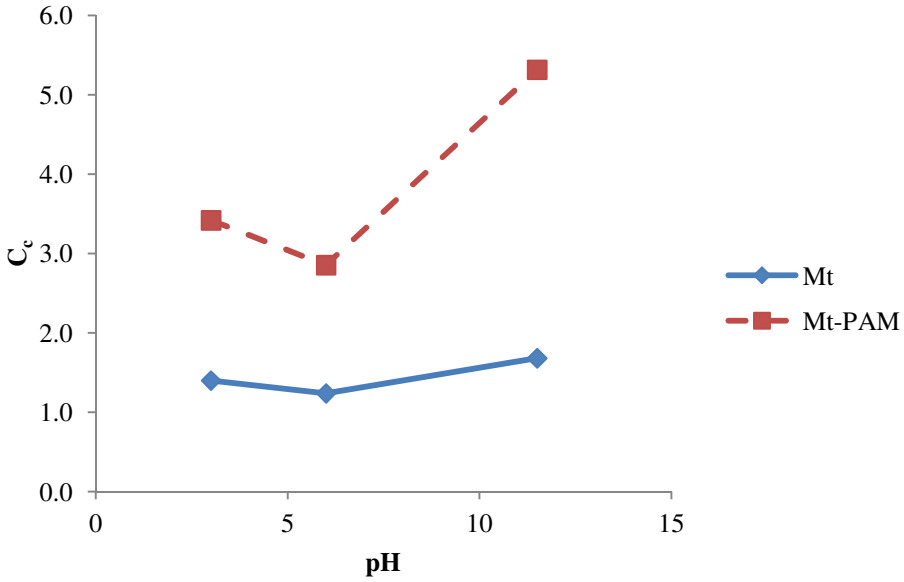
FIG 5.23: Coefficient of consolidation results for Mt and Mt-PAM under varying (a) pH levels and (b) ionic concentrations

The compression index and recompression index summary plots are shown in Figures 5.24 and 5.25, respectively. (A complete list of these values is provided in Appendix B). Consistent with the results for the kaolinitic samples, the C_c and C_r values are higher for the Mt-PAM samples than the Mt samples. This conclusion is consistent regardless of the pore fluid condition. However, there does not appear to be a relationship between C_c and C_r and increasing levels of pH or ionic concentration.

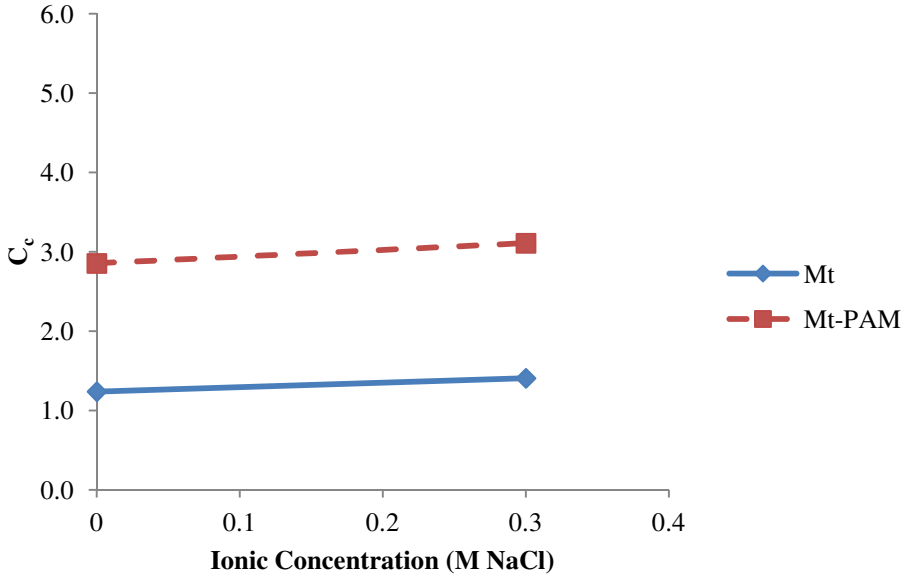
5.4 Discussion of Results

Figure 5.13, 5.14, and 5.21 show void ratio changes with the addition of polymer to the different types of clay. For both kaolinite-based samples and montmorillonite-based samples, larger changes in void ratio were observed throughout the test with the addition of polymers. Since the composite samples experienced higher change in their void ratios, it can be concluded that these materials are more compressible.

Montmorillonite-based materials showed higher changes in void ratios, but there was not a clear trend linking pore fluid conditions to these changes. For the kaolinite-based materials, increasing pH and decreasing ionic concentration resulted in an increase in the compressibility of these materials. From a micro-scale perspective, it was shown that high pH and low ionic concentration induce an extended conformation in materials that contained polymers (see Figure 2.8). The results from this study showed an increase in the compressibility of these

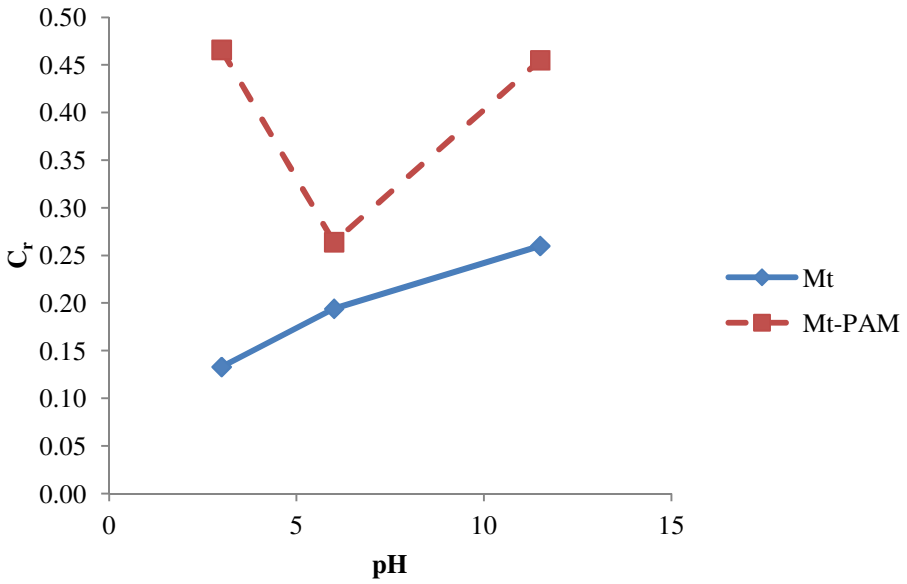


(a)

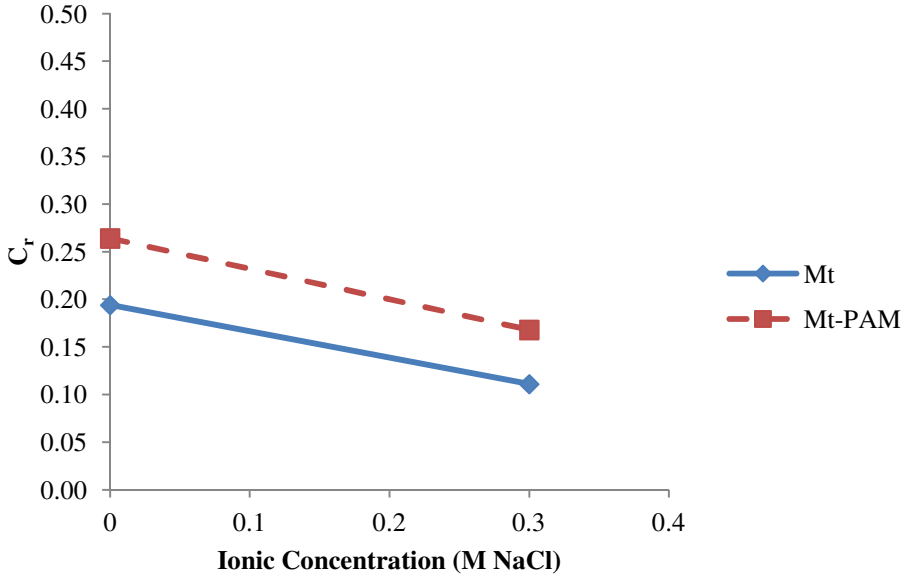


(b)

FIG 5.24: Compression index results for Mt and Mt-PAM under varying (a) pH levels and (b) ionic concentrations



(a)



(b)

FIG 5.25: Recompression index results for Mt and Mt-PAM under varying (a) pH levels and (b) ionic concentrations

materials at these same pore fluid conditions; therefore, an extended polymer conformation increases the compressibility of these materials. This could be attributed to the orientation and spacing of the composites under these conditions. It appears that a polymer that adopts a coiled conformation is "stiffer" than a polymer that adopts an extended conformation. Referencing Figure 2.8, the spacing between the clay particles is also shown to increase with increasing pH and decreasing ionic concentration. Therefore, the potential for compressibility could be increased for these same conditions, as the particles could travel further distances during compression.

This hypothesis can also be applied to the results from the coefficient of consolidation. This parameter is an indicator of how quickly water can be expelled from the particulate system, and thus, the time required for consolidation to take place. The Kt samples exhibited higher C_v values than the Kt-PAM samples, indicating that the addition of polymers adds to the time required for consolidation to occur. Due to PAM's hydrophilic nature, more water molecules are attracted to the composite. Therefore, this phenomenon could be increasing the time required to expel these water molecules from the system. Similar observations were made with the Mt-PAM samples, but only at certain conditions. As mentioned in Chapter 2, the consolidation behavior of montmorillonite is more heavily influenced by electrical forces versus physical interactions. Also, whereas Kt-PAM experiences only interparticle interactions, Mt-PAM experiences both interparticle and interlayer

interactions. Thus, these samples likely are exhibiting additional mechanisms other than PAM's influence that are affecting their coefficient of consolidation values.

It was also shown that Kt-PAM and Mt-PAM samples exhibited higher values of C_c and C_r than their Kt and Mt counterparts, respectively. Higher values for these parameters coincide with larger changes in their void ratios during the test. Higher C_c values indicate that the void ratio of the sample decreases more during loading, and a higher C_r value means that the sample experiences a larger rebound during unloading. These results indicate that the composite samples are more sensitive to load than the control samples. Furthermore, increasing pH and decreasing ionic concentration led to increases in C_c and C_r values for most cases. Therefore, the increasingly compressible nature of extended polymers (pH 11.5, distilled water) appears to lead to higher rates of consolidation and rebound.

Finally, the results from shear wave velocity testing do not significantly distinguish between the control and composite samples. For a given effective stress, the shear wave velocity values are similar regardless of the pore fluid condition and the addition of polymer. However, a preliminary conclusion resulted from the test on montmorillonite-based samples. In this study, it was observed that at the higher ionic concentration there was a significant increase in shear wave velocity for both control and composite samples.

5.5 Conclusions

The compressibility and shear wave velocity testing showed that the composite sample exhibited different behaviors as compared to the control samples. With the addition of polymer to the clay minerals, the compressibility, C_c, and C_r were all increased. The addition of polymer was also shown to decrease the coefficient of consolidation for kaolinite-based samples, likely due to the polymer's hydrophilic nature. The same conclusion was not reached for montmorillonite-based samples, likely due the influence of electrical forces and interlayer interactions.

The shear wave velocities between control and composite materials are not significantly different. Therefore, it can be concluded that these differing materials exhibit approximately the same levels of shear wave velocity for a given effective stress. The only exception to this led to a preliminary conclusion in which Mt-PAM has increasing shear wave velocity with increasing ionic concentration. Furthermore, shear wave velocity is also directly related to the stiffness of the material. Because the shear wave velocities of these materials are relatively the same, it can be concluded that this testing may not be a useful method of distinguishing between the stiffness of control and composite samples. However, further analysis needs to be performed on these tests to confirm these conclusions.

Finally, "tunability" was shown in these tests for Kt-PAM samples. The compressibility, C_v values, C_c values, and C_r values all appear to depend on the pH and ionic concentration of the saturating fluid. It was concluded that with increasing pH and decreasing ionic concentration, the polymers' extended conformation at these

conditions significantly affected these values. PAM's extended conformation led to greater increases in compressibility, greater decreases in C_v, greater increases in C_c, and greater increases in C_r. Therefore, an extended polymer conformation has been determined to be more compressible and can exhibit greater changes in its compressibility than a coiled polymer conformation.

CHAPTER 6: CONCLUSIONS AND FUTURE WORK

The development of the specific clay-polymer composites used in this study was motivated by the idea of creating a geomaterial that could be modified over time by adjusting its fabric, namely in the form of controlling interparticle and interlayer spacings. The scope of this project was to investigate the clay-polymer composites behaviors at the meso-scale level through laboratory bench-scale testing.

This study aimed to determine the shear strength and compressibility of the composites through the use of direct shear tests, 1D consolidation tests, and shear wave velocity measurements. The "tunability" of these materials at the meso-scale was also of interest. Links were made between known micro-scale particle and particle-polymer response to observations made through bench-scale testing.

6.1 Conclusions

The main purpose of this study was to determine if the behavior of the tunable clay-polymer composites at the meso-scale would follow the known micro-scale observations. In other words, it was predicted that the composites would maintain their "tunability" at the meso-scale. The main conclusions are as follows:

(1) Direct Shear:

a. The composite samples (Kt-PAM and Mt-PAM) were not shown to have clear trends when comparing the effects of their polymer conformation or when comparing them to the control samples (Kt and

Mt). Therefore, the "tunability" of the PAM composites was not evident based on direct shear test results.

b. Because the direct shear test is best for a drained test on clays, the different normal stresses and resulting changes in excess pore water pressure were shown to affect the normalized shear stresses of the samples.

c. Regardless of any variables considered, the clay-PAM composites exhibited greater values of shear strength when compared to the control samples.

d. For Kt, the high ionic concentration and high solids content were shown to be more influential in determining shear strength. For Kt-PAM, it was shown that the soil fabric was the most influential factor for determining the shear strength of the composites.

(2) 1D Consolidation:

a. "Tunability" was shown for Kt-PAM samples. PAM's extended conformation at high pH and low ionic concentration led to greater increases in compressibility, greater decreases in C_v, greater increases in C_c, and greater increases in C_r.

b. With the addition of polymer to the clay minerals, the compressibility, C_c, and C_r all increased.

c. The addition of polymer was shown to decrease the coefficient of consolidation for kaolinite-based samples, likely due to the polymer's

hydrophilic nature. The same conclusion was not reached for montmorillonite-based samples, likely due the greater influence of electrical forces.

d. An extended polymer conformation was determined to be more compressible and can exhibit greater changes in its behavior than a coiled polymer conformation.

(3) Shear Wave Velocity:

a. The shear wave velocities between control and composite materials were not significantly different. Because the shear wave velocities of these materials are relatively the same, it can be concluded that this testing may not be a useful method of distinguishing between the stiffness of control and composite samples. However, further analysis needs to be performed on these tests to confirm these conclusions.

b. Mt-PAM behaved slightly differently, as it showed an increasing stiffness with increasing ionic concentration. Due to limited data, however, this is only a preliminary conclusion.

The conclusions show that the composite samples behave differently than the control samples. For the composites, the "tunability" seen at the micro-scale was only evident at the meso-scale through their compressibility parameters. The shear strength of the composites was greatly increased and the shear wave velocity remained the same; however, changes in the material due to the polymer molecule conformation were only evident in the 1D consolidation test.

Careful consideration must be used when determining the large-scale, practical applications of these clay-polymer composites. Some practical applications for these materials relating to their "tunable" nature could be in landfill liners or in chemical spill control, as noted in Chapter 1. This study also showed that while these materials experienced gains in shear strength, their compressibility was also increased. Therefore, these materials would most likely not be suitable in situations where compressibility is of concern. Because of their increased shear strength, these materials could also be used to increase a slope's stability, as long as compressibility is not of concern.

6.2 Future Work

This testing has focused solely on the polymer effects for kaolinite and montmorillonite clays. In order to verify the significance of adding polymer to other clays, future research still needs to performed to determine polymer effects on other, dissimilar clays such as illite Also, this research has solely focused on the shear strength, compressibility, and stiffness aspects of the composites' engineering behavior. There are other methods in which to characterize the engineering behaviors of these materials that can be utilized, such as plasticity, permeability, etc.

Questions remain regarding whether other "responsive" polymers would produce similar results. Whereas PAM conformation is influenced solely by pH levels and ionic concentrations, there are other environmental factors as well. It was not determined in this study if dissimilar polymers would respond to environmental

triggers that are relevant to their behavior as well. While these questions still remain, there is now a baseline of results to begin to understand fundamental engineering behaviors of these materials.

In addition, improvements can be made into the some of the test methods used in this study. During sample preparation, large variations in void ratio and water content were seen in the preconsolidation tubes. It was noted that this occurrence was likely due to the doubly drained nature of this test setup. Even though there were drainage holes placed alongside the tube, they became clogged quickly with the specimens. In the future, these drainage holes can be utilized by using a filter paper lines along the tube walls. This will likely allow for a fully drained condition during preconsolidation.

The direct shear was performed in a manner in which the samples were undrained; however, this is not the most effective way to determine the shear strength of clays. Therefore, future shear strength testing can be performed in a triaxial device, in which undrained or drained tests can be accurately performed. If the direct shear test is to be used for these materials in the future, an excess pore pressure measuring device should be included in the direct shear box. This would allow for the measurement of the excess pore water pressures during the test, from which the effective shear stresses could then be calculated.

The 1D consolidation and shear wave velocity testing on montmorillonite-based materials was performed at differing maximum effective stresses. As a result, the unloading curves for the consolidation plots and shear wave velocity plots were

not able to be effectively compared between samples. If using the same test equipment as in this study, future research should be conducted at a maximum effective stress of 87 kPa for all samples. This would allow all Mt and Mt-PAM samples to be compared effectively.

LIST OF REFERENCES

Alexandre, M., and Dubois, P. (2000). "Polymer-Layered Silicate Nanocomposites: Preparation, Properties and Uses of a New Class of Materials." *Materials Science and Engineering: R: Reports*, 28(1–2), 1-63.

Alvarado, G., and Coop, M. (2012). "On the Performance of Bender Elements in Triaxial Tests." *Géotechnique*, 62(1), 1-17.

Ashland, F. X. (2013). "Average Shear Wave Velocity References." <http://www.seis.utah.edu/urban/response.shtml>. (March 29, 2013).

ASTM Standard D422 (1963). "Standard Test Method for Particle-Size Analysis of Soils." ASTM International, West Conshohocken, PA, 2011, www.astm.org.

ASTM Standard D2435 (2011). "Standard Test Methods for One-Dimensional Consolidation Properties of Soils Using Incremental Loading." ASTM International, West Conshohocken, PA, 2011, www.astm.org.

ASTM Standard D3080 (2011). "Standard Test Method for Direct Shear Test of Soils Under Consolidated Drained Conditions." ASTM International, West Conshohocken, PA, 2011, www.astm.org.

Bailey, S. W. (1993). "Review of the Structural Relationships of the Kaolin Minerals." *Kaolin Genesis and Utilization: A Collection of Papers Presented at the Keller '90 Kaolin Symposium*, H. H. Murray, W. M. Bundy, and C. C. Harvey, eds., The Clay Minerals Society, Boulder.

Barak, P., and Nater, E. A. (2003). "The Virtual Museum of Minerals and Molecules." <http://virtual-museum.soils.wisc.edu/index.html>. (Feb. 11, 2013).

Berend, I., Cases, J.-M., Francois, M., Uriot, J.-P., Michot, L., Masion, A., and Thomas, F. (1995). "Mechanism of Adsorption and Desorption of Water Vapor by Homoionic Montmorillonites: 2. The Li+, Na+, K+, Rb+, and Cs+-Exchanged Forms." *Clays and Clay Minerals*, 43(3), 324-336.

Besra, L., Sengupta, D. K., Roy, S. K., and Ay, P. (2002). "Flocculation and Dewatering of Kaolin Suspensions in the Presence of Polyacrylamide and Surfactants." *International Journal of Mineral Processing*, 66(1–4), 203-232.

Borden, D., and Giese, R. (2001). "Baseline Studies of the Clay Minerals Society Source Clays: Cation Exchange Capacity Measurements by the Ammonia-Electrode Method." *Clays and Clay Minerals*, 49(5), 444-445.

Brandrup, J., and Immergut, E. H. (1989). *Polymer Handbook*, Wiley, New York.

Brindley, G. W., and Brown, G. (1980). *Crystal Structures of Clay Minerals and Their X-ray Identification*, Mineralogical Society, London.

Brown, G., and Nadeau, P. (1984). "Crystal Structures of Clay Minerals and Related Phyllosilicates [and Discussion]." *Philosophical Transactions of the Royal Society of London. Series A, Mathematical and Physical Sciences*, 311(1517), 221-240.

Budhu, M. (2011). *Soil Mechanics and Foundations*, John Wiley & Sons, New Jersey.

Chang, F.-R. C., Skipper, N. T., and Sposito, G. (1995). "Computer Simulation of Interlayer Molecular Structure in Sodium Montmorillonite Hydrates." *Langmuir*, 11(7), 2734-2741.

Chen, J., Anandarajah, A., and Inyang, H. (2000). "Pore Fluid Properties and Compressibility of Kaolinite." *Journal of Geotechnical and Geoenvironmental Engineering*, 126(9), 798-807.

Coduto, D. P. (1999). *Geotechnical Engineering*, Prentice Hall, New Jersey.

Day, S. R., O'Hannesin, S. F., and Marsden, L. (1999). "Geotechnical Techniques for the Construction of Reactive Barriers." *Journal of Hazardous Materials*, 67(3), 285-297.

Deng, Y., Dixon, J. B., White, G. N., Loeppert, R. H., and Juo, A. S. R. (2006). "Bonding Between Polyacrylamide and Smectite." *Colloids and Surfaces A: Physicochemical and Engineering Aspects*, 281(1–3), 82-91.

Di Maio, C., Hueckel, T., and Loret, B. (2002). *Chemo-Mechanical Coupling in Clays: From Nano-scale to Engineering Applications*, Balkema, The Netherlands.

Douillard, J. M., Salles, F., Devautour-Vinot, S., Manteghetti, A., and Henry, M. (2007). "Study of the Surface Energy of Montmorillonite Using PACHA Formalism." *Journal of Colloid and Interface Science*, 306(1), 175-182.

Dyvik, R., and Madshus, C. "Lab Measurements of G_{max} Using Bender Elements." *Proc., Advances in the art of testing soils under cyclic conditions*, ASCE, 186-196.

Fernandez, A. L. (2000). "Tomographic Imaging the State of Stress." PhD Thesis, Georgia Institute of Tech., Atlanta, GA.

Fox, P. (2004). "Analytical Solutions for Stability of Slurry Trench." *Journal of Geotechnical and Geoenvironmental Engineering*, 130(7), 749-758.

Fu, X., and Qutubuddin, S. (2001). "Polymer–Clay Nanocomposites: Exfoliation of Organophilic Montmorillonite Nanolayers in Polystyrene." *Polymer*, 42(2), 807-813.

Gajo, A., and Maines, M. (2007). *Mechanical Effects of Aqueous Solutions of Inorganic Acids and Bases on a Natural Active Clay*, Telford, London.

Gao, D., and Heimann, R. B. (1993). "Structure and Mechanical Properties of Superabsorbent Poly(acrylamide)-montmorillonite Composite Hydrogels." *Polymer Gels and Networks*, 1(4), 225-246.

Giannelis, E. P., Krishnamoorti, R., and Manias, E. (1999). "Polymer-Silicate Nanocomposites: Model Systems for Confined Polymers and Polymer Brushes." *Polymers in Confined Environments*, S. Granick, K. Binder, P. G. Gennes, E. P. Giannelis, G. S. Grest, H. Hervet, R. Krishnamoorti, L. Léger, E. Manias, E. Raphaël, and S. Q. Wang, eds., Springer, Berlin, 107-147.

Gregory, J. (1988). "Polymer Adsorption and Flocculation in Sheared Suspensions." *Colloids and Surfaces*, 31, 231-253.

Grim, R. E. (1968). *Clay Mineralogy*, McGraw-Hill, New York.

Gudeman, L. F., and Peppas, N. A. (1995). "Preparation and Characterization of pH-Sensitive, Interpenetrating Networks of Poly(vinyl alcohol) and Poly(acrylic acid)." *Journal of Applied Polymer Science*, 55(6), 919-928.

Hanwell, M. D., Curtis, D. E., Lonie, D. C., Vandermeersch, T., Zurek, E., and Hutchison, G. R. 2012. Avogadro: An Open-Source Molecular Builder and Visualization Tool, version 1.1.0.

Hatami, F., Ghamari, A., and Rahai, A. (2012). "Investigating the Properties of Steel Shear Walls Reinforced with Carbon Fiber Polymers (CFRP)." *Journal of Constructional Steel Research*, 70, 36-42.

Hibbeler, R. C. (2003). *Mechanics of Materials*, Pearson Education, New Jersey.

Horpibulsuk, S., Yangsukkaseam, N., Chinkulkijniwat, A., and Du, Y. J. (2011). "Compressibility and Permeability of Bangkok Clay Compared with Kaolinite and Bentonite." *Applied Clay Science*, 52(1–2), 150-159.

Kim, S., Motyka, M. A., Palomino, A. M., and Podraza, N. J. (2012). "Conformational Effects of Adsorbed Polymer on the Swelling Behavior of Engineered Clay Minerals." *Clays and Clay Minerals*, 60(4), 363-373.

Kim, S., and Palomino, A. (2009). "Polyacrylamide-Treated Kaolin: A Fabric Study." *Applied Clay Science*, 45(4), 270-279.

Kim, S., and Palomino, A. (2011). "Factors Influencing the Synthesis of Tunable Clay-Polymer Nanocomposites using Bentonite and Polyacrylamide." *Applied Clay Science*, 51(4), 491-198.

Kim, S., Palomino, A. M., and Colina, C. M. (2012). "Responsive Polymer Conformation and Resulting Permeability of Clay–Polymer Nanocomposites." *Molecular Simulation*, 38(8-9), 723-734.

Kim, S. J., Kim, M. S., Kim, S. I., Spinks, G. M., Kim, B. C., and Wallace, G. G. (2006). "Self-Oscillatory Actuation at Constant DC Voltage with pH-Sensitive Chitosan/Polyaniline Hydrogel Blend." *Chemistry of Materials*, 18(24), 5805-5809.

Klenina, O. V., and Lebedeva, L. G. (1983). "Viscometric Properties of Dilute Solutions of Hydrolyzed Polyacrylamide." *Polymer Science U.S.S.R.*, 25(10), 2380-2389.

Kulicke, W. M., Kniewske, R., and Klein, J. (1982). "Preparation, Characterization, Solution Properties and Rheological Behaviour of Polyacrylamide." *Progress in Polymer Science*, 8(4), 373-468.

Kurenkov, V. F. (1997). "Acrylamide Polymers." *Handbook of Engineering Polylmeric Materials*, N. P. Cheremisinoff, ed., Marcel Dekker, New York.

Laird, D. A. (1997). "Bonding Between Polyacrylamide and Clay Mineral Surfaces." *Soil Science*, 162(11), 826-832.

Lambe, T. W., and Whitman, R. V. (1969). "Soil Mechanics." John Wiley, New York.

Lee, J.-S. (2003). "High-Resolution Geophysical Techniques for Small-Scale Soil Model Testing." PhD Thesis, Georgia Institute of Tech., Atlanta, GA.

Lee, J.-S. (2012). "Personal correspondence."

Lee, J.-S., and Santamarina, J. (2005). "Bender Elements: Performance and Signal Interpretation." *Journal of Geotechnical and Geoenvironmental Engineering*, 131(9), 1063-1070.

Liaki, C., Rogers, C. D. F., and Boardman, D. I. (2008). "Physicochemical Effects on Uncontaminated Kaolinite due to Electrokinetic Treatment Using Inert Electrodes." *Journal of Environmental Science and Health, Part A*, 43(8), 810-822.

Liu, C., and Evett, J. B. (2004). *Soils and Foundations*, Prentice Hall, New Jersey.

Luckham, P. F., and Rossi, S. (1999). "The Colloidal and Rheological Properties of Bentonite Suspensions." *Advances in Colloid and Interface Science*, 82(13), 43-92.

Maltesh, C., Somasundaran, P., Pradip, Kulkarni, R. A., and Gundiah, S. (1991). "Effect of the Degree of Hydrolysis of Polyacrylamide on its Interactions with Poly(ethylene oxide) and Poly(vinylpyrrolidone)." *Macromolecules*, 24(21), 5775-5778.

McCarthy, D. F. (2002). *Essentials of Soil Mechanics and Foundations: Basic Geotechnics*, Prentice Hall, New Jersey.

Meade, R. H. (1964). *Removal of Water and Rearrangement of Particles During the Compaction of Clayey Sediments: Review*, US Government Printing Office, Washington, D. C.

Mesri, G., and Olson, R. E. (1971). "Consolidation Characteristics of Montmorillonite." *Géotechnique*, 21(4), 341-352.

Meunier, A. (2005). *Clays*, Springer, Berlin.

Miranda-Trevino, J. C., and Coles, C. A. (2003). "Kaolinite Properties, Structure and Influence of Metal Retention on pH." *Applied Clay Science*, 23(1–4), 133-139.

Mitchell, J. K. (1960). "The Application of Colloidal Theory to the Compressibility of Clays." *Interparticle Forces in Clay–Water–Electrolyte Systems*, R. H. G. Parry, ed., Commonwealth Science and Industry Research Organization, Melbourne, 2.92-92.97.

Mitchell, J. K., and Soga, K. (2005). *Fundamentals of Soil Behavior*, Wiley, New Jersey.

Mpofu, P., Addai-Mensah, J., and Ralston, J. (2003). "Investigation of the Effect of Polymer Structure Type on Flocculation, Rheology and Dewatering Behaviour of Kaolinite Dispersions." *International Journal of Mineral Processing*, 71(1–4), 247-268.

Müller-Vonmoos, M., and Løken, T. (1989). "The Shearing Behaviour of Clays." *Applied Clay Science*, 4(2), 125-141.

Newman, A. C. D. (1987). *Chemistry of Clays and Clay Minerals*, Wiley-Interscience, New York.

Nugent, R. A. (2011). "The Effect of Exopolymers on the Compressibility and Shear Strength of Kaolinite." PhD thesis, Louisiana State Univ., Baton Rouge, La.

O'Rourke, T., Druschel, S., and Netravali, A. (1990). "Shear Strength Characteristics of Sand-Polymer Interfaces." *Journal of Geotechnical Engineering*, 116(3), 451-469.

Painter, P. C., and Coleman, M. M. (1997). *Fundamentals of Polymer Science: An Introductory Text*, Technomic Publishing Company, Lancaster.

Palomino, A. M., and Santamarina, J. C. (2005). "Fabric Map for Kaolinite: Effects of pH and Ionic Concentration on Behavior." *Clays and Clay Minerals*, 53(3), 211-223.

Park, T., and Tan, S. A. (2005). "Enhanced Performance of Reinforced Soil Walls by the Inclusion of Short Fiber." *Geotextiles and Geomembranes*, 23(4), 348-361.

Park, T. G., and Hoffman, A. S. (1992). "Synthesis and Characterization of pH- and/or Temperature-Sensitive Hydrogels." *Journal of Applied Polymer Science*, 46(4), 659-671.

Rajasekaran, G., and Narasimha Rao, S. (1997). "The Microstructure of Lime-Stabilized Marine Clay." *Ocean Engineering*, 24(9), 867-878.

Ranjan, G., and Rao, A. S. R. (2000). *Basic And Applied Soil Mechanics*, New Age International, India.

Ranjbar, M., and Schaffie, M. (2000). "Improved Treatment of Acrylamide Co- and Terpolymers for Water Control in Gas-Producing and Storage Wells." *Journal of Petroleum Science and Engineering*, 26(1–4), 133-141.

Rao, F., Song, S., and Lopez-Valdivieso, A. (2011). "Specific Adsorption of Chromium Species on Kaolinite Surface." *Mineral Processing and Extractive Metallurgy Review*, 33(3), 180-189.

Razakamanantsoa, A. R., Barast, G., and Djeran-maigre, I. (2012). "Hydraulic Performance of Activated Calcium Bentonite Treated by Polyionic Charged Polymer." *Applied Clay Science*, 59, 103-114.

Rizkalla, S., Lucier, G., and Dawood, M. (2012). "Innovative Use of FRP for the Precast Concrete Industry." *Advances in Structural Engineering*, 15(4), 565-574.

Santamarina, J., Klein, K., Wang, Y., and Prencke, E. (2002). "Specific Surface: Determination and Relevance." *Canadian Geotechnical Journal*, 39(1), 233-241.

Santamarina, J. C., Klein, K. A., and Fam, M. A. (2001). *Soils and Waves*, John Wiley & Sons, Chichester.

Shang, J. Q., Lo, K. Y., and Quigley, R. M. (1994). "Quantitative Determination of Potential Distribution in Stern–Gouy Double-Layer Model." *Canadian Geotechnical Journal*, 31(5), 624-636.

Shroff, A. V., and Shah, D. L. (2003). *Soil Mechanics and Geotechnical Engineering*, A.A. Balkema, India.

Sinha Ray, S., and Okamoto, M. (2003). "Polymer/layered Silicate Nanocomposites: A Review from Preparation to Processing." *Progress in Polymer Science*, 28(11), 1539-1641.

Spagnoli, G., Rubinos, D., Stanjek, H., Fernández-Steeger, T., Feinendegen, M., and Azzam, R. (2012). "Undrained Shear Strength of Clays as Modified by pH Variations." *Bull Eng Geol Environ*, 71(1), 135-148.

Sposito, G. (1989). *The Chemistry of Soils*, Oxford Univerity Press, New York.

Sridharan, A., El-Shafei, A., and Miura, N. (2002). "Mechanisms Controlling the Undrained Strength Behavior of Remolded Ariake Marine Clays." *Marine Georesources & Geotechnology*, 20(1), 21-50.

Sridharan, A., and Prakash, K. (1999). "Mechanisms Controlling the Undrained Shear Strength Behaviour of Clays." *Canadian Geotechnical Journal*, 36(6), 1030-1038.

Sridharan, A., and Rao, G. V. (1979). "Shear Strength Behaviour of Saturated Clays and the Role of the Effective Stress Concept." *Géotechnique*, 29(2), 177-193.

Stumm, W. (1992). *Chemistry of the Solid-Water Interface: Processes at the Mineral-Water and Particle-Water Interface in Natural Systems*, Wiley, New York.

Stutzmann, T., and Siffert, B. (1977). "Contribution to the Adsorption Mechanism of Acetamide and Polyacrylamide on to Clays." *Clays and Clay Minerals*, 25(6), 392-406.

Theng, B. K. G. (1979). *Formation and Properties of Clay-Polymer Complexes*, Elsevier, Amsterdam.

Theng, B. K. G. (1982). "Clay-Polymer Interactions; Summary and Perspectives." *Clays and Clay Minerals*, 30(1), 1-10.

Tiwari, B., and Ajmera, B. (2011). "Consolidation and Swelling Behavior of Major Clay Minerals and Their Mixtures." *Applied Clay Science*, 54(3–4), 264-273.

van Olphen, H. (1977). *An Introduction to Clay Colloid Chemistry: For Clay Technologists, Geologists, and Soil Scientists*, Wiley-Interscience, New York.

Wahid, A. S., Gajo, A., and Di Maggio, R. (2011). *Chemo-Mechanical Effects in Kaolinite. Part 1: Prepared Samples*, Telford, London.

White, I. D., Mottershead, D. N., and Harrison, S. J. (1992). *Environmental Systems: An Introductory Text*, Chapman & Hall, London.

Whitley, H. D., and Smith, D. E. (2004). "Free Energy, Energy, and Entropy of Swelling in Cs--, Na--, and Sr--Montmorillonite Clays." *The Journal of Chemical Physics*, 120(11), 5387-5395.

Wood, D., and Wroth, C. (1978). "The Use of the Cone Penetrometer to Determine the Plastic Limit of Soils." *Ground Engineering*, 11(3).

Xu, Q., Tolaymat, T., and Townsend, T. (2012). "Impact of Pressurized Liquids Addition on Landfill Slope Stability." *Journal of Geotechnical and Geoenvironmental Engineering*, 138(4), 472-480.

Zeng, Q. H., Yu, A. B., Lu, G. Q., and Paul, D. R. (2005). "Clay-Based Polymer Nanocomposites: Research and Commercial Development." *Journal of Nanoscience and Nanotechnology*, 5(10), 1574-1592.

APPENDICES

Appendix A

This appendix contains data gathered from all measurements related to the direct shear testing (Chapter 4). Tables A.1 and A.2 show data from tests on kaolinite and montmorillonite samples, respectively. In these tables, S_u is defined as the shear stress value of the control samples when the residual state is just reached. Disp is the horizontal deflection where the shear stress of the control sample was recorded, S_{comp} is defined as the shear stress at the same displacement defined from the comparable control sample, σ_v is the normal stress, S_u/σ_v is the normalized shear stress, M_w is the wet mass after the test, M_d is the dry mass after the test, and w is the water content after the test. S_u was defined based on the methodology shown in Section 4.1.3.

Figure A.1 shows the shear stress vs. lateral displacement graphs for all samples tested. There are 48 graphs included, from which the values for S_u and σ_v were determined and summarized in Tables A.1 and A.2.

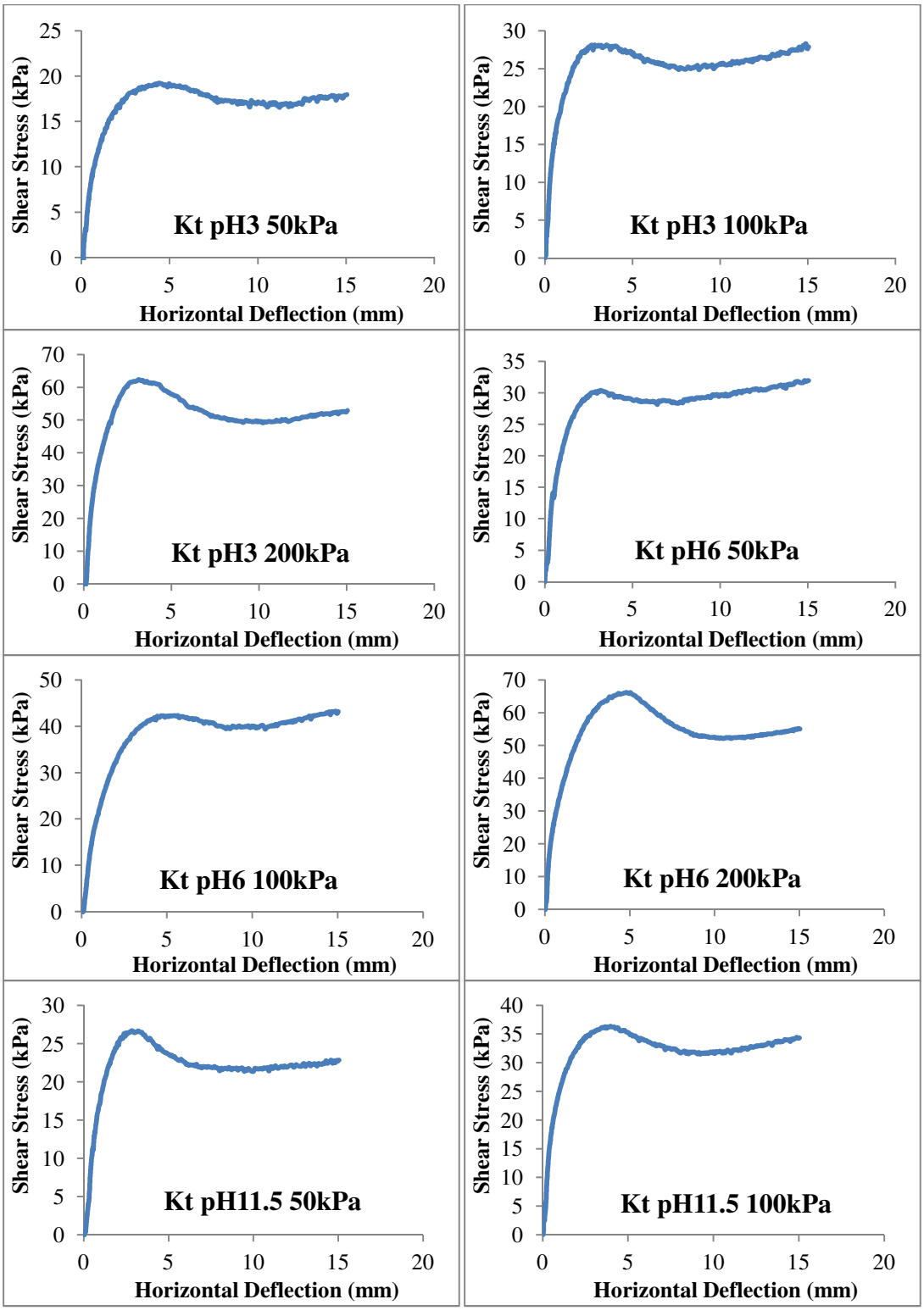
TABLE A.1: Direct shear measurements from tests on Kt and Kt-PAM samples

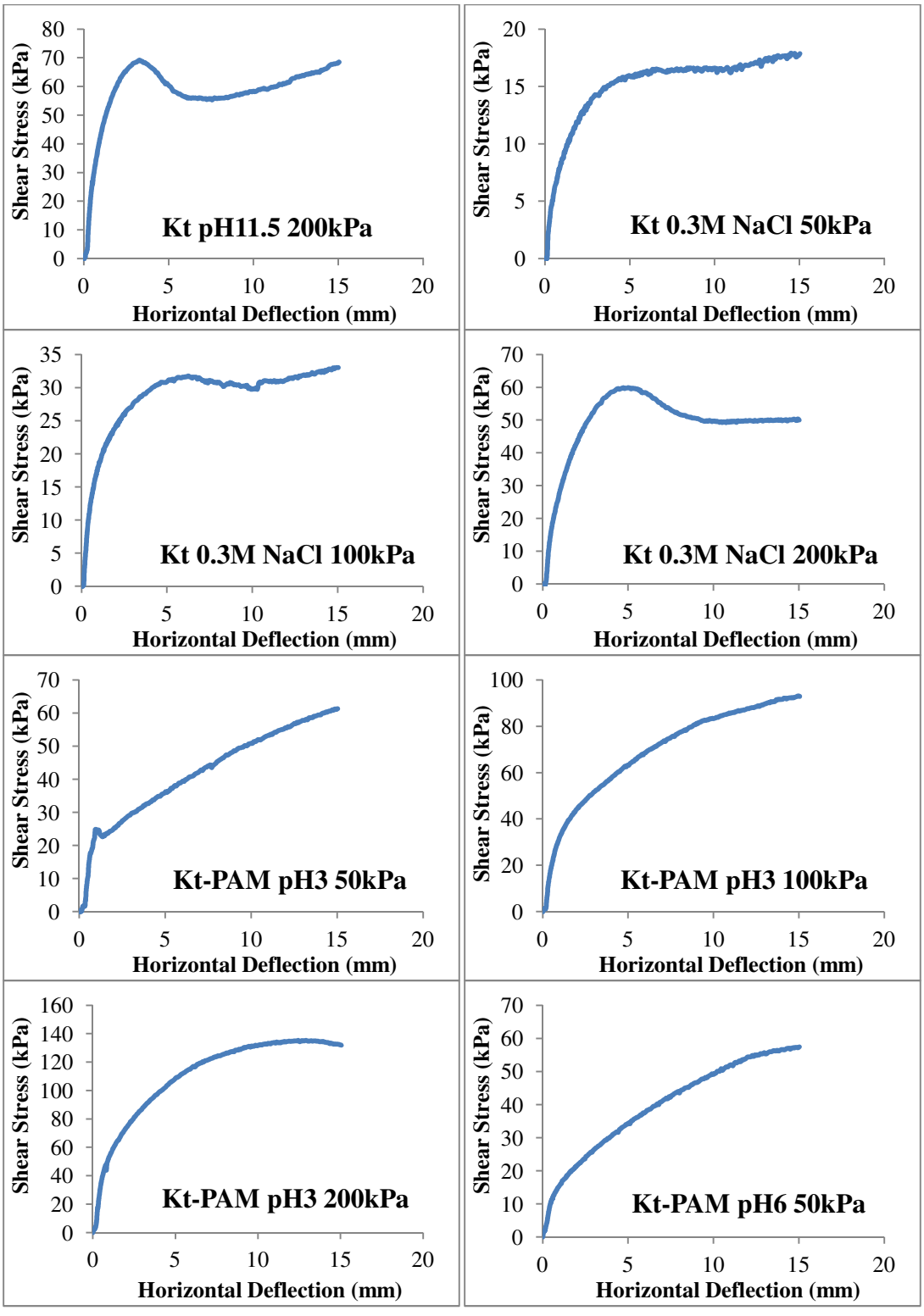
Sample	S_u or S_{comp} (kPa)	Disp. (mm)	σ_v (kPa)	S_u/σ_v or S_{comp}/σ_v	M_w (g)	M_d (g)	w (%)
Kt pH3 50kPa	16.5	11.2	50	0.33	151.78	111.91	35.63
Kt pH3 100kPa	24.9	8.8	100	0.25	162.65	120.38	35.11
Kt pH3 200kPa	49.1	10.2	200	0.25	172.91	131.01	31.98
Kt pH6 50kPa	28.2	6.4	50	0.56	161.67	120.77	33.87
Kt pH6 100kPa	39.4	10.8	100	0.39	149.4	111.12	34.45
Kt pH6 200kPa	52.1	11.0	200	0.26	148.05	112.21	31.94
Kt pH11.5 50kPa	21.3	11.6	50	0.43	163.4	121.54	34.44
Kt pH11.5 100kPa	31.5	9.2	100	0.31	152.5	113	34.96
Kt pH11.5 200kPa	55.3	7.8	200	0.28	168.41	128.04	31.53
Kt 0.3M NaCl 50kPa	16.2	10.9	50	0.32	152.39	111.44	36.75
Kt 0.3M NaCl 100kPa	29.7	9.9	100	0.30	156.68	115.97	35.10
Kt 0.3M NaCl 200kPa	49.2	10.5	200	0.25	121.95	91.95	32.63
Kt-PAM pH3 50kPa	53.5	11.2	50	1.07	157.23	105.03	49.70
Kt-PAM pH3 100kPa	80.1	8.8	100	0.80	152.77	107.24	42.46
Kt-PAM pH3 200kPa	132.1	10.2	200	0.66	152.3	111.65	36.41
Kt-PAM pH6 50kPa	39.1	6.4	50	0.78	142.17	96.21	47.77
Kt-PAM pH6 100kPa	80.5	10.8	100	0.81	138.85	96.1	44.48
Kt-PAM pH6 200kPa	134.6	11.0	200	0.67	133.03	95.43	39.40
Kt-PAM pH11.5 50kPa	52.2	11.6	50	1.04	127.73	90.37	41.34
Kt-PAM pH11.5 100kPa	91.7	9.2	100	0.92	155.06	106.94	45.00
Kt-PAM pH11.5 200kPa	128.6	7.8	200	0.64	152.73	107.61	41.93
Kt-PAM 0.3M NaCl 50kPa	67.4	10.9	50	1.35	171.91	121.57	41.41
Kt-PAM 0.3M NaCl 100kPa	91.3	9.9	100	0.91	156.1	110.47	41.31
Kt-PAM 0.3M NaCl 200kPa	146.5	10.5	200	0.73	157.61	117.25	34.42

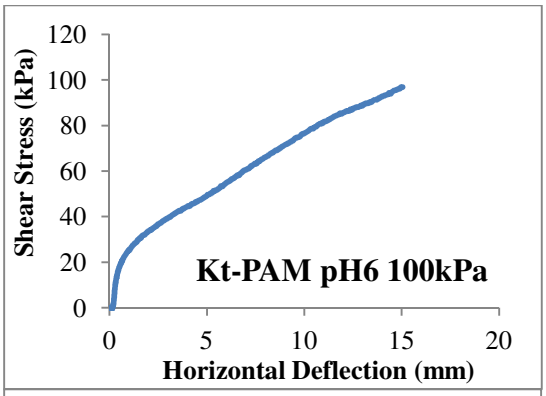
TABLE A.2: Direct shear measurements from tests on Mt and Mt-PAM samples

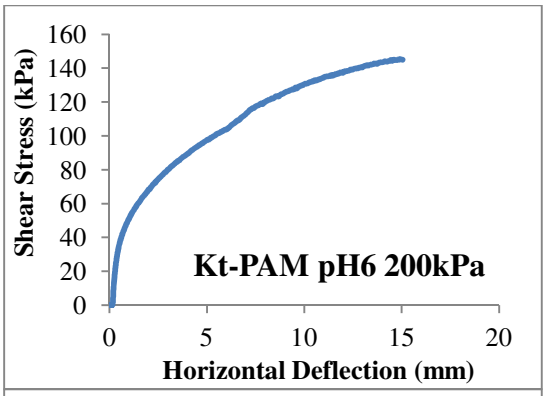
Sample	S_u or S_{comp} (kPa)	Disp. (mm)	σ_v (kPa)	S_u/σ_v or S_{comp}/σ_v	M_w (g)	M_d (g)	w (%)
Mt pH3 50kPa	6.7	9.6	50	0.13	94.04	31.6	197.59
Mt pH3 100kPa	9.4	9.9	100	0.09	84.59	42.16	100.64
Mt pH3 2000kPa	19.6	7.2	200	0.10	85.63	38.75	120.98
Mt pH6 50kPa	12.4	6.8	50	0.25	98.73	35.39	178.98
Mt pH6 100kPa	14.9	6.6	100	0.15	82.88	30.84	168.74
Mt pH6 200kPa	15.8	5.8	200	0.08	74.65	30.76	142.69
Mt pH11.5 50kPa	9.6	6.2	50	0.19	95.74	29.86	220.63
Mt pH11.5 100kPa	14.6	7.1	100	0.15	85.35	30.21	182.52
Mt pH11.5 200kPa	19.5	4.3	200	0.10	76.35	34.7	120.03
Mt 0.3M NaCl 50kPa	8.8	5.3	50	0.18	86.87	29.29	196.59
Mt 0.3M NaCl 100kPa	15.7	5.9	100	0.16	76.35	30.51	150.25
Mt 0.3M NaCl 200kPa	14.8	8.2	200	0.07	62.67	28.42	120.51
Mt-PAM pH3 50kPa	16.2	9.6	50	0.32	89.03	23.85	273.29
Mt-PAM pH3 100kPa	26.3	9.9	100	0.26	92.97	29.21	218.28
Mt-PAM pH3 200kPa	36.1	7.2	200	0.18	76.58	29.92	155.95
Mt-PAM pH6 50kPa	15.8	6.8	50	0.32	79.73	20.29	292.95
Mt-PAM pH6 100kPa	26.8	6.6	100	0.27	110.7	35.68	210.26
Mt-PAM pH6 200kPa	37.9	5.8	200	0.19	87.56	36.57	139.43
Mt-PAM pH11.5 50kPa	11.7	6.2	50	0.23	96.45	27.1	255.90
Mt-PAM pH11.5 100kPa	30.2	7.1	100	0.30	83.3	26.93	209.32
Mt-PAM pH11.5 200kPa	41.2	4.3	200	0.21	83.1	31.76	161.65
Mt-PAM 0.3M NaCl 50kPa	19.3	5.3	50	0.39	92.72	28.95	220.28
Mt-PAM 0.3M NaCl 100kPa	31.5	5.9	100	0.32	85.06	31.9	166.65
Mt-PAM 0.3M NaCl 200kPa	48.1	8.2	200	0.24	78.1	34.13	128.83

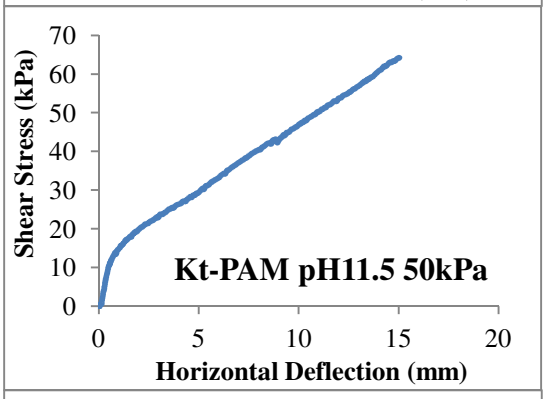
FIG. A.1: Shear stress vs. lateral displacement graphs for all 48 samples tested

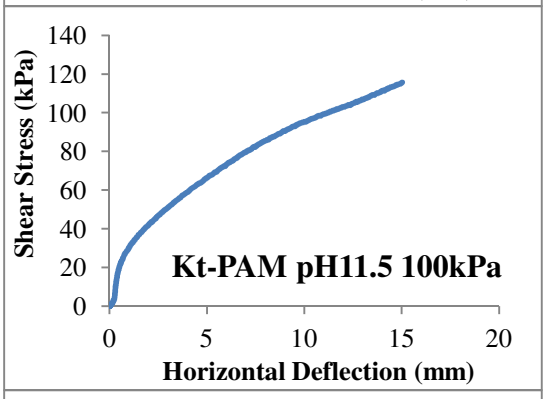

Shear Stress (kPa)
Horizontal Deflection (mm)
Kt pH3 50kPa
Kt pH3 100kPa
Kt pH3 200kPa
Kt pH6 50kPa
Kt pH6 100kPa
Kt pH6 200kPa
Kt pH11.5 50kPa
Kt pH11.5 100kPa

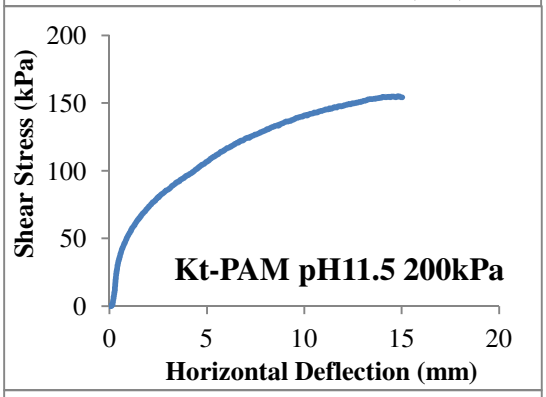

Kt pH11.5 200kPa
Kt 0.3M NaCl 50kPa
Kt 0.3M NaCl 100kPa
Kt 0.3M NaCl 200kPa
Kt-PAM pH3 50kPa
Kt-PAM pH3 100kPa
Kt-PAM pH3 200kPa
Kt-PAM pH6 50kPa
Shear Stress (kPa)
Horizontal Deflection (mm)

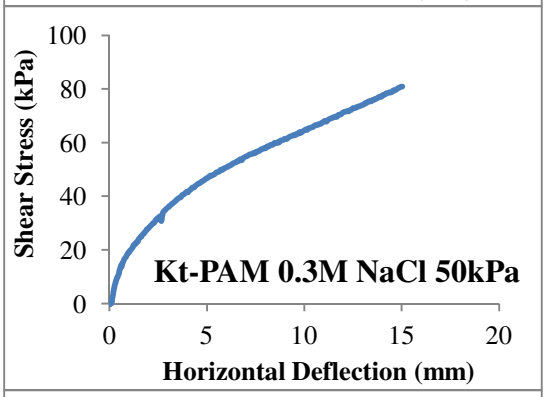

Shear Stress (kPa)
120
100
80
60
40
20
0
0
5
10
15
20
Horizontal Deflection (mm)
Kt-PAM pH6 100kPa

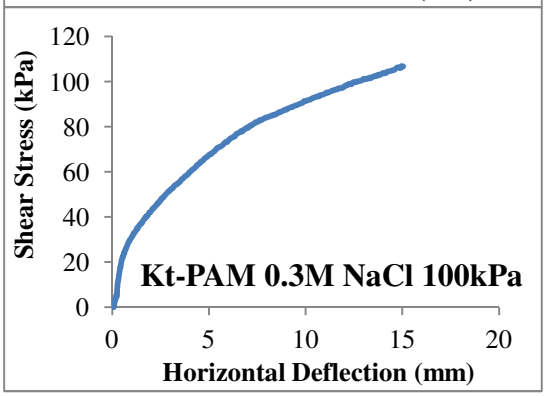

Shear Stress (kPa)
160
140
120
100
80
60
40
20
0
0
5
10
15
20
Horizontal Deflection (mm)
Kt-PAM pH6 200kPa

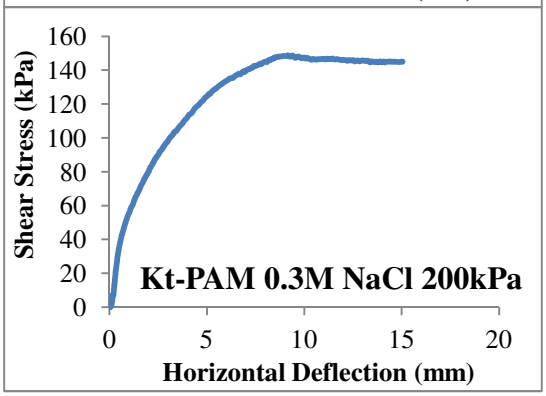

Shear Stress (kPa)
70
60
50
40
30
20
10
0
0
5
10
15
20
Horizontal Deflection (mm)
Kt-PAM pH11.5 50kPa

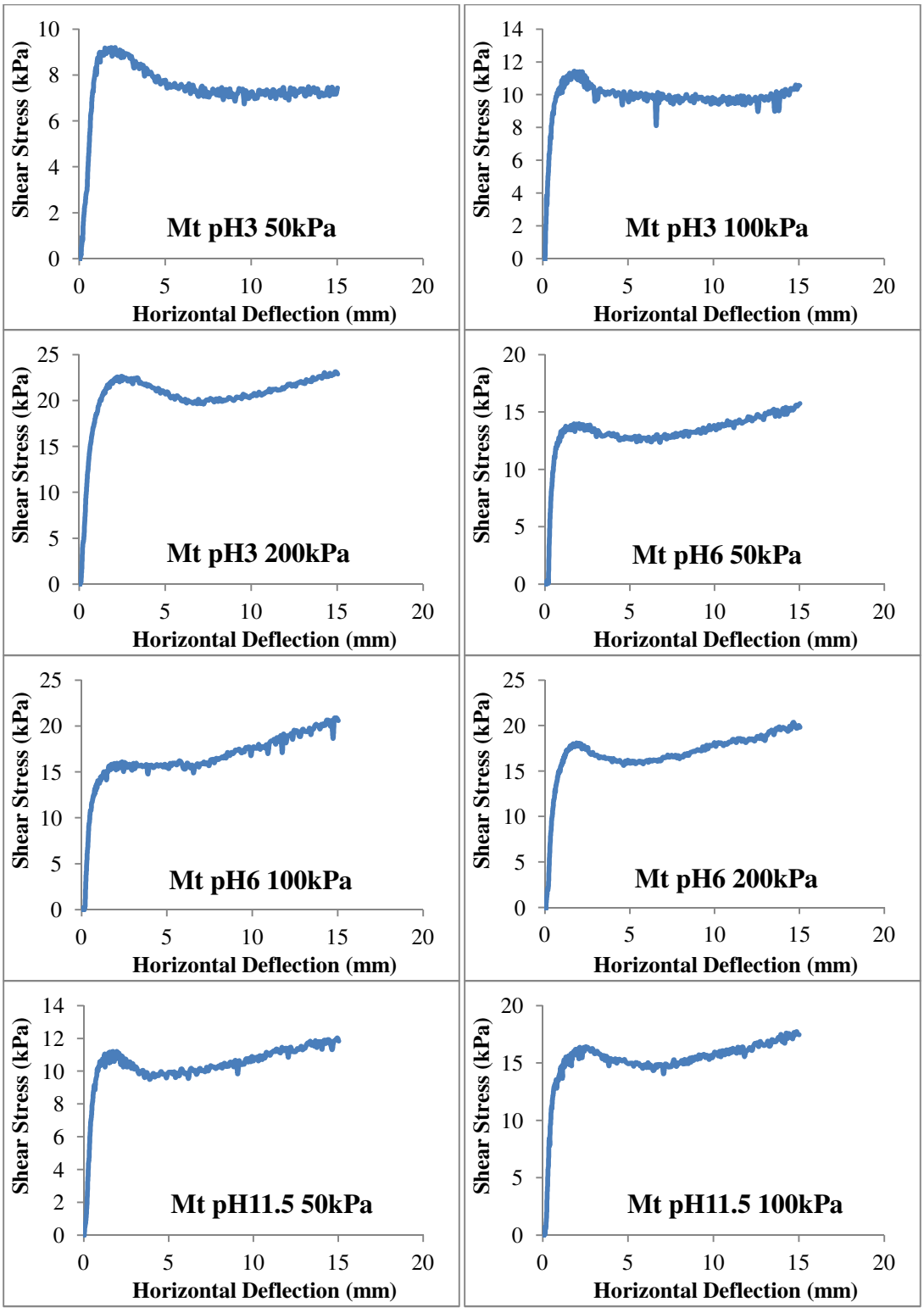

Shear Stress (kPa)
140
120
100
80
60
40
20
0
0
5
10
15
20
Horizontal Deflection (mm)
Kt-PAM pH11.5 100kPa

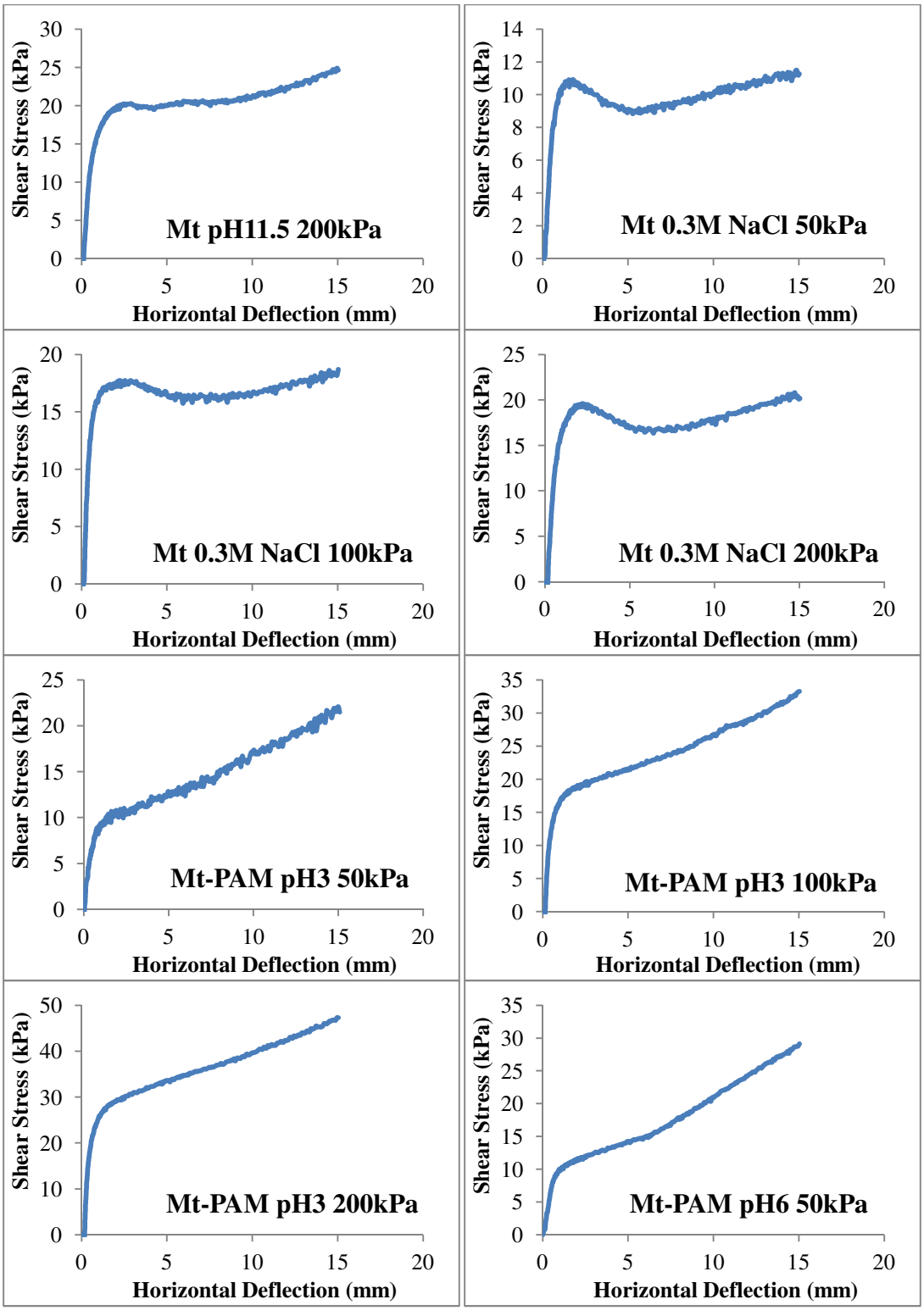

Shear Stress (kPa)
200
150
100
50
0
0
5
10
15
20
Horizontal Deflection (mm)
Kt-PAM pH11.5 200kPa

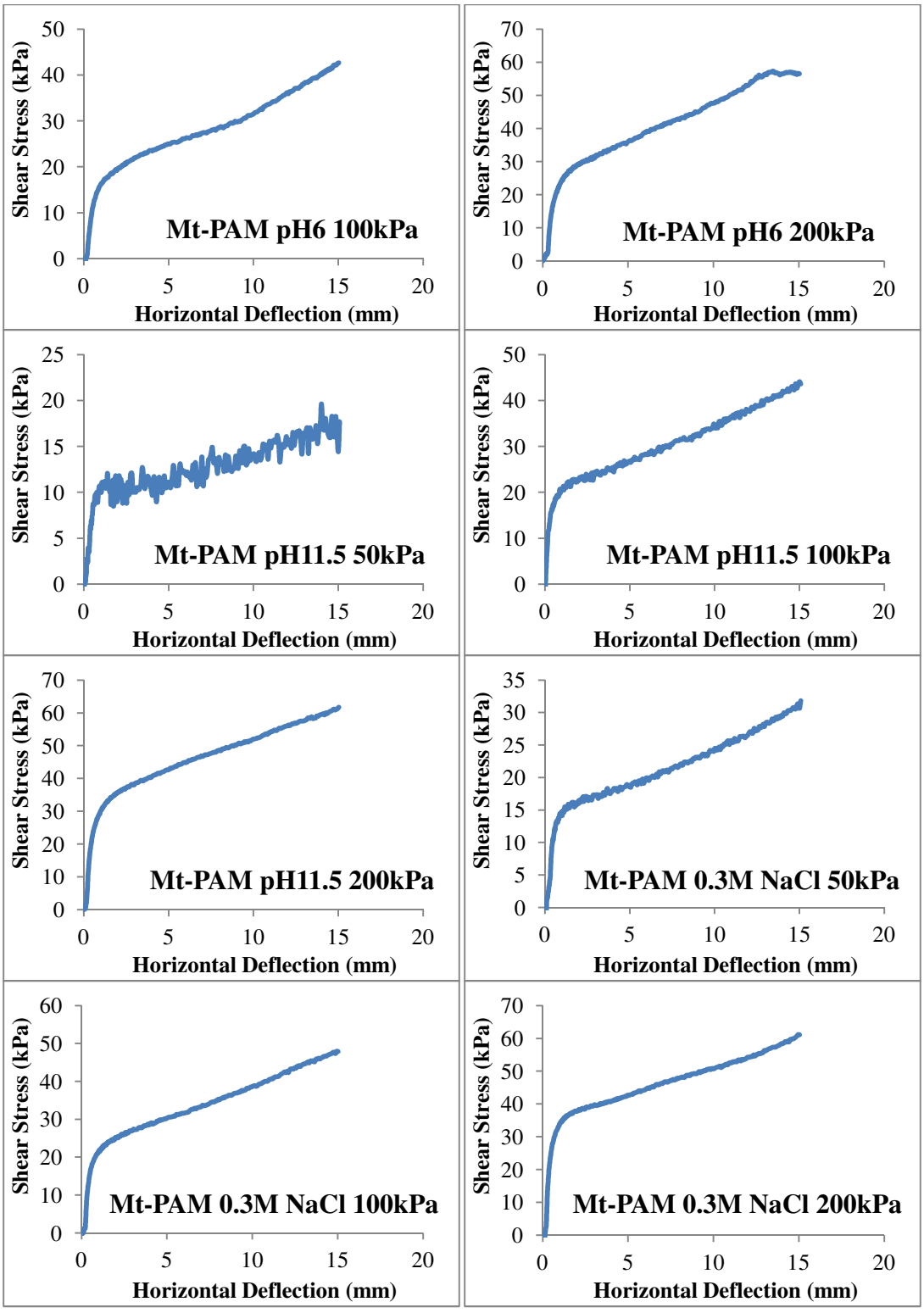

Shear Stress (kPa)
100
80
60
40
20
0
0
5
10
15
20
Horizontal Deflection (mm)
Kt-PAM 0.3M NaCl 50kPa


Shear Stress (kPa)
120
100
80
60
40
20
0
0
5
10
15
20
Horizontal Deflection (mm)
Kt-PAM 0.3M NaCl 100kPa


Shear Stress (kPa)
160
140
120
100
80
60
40
20
0
0
5
10
15
20
Horizontal Deflection (mm)
Kt-PAM 0.3M NaCl 200kPa


Shear Stress (kPa)
Horizontal Deflection (mm)
Mt pH3 50kPa
Mt pH3 100kPa
Mt pH3 200kPa
Mt pH6 50kPa
Mt pH6 100kPa
Mt pH6 200kPa
Mt pH11.5 50kPa
Mt pH11.5 100kPa


Shear Stress (kPa)
Horizontal Deflection (mm)
Mt pH11.5 200kPa
Mt 0.3M NaCl 50kPa
Mt 0.3M NaCl 100kPa
Mt 0.3M NaCl 200kPa
Mt-PAM pH3 50kPa
Mt-PAM pH3 100kPa
Mt-PAM pH3 200kPa
Mt-PAM pH6 50kPa


Shear Stress (kPa)
Horizontal Deflection (mm)
Mt-PAM pH6 100kPa
Mt-PAM pH6 200kPa
Mt-PAM pH11.5 50kPa
Mt-PAM pH11.5 100kPa
Mt-PAM pH11.5 200kPa
Mt-PAM 0.3M NaCl 50kPa
Mt-PAM 0.3M NaCl 100kPa
Mt-PAM 0.3M NaCl 200kPa

Appendix B

This appendix contains data gathered from all testing related to the 1D consolidation and shear wave velocity measurements. Table B.1 lists measurements recorded during the 1D consolidation tests on all samples, and Table B.2 includes the calculations performed on all samples. Table B.3 shows the values and calculations performed to determine average C_v values for all samples.

Figure B.1 includes the consolidation plots for all samples tested. On these plots, trendlines were added to determine the C_c and C_r values, which were determined from the slope of the trendlines.

TABLE B.1: Measurements recorded during 1D consolidation testing

Sample	h_i (mm)	h_0 (mm)	h_{87} (mm)	h_{1643} (mm)	h_f (mm)	$M_{w,i}$ (g)	$M_{w,0}$ (g)	$M_{w,f}$ (g)	M_d (g)
Kt pH3	50	61.857	52.223	38.743	44.560			369	286.9
Kt pH6	50	56.622	52.279	41.593	46.500		400.08	384.05	298.36
Kt pH11.5	50	51.116	45.762	37.228	41.030		349.62	330.72	259.52
Kt 0.3M NaCl	50	56.332	48.306	35.835	41.580			348.96	272.75
Kt-PAM pH3	50	54.552	52.051	38.86	43.600			357.47	267.8
Kt-PAM pH6	50	53.671	49.785	38.723	43.300			358.81	268.9
Kt-PAM pH11.5	50	52.856	44.855	33.272	38.200			323.69	249.49
Kt-PAM 0.3M NaCl	50	52.839	48.737	36.837	42.438			343.91	249.74
Mt pH3	50	62.301	43.327		38.885			229.54	89.64
Mt pH6	50	58.518	41.665		38.355			224.7	87.98
Mt pH11.5	35	49.142	30.471		19.143			121.31	58.25
Mt 0.3M NaCl	40	44.768	26.154		16.510			114.19	66.42
Mt-PAM pH3	50	57.443	24.677		28.030	249.62	288	157.59	47.08
Mt-PAM pH6	50	57.417	31.001		26.990			158.2	52.74
Mt-PAM pH11.5	50	60.818	24.636		27.620		295.5	151.36	42.98
Mt-PAM 0.3M NaCl	50	55.258	21.806		23.190	261.02	280.87	137.92	54.1

h_i = Height of sample after trimming, before saturation

h_0 = Height of sample after saturation, before first load

h_{87} = Height of sample after 87 kPa normal stress

h_{1643} = Height of sample after 1643 kPa normal stress

h_f = Height of sample after final loading

$M_{w,i}$ = Mass of wet sample after trimming, before saturation

$M_{w,0}$ = Mass of wet sample after saturation, before first load

$M_{w,f}$ = Mass of wet sample after final loading

M_d = Mass of dry sample after final loading

TABLE B.2: Calculated values obtained from 1D consolidation testing

Sample	w_i (%)	w_0 (%)	w_f (%)	V_s (cm^3)	H_s (cm)	e_i	e_0	e_{87}	e_{1643}	e_f
Kt pH3			28.62	110.35	2.51	0.99	1.47	1.08	0.54	0.78
Kt pH6		34.09	28.72	114.75	2.61	0.92	1.17	1.00	0.59	0.78
Kt pH11.5		34.72	27.44	99.82	2.27	1.20	1.25	1.02	0.64	0.81
Kt 0.3M NaCl			27.94	104.90	2.38	1.10	1.36	1.03	0.50	0.74
Kt-PAM pH3			33.48	103.00	2.34	1.14	1.33	1.22	0.66	0.86
Kt-PAM pH6			33.44	103.42	2.35	1.13	1.28	1.12	0.65	0.84
Kt-PAM pH11.5			29.74	95.96	2.18	1.29	1.42	1.06	0.53	0.75
Kt-PAM 0.3M NaCl			37.71	96.05	2.18	1.29	1.42	1.23	0.69	0.94
Mt pH3			156.07	34.48	0.78	5.38	6.95	4.53		3.96
Mt pH6			155.40	33.84	0.77	5.50	6.61	4.42		3.99
Mt pH11.5			108.26	22.40	0.51	5.87	8.65	4.98		2.76
Mt 0.3M NaCl			71.92	25.55	0.58	5.89	6.71	3.50		1.84
Mt-PAM pH3	430.20	511.72	234.73	18.11	0.41	11.15	12.96	5.00		5.81
Mt-PAM pH6			199.96	20.28	0.46	9.85	11.46	5.72		4.85
Mt-PAM pH11.5		587.53	252.16	16.53	0.38	12.31	15.19	5.56		6.35
Mt-PAM 0.3M NaCl	382.48	419.17	154.94	20.81	0.47	9.57	10.69	3.61		3.90

w_i = Water content after trimming, before saturation

w_0 = Water content after saturation, before first load

w_f = Water content after final loading

e_i = Void ratio after trimming, before saturation

e_0 = Void ratio after saturation, before first load

e_{87} = Void ratio after 87 kPa normal stress

e_{1643} = Void ratio after 1643 kPa normal stress

e_f = Void ratio after final loading

TABLE B.3: Values used to calculate an average C_v for each sample

Sample	ε_{100} (%)	ε_0 (%)	ε_{50} (%)	t_{50} (min)	H_{dr} (mm)	C_v (cm^2/s)
Kt pH3 15kPa	6.7	0.40	3.55	76	59.66	1.54E-03
Kt pH3 38kPa	3.5	0.68	2.09	60	55.60	1.69E-03
Kt pH3 87kPa	4.3	1.02	2.66	30	53.20	3.10E-03
Kt pH3 136kPa	2.5	0.56	1.53	27	51.42	3.22E-03
Kt pH3 439kPa	8.95	3.20	6.07	12	47.74	6.24E-03
Kt pH3 841kPa	6.08	2.24	4.16	7.3	44.11	8.75E-03
Kt pH3 1643kPa	8.65	3.27	5.96	4	40.37	1.34E-02
Kt pH3						**5.42E-03**
Kt pH6 87kPa	7.6	1.55	4.57	27	54.03	3.55E-03
Kt pH6 136kPa	1.48	0.43	0.95	9.7	51.78	9.08E-03
Kt pH6 239kPa	2.43	1.04	1.73	7.7	50.54	1.09E-02
Kt pH6 439kPa	3.21	1.32	2.26	5	48.87	1.57E-02
Kt pH6 841kPa	5.08	1.96	3.52	4.7	46.52	1.51E-02
Kt pH6 1643kPa	7.16	3.17	5.16	1.4	43.32	4.40E-02
Kt pH6						**1.64E-02**
Kt pH11.5 87kPa	10.08	3.63	6.85	37	47.61	2.01E-03
Kt pH11.5 136kPa	1.9	0.33	1.12	17	45.25	3.95E-03
Kt pH11.5 239kPa	2.3	0.78	1.54	11	44.14	5.82E-03
Kt pH11.5 439kPa	2.84	1.18	2.01	6	42.84	1.00E-02
Kt pH11.5 841kPa	2.77	1.50	2.14	0.5	41.39	1.13E-01
Kt pH11.5 1643kPa	6.9	1.89	4.39	2	38.60	2.45E-02
Kt pH11.5						**2.65E-02**
Kt 0.3M NaCl 15kPa	4.73	0.14	2.43	80	54.96	1.24E-03
Kt 0.3M NaCl 38kPa	5.4	1.19	3.30	49	51.48	1.78E-03
Kt 0.3M NaCl 87kPa	3.88	0.96	2.42	22	49.08	3.60E-03
Kt 0.3M NaCl 136kPa	2.32	0.54	1.43	28	47.62	2.66E-03
Kt 0.3M NaCl 439kPa	8.55	3.39	5.97	9.5	44.32	6.79E-03
Kt 0.3M NaCl 841kPa	6.2	2.39	4.30	5.6	40.97	9.84E-03
Kt 0.3M NaCl 1643kPa	8.55	3.57	6.06	4	37.38	1.15E-02
Kt 0.3M NaCl						**5.34E-03**

TABLE B.3 (cont.): Values used to calculate an average C_v for each sample

Sample	ε_{100} (%)	ε_0 (%)	ε_{50} (%)	t_{50} (min)	H_{dr} (mm)	C_v (cm^2/s)
Kt-PAM pH3 15kPa						N/A
Kt-PAM pH3 38kPa						N/A
Kt-PAM pH3 87kPa	3.78	0.13	1.95	120	53.23	7.75E-04
Kt-PAM pH3 136kPa	2.85	0.27	1.56	34	51.24	2.54E-03
Kt-PAM pH3 439kPa	8.02	1.66	4.84	14	47.97	5.40E-03
Kt-PAM pH3 841kPa	5.16	1.52	3.34	10	44.33	6.45E-03
Kt-PAM pH3 1643kPa	7.45	2.57	5.01	4	40.83	1.37E-02
Kt-PAM pH3						**5.77E-03**
Kt-PAM pH6 87kPa	6.9	0.29	3.59	23	51.74	3.82E-03
Kt-PAM pH6 136kPa	1.85	0.27	1.06	30	49.26	2.66E-03
Kt-PAM pH6 439kPa	7.05	1.36	4.21	10.5	46.73	6.83E-03
Kt-PAM pH6 841kPa	4.73	1.34	3.04	9.8	43.64	6.38E-03
Kt-PAM pH6 1643kPa	7.02	2.81	4.92	3.8	40.39	1.41E-02
Kt-PAM pH6						**6.76E-03**
Kt-PAM pH11.5 87kPa	13.7	-0.21	6.74	72	49.29	1.11E-03
Kt-PAM pH11.5 136kPa	2.6	0.18	1.39	53	44.23	1.21E-03
Kt-PAM pH11.5 239kPa	3.7	0.46	2.08	34	42.57	1.75E-03
Kt-PAM pH11.5 439kPa	4.33	0.88	2.60	18	40.52	2.99E-03
Kt-PAM pH11.5 841kPa	5.6	1.74	3.67	10	38.05	4.75E-03
Kt-PAM pH11.5 1643kPa	8	2.98	5.49	4.5	34.87	8.87E-03
Kt-PAM pH11.5						**3.45E-03**
Kt-PAM 0.3M NaCl 15kPa	0.9	0.08	0.49	26	52.58	3.49E-03
Kt-PAM 0.3M NaCl 38kPa	2.87	0.57	1.72	30.5	51.46	2.85E-03
Kt-PAM 0.3M NaCl 87kPa	3.28	0.31	1.80	38	49.70	2.13E-03
Kt-PAM 0.3M NaCl 136kPa	2.15	0.26	1.21	40.5	48.15	1.88E-03
Kt-PAM 0.3M NaCl 439kPa	7.6	1.69	4.64	12	45.30	5.61E-03
Kt-PAM 0.3M NaCl 841kPa	4.95	1.49	3.22	4.8	42.04	1.21E-02
Kt-PAM 0.3M NaCl 1643kPa	7.57	3.04	5.30	3.1	38.58	1.58E-02
Kt-PAM 0.3M NaCl						**6.26E-03**

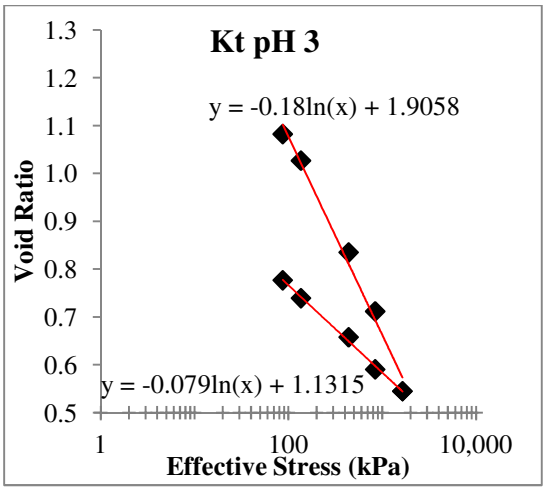
TABLE B.3 (cont.): Values used to calculate an average C_v for each sample

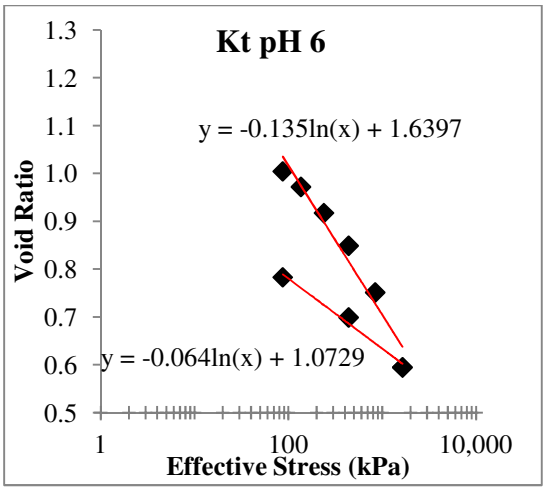
Sample	ε_{100} (%)	ε_0 (%)	ε_{50} (%)	t_{50} (min)	H_{dr} (mm)	C_v (cm^2/s)
Mt pH3 15kPa						N/A
Mt pH3 38kPa	13.2	1.21	7.21	510	57.29	2.11E-04
Mt pH3 87kPa	17.6	-0.05	8.78	900	48.55	8.60E-05
Mt pH3 136kPa	12.6	0.35	6.47	1700	40.52	3.17E-05
Mt pH3						**1.10E-04**
Mt pH6 15kPa						N/A
Mt pH6 38kPa	12.85	1.41	7.13	540	53.71	1.75E-04
Mt pH6 87kPa	15.9	0.85	8.38	980	45.82	7.03E-05
Mt pH6 136kPa	11.1	0.27	5.69	1600	39.30	3.17E-05
Mt pH6						**9.25E-05**
Mt pH11.5 15kPa	6.17	0.04	3.11	180	47.62	4.14E-04
Mt pH11.5 38kPa	17	1.36	9.18	410	41.55	1.38E-04
Mt pH11.5 87kPa	18.5	0.90	9.70	700	33.99	5.42E-05
Mt pH11.5 136kPa	13	0.34	6.67	840	28.44	3.16E-05
Mt pH11.5 439kPa	35.5	4.08	19.79	1000	21.14	1.47E-05
Mt pH11.5						**1.30E-04**
Mt 0.3M NaCl 15kPa	5.2	0.74	2.97	390	43.44	1.59E-04
Mt 0.3M NaCl 38kPa	17.9	1.25	9.57	700	38.28	6.87E-05
Mt 0.3M NaCl 87kPa	22.5	0.93	11.71	830	30.27	3.62E-05
Mt 0.3M NaCl 136kPa	15	-0.48	7.26	700	24.26	2.76E-05
Mt 0.3M NaCl 439kPa	26.8	1.95	14.37	700	18.76	1.65E-05
Mt 0.3M NaCl						**6.16E-05**

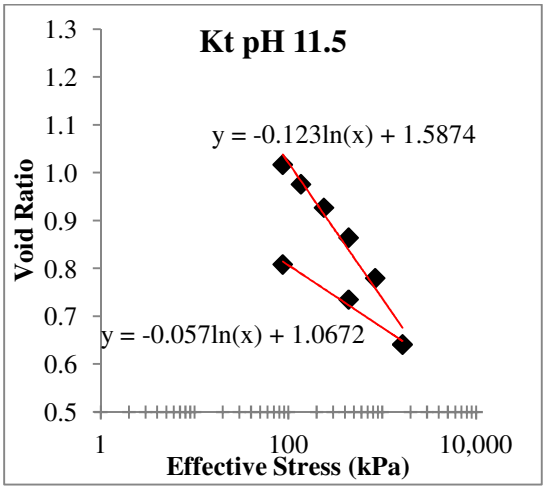
TABLE B.3 (cont.): Values used to calculate an average C_v for each sample

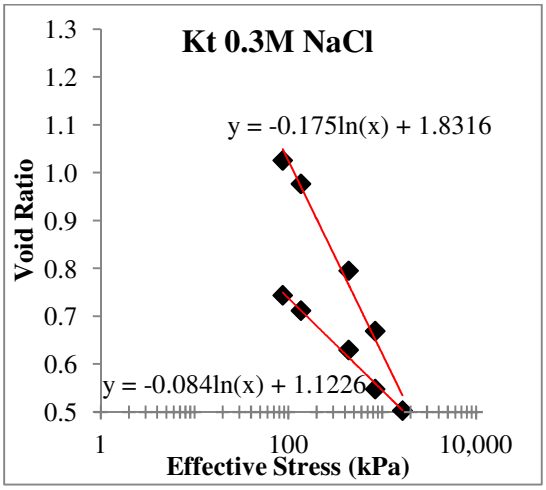
Sample	ε_{100} (%)	ε_0 (%)	ε_{50} (%)	t_{50} (min)	H_{dr} (mm)	C_v (cm^2/s)
Mt-PAM pH3 15kPa	13	0.27	6.63	750	53.63	1.26E-04
Mt-PAM pH3 38kPa	29.7	0.59	15.15	1700	41.85	3.38E-05
Mt-PAM pH3 87kPa	25.3	0.45	12.87	1700	29.71	1.70E-05
Mt-PAM pH3						**5.89E-05**
Mt-PAM pH6 15kPa	4.9	0.09	2.50	450	55.98	2.29E-04
Mt-PAM pH6 38kPa	24	0.33	12.17	1400	47.93	5.39E-05
Mt-PAM pH6 87kPa	24.2	-2.34	10.93	1600	36.71	2.77E-05
Mt-PAM pH6 136kPa	17.8	-2.05	7.88	1900	28.56	1.41E-05
Mt-PAM pH6						**8.11E-05**
Mt-PAM pH11.5 15kPa	2.14	0.26	1.20	180	60.09	6.59E-04
Mt-PAM pH11.5 38kPa	39.5	0.32	19.91	1400	47.64	5.32E-05
Mt-PAM pH11.5 87kPa	27.35	-0.07	13.64	1500	29.86	1.95E-05
Mt-PAM pH11.5						**2.44E-04**
Mt-PAM 0.3M NaCl 15kPa	12.9	0.55	6.72	540	51.54	1.62E-04
Mt-PAM 0.3M NaCl 38kPa	31	-0.43	15.29	1050	40.30	5.08E-05
Mt-PAM 0.3M NaCl 87kPa	29.7	0.40	15.05	1050	27.11	2.30E-05
Mt-PAM 0.3M NaCl						**7.84E-05**

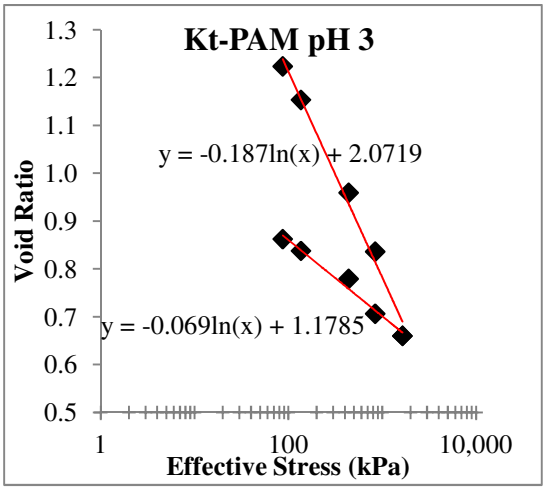
FIG. B.1: Consolidation curves for each sample tested displaying the trendlines used to determine C_c and C_r values

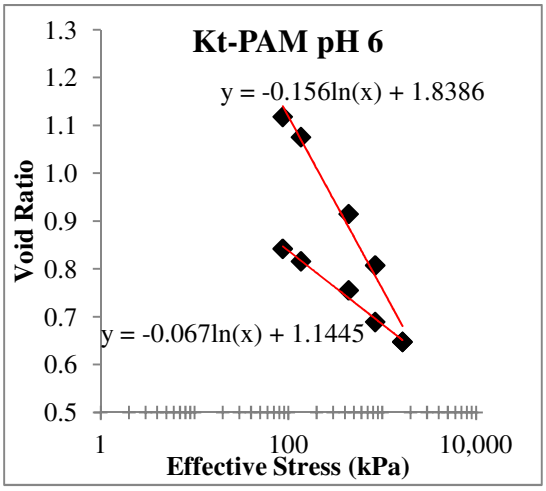

Kt pH 3
y = -0.18ln(x) + 1.9058
y = -0.079ln(x) + 1.1315
Void Ratio
Effective Stress (kPa)
1.3
1.2
1.1
1.0
0.9
0.8
0.7
0.6
0.5
1
100
10,000

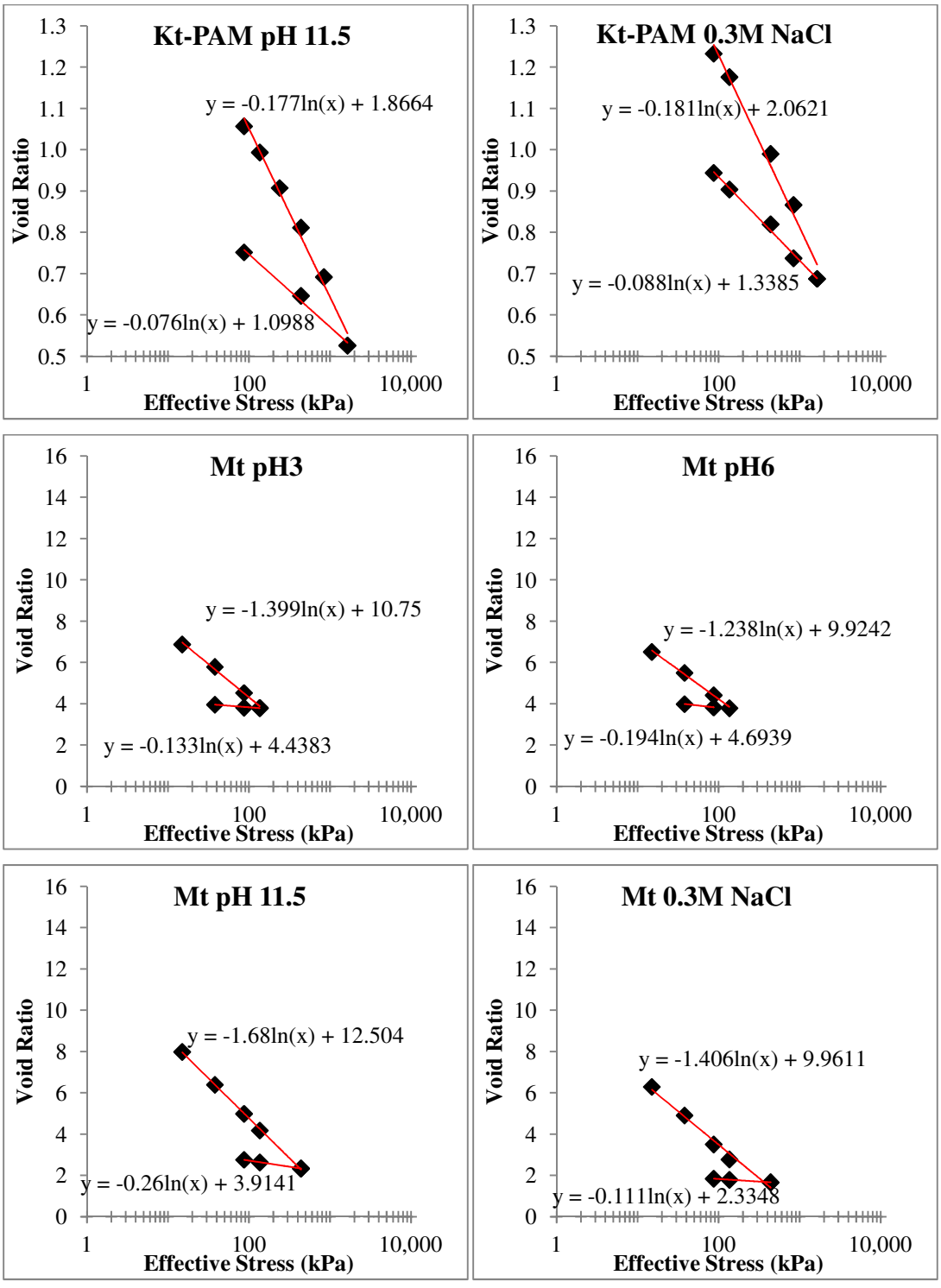

Kt pH 6
y = -0.135ln(x) + 1.6397
y = -0.064ln(x) + 1.0729
Void Ratio
Effective Stress (kPa)
1.3
1.2
1.1
1.0
0.9
0.8
0.7
0.6
0.5
1
100
10,000

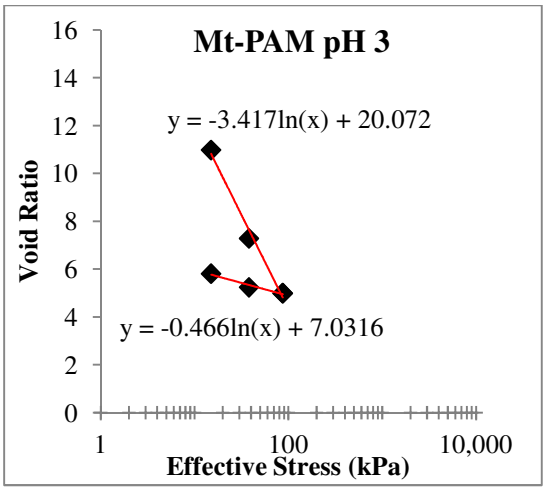

Kt pH 11.5
y = -0.123ln(x) + 1.5874
y = -0.057ln(x) + 1.0672
Void Ratio
Effective Stress (kPa)
1.3
1.2
1.1
1.0
0.9
0.8
0.7
0.6
0.5
1
100
10,000

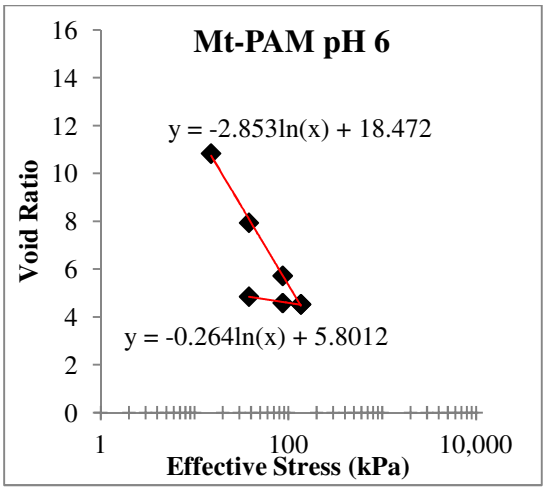

Kt 0.3M NaCl
y = -0.175ln(x) + 1.8316
y = -0.084ln(x) + 1.1226
Void Ratio
Effective Stress (kPa)
1.3
1.2
1.1
1.0
0.9
0.8
0.7
0.6
0.5
1
100
10,000

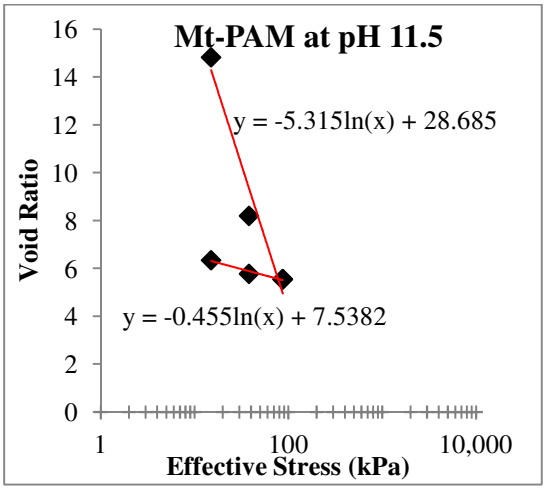

Kt-PAM pH 3
y = -0.187ln(x) + 2.0719
y = -0.069ln(x) + 1.1785
Void Ratio
Effective Stress (kPa)
1.3
1.2
1.1
1.0
0.9
0.8
0.7
0.6
0.5
1
100
10,000

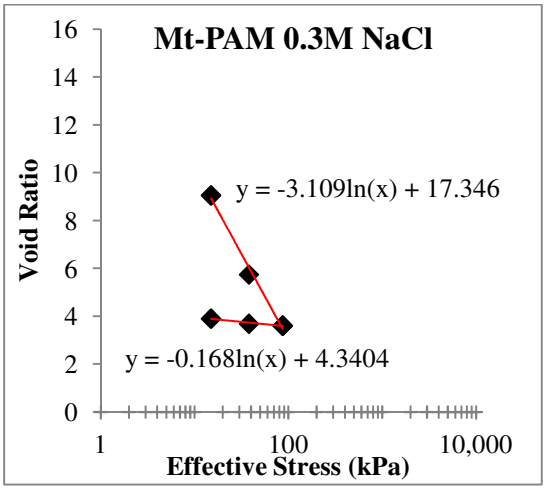

Kt-PAM pH 6
y = -0.156ln(x) + 1.8386
y = -0.067ln(x) + 1.1445
Void Ratio
Effective Stress (kPa)
1.3
1.2
1.1
1.0
0.9
0.8
0.7
0.6
0.5
1
100
10,000


Kt-PAM pH 11.5
y = -0.177ln(x) + 1.8664
y = -0.076ln(x) + 1.0988
Void Ratio
Effective Stress (kPa)
Kt-PAM 0.3M NaCl
y = -0.181ln(x) + 2.0621
y = -0.088ln(x) + 1.3385
Mt pH3
y = -1.399ln(x) + 10.75
y = -0.133ln(x) + 4.4383
Mt pH6
y = -1.238ln(x) + 9.9242
y = -0.194ln(x) + 4.6939
Mt pH 11.5
y = -1.68ln(x) + 12.504
y = -0.26ln(x) + 3.9141
Mt 0.3M NaCl
y = -1.406ln(x) + 9.9611
y = -0.111ln(x) + 2.3348


Mt-PAM pH 3
y = -3.417ln(x) + 20.072
y = -0.466ln(x) + 7.0316
Void Ratio
Effective Stress (kPa)
16
14
12
10
8
6
4
2
0
1
100
10,000


Mt-PAM pH 6
y = -2.853ln(x) + 18.472
y = -0.264ln(x) + 5.8012
Void Ratio
Effective Stress (kPa)
16
14
12
10
8
6
4
2
0
1
100
10,000


Mt-PAM at pH 11.5
y = -5.315ln(x) + 28.685
y = -0.455ln(x) + 7.5382
Void Ratio
Effective Stress (kPa)
16
14
12
10
8
6
4
2
0
1
100
10,000


Mt-PAM 0.3M NaCl
y = -3.109ln(x) + 17.346
y = -0.168ln(x) + 4.3404
Void Ratio
Effective Stress (kPa)
16
14
12
10
8
6
4
2
0
1
100
10,000

VITA

Matthew Bishop was raised in New Tazewell, TN, by his parents David and Debbie Bishop. He attended Claiborne High School, where he graduated as a co-valedictorian of his class in 2007. After graduation, he attended the University of Tennessee, Knoxville, to study Civil Engineering. During his college career, he was heavily involved with the American Society of Civil Engineers (ASCE) student chapter, where he served as Treasurer and Concrete Canoe captain his senior year. He also worked as a Civil Engineering intern at the U.S. Department of Veterans Affairs campus in Johnson City, TN. He completed his Bachelor of Science degree in Civil Engineering with a minor in Business Administration in 2011.

Matthew continued his education at the University of Tennessee, Knoxville, in the Dual MS-MBA program. He worked as both a teaching assistant and research assistant during this time in the department of Civil Engineering. He concentrated in the field of Geotechnical Engineering and will be graduating in Summer 2013. Upon graduation, Matthew will be working as a Geotechnical Engineer in Knoxville, TN.